8-2003

Effects of Fiberimatiux Interactions on the Interfacial Deformation Micromechanics of Cellulose-Fiberipolymer Composites

William tai-Yin Tze

EFFECTS OF FIBER/MATRIX INTERACTIONS ON THE INTERFACIAL DEFORMATION MICROMECHANICS OF CELLULOSE-FIBER/POLYMER COMPOSITES

By

William Tai-Yin Tze

B. For. Sc. Agricultural University of Malaysia (UPM), 1992

M.S. Michigan Technological University, 1998

A THESIS

Submitted in Partial Fulfillment of the

Requirements for the Degree of

Doctor of Philosophy

(in Forest Resources)

The Graduate School

The University of Maine

August, 2003

Advisory Committee:

Douglas Gardner, Professor of Wood Science and Technology, Co-Advisor

Carl Tripp, Professor of Chemistry, Co-Advisor

Stephen Shaler, Professor of Wood Science and Technology

William Unertl, Professor of Physics

Timothy Rials, Professor of Wood Science, University of Tennessee

LIBRARY RIGHTS STATEMENT

In presenting this thesis in partial fulfillment of the requirements for an advanced degree at The University of Maine, I agree that the Library shall make it freely available for inspection. I further agree that permission for "fair use" copying of this thesis for scholarly purposes may be granted by the Librarian. It is understood that any copying or publication of this thesis for financial gain shall not be allowed without my written permission.

Signature: 

Date: AUG 22, 2003

EFFECTS OF FIBER/MATRIX INTERACTIONS ON THE INTERFACIAL DEFORMATION MICROMECHANICS OF CELLULOSE-FIBER/POLYMER COMPOSITES

By William Tai-Yin Tze

Thesis Co-Advisors: Dr. Douglas Gardner and Dr. Carl Tripp

An Abstract of the Thesis Presented
in Partial Fulfillment of the Requirements for the
Degree of Doctor of Philosophy
(in Forest Resources)
August, 2003

The overall objective of this dissertation was to gain an understanding of the relationship between interfacial chemistry and the micromechanics of the cellulose-fiber/polymer composites. Regenerated cellulose (lyocell) fibers were treated with amine-, phenylamine-, phenyl-, and octadecyl-silanes, and also styrene-maleic anhydride copolymer. Inverse gas chromatography was conducted to evaluate the modified surfaces and to examine the adsorption behavior of ethylbenzene, a model compound for polystyrene, onto the fibers. Micro-composites were formed by depositing micro-droplets of polystyrene onto single fibers. The fiber was subjected to a tensile strain, and Raman spectroscopy was employed to determine the point-to-point variation of the strain- and stress-sensitive 895 cm^{-1} band of cellulose along the embedded region.

Inverse gas chromatography studies reveal that the I_{a-b} values, calculated by matching the Lewis acid parameter (K_A) and basic parameter (K_B) between

polystyrene and different fibers, were closely correlated to the acid-base adsorption enthalpies of ethylbenzene onto the corresponding fibers. Hence, I_{a-b} was subsequently used as a convenient indicator for fiber/matrix acid-base interaction.

The Raman micro-spectroscopic studies demonstrate that the interfacial tensile strain and stress are highest at the edge of the droplet, and these values decline from the edge region to the middle region of the embedment. The maximum of these local strains corresponds to a strain-control fracture of the matrix polymer. The minimum of the local tensile stress corresponds to the extent of fiber-to-matrix load transfer. The slope of the tensile stress profile allows for an estimation of the maximum interfacial shear stress, which is indicative of fiber/polymer (practical) adhesion. As such, a novel micro-Raman tensile technique was established for evaluating the ductile-fiber/brittle-polymer system in this study.

The micro-Raman tensile technique provided maximum interfacial shear stress values of 8.0 to 13.8 MPa, ranking functional groups according to their practical adhesion to polystyrene: alkyl< untreated < phenyl = phenylamine = styrene copolymer < amine. Overall, interfacial bonding can be increased by increasing the acid-base interactions (I_{a-b}) or reducing the chemical incompatibility ($\overline{\Delta\delta}$) between the fibers and matrix. Therefore, interfacial chemistry can be employed to enhance and predict cellulose-fiber/polymer adhesion to better engineer composite properties and ultimately better utilize bio-resources.

ACKNOWLEDGEMENTS

I would like to express my sincere gratitude to my co-advisors, Dr. Douglas Gardner and Dr. Carl Tripp, for their invaluable advice of this dissertation. Dr. Gardner has provided me with unfailing support without which, I could not have completed my Ph.D. program. Dr. Carl Tripp has spent countless hours with me in making the Raman spectroscopic studies a success. Also acknowledged are other members of my dissertation committee: Dr. Stephen Shaler, Dr. William Unertl, and Dr. Timothy Rials for their constructive suggestions in my research work.

I owe a debt of gratitude to Research Associate Shane O' Neill who built the micro-Raman tensile stage and the data acquisition system that allowed me to proceed with my proposed research. Dr. Magnus Wålinder, now of the Swedish Institute for Wood Technology Research (Trätek), was a resourceful colleague and mentor during his fellowship as the post-doctorate researcher in Dr. Gardner's group. Dr. Sofian Kanan, now of the American University of Sharjah, U.A.E., was practically my problem solver in the early stage of my research with Dr. Tripp. I also derived numerous benefits from interacting with chemists of Dr. Tripp's research group: Dr. Anil Waghe (now with the University of Oklahoma), Mr. Zhixiang Lu (now a Ph.D. student in the University of Massachusetts), Ms. Haiyan Li, Ms. Cuihong Jiang, and Mr. Wei Gu, whose support and assistance are greatly appreciated.

It has been a good experience working in two of the dynamic and scientific-excel groups of UMaine: the Advanced Engineered Wood Composites Center (AEWC) and the Laboratory for Surface Science and Technology (LASST). I thank the administrative and technical staff of both the centers. Of notable mention is the kind personal attention provided by Ms. Doreen Parent and Ms. Marcy Smith.

Also deserving to be mentioned is my official affiliation at UMaine: the Department of Forest Management. I thank Dr. David Field, the head of the department, for opening up a wonderful learning experience by accepting me to the Ph.D. program. I am grateful to Ms. Cindy Paschal and Ms. Dolores Stone, for taking care of my administrative-related business.

Other people who have improved the quality of my educational experience are (1) Dr. Joseph Genco, my advisor for the Pulp and Paper Certificate Program during my initial year at UMaine, (2) Ms. Jane Morse of the Writing Center, and (3) Ms. Kylie Gallant, my speech tutor who worked with the Conley Speech and Hearing Center. Also provided equal, if not more, significant contributions are staff from the Office of International Program especially Mr. James Leck and Ms. Mireille Le Gal.

During my five years of stay at UMaine, I have acquainted many nice people. Among them, I would like to mention Dr. Lech Muzynski and Ms. Danuta Muzynska who generously shared with me many important celebrations and precious moments of their time. Other people who have been supportive and providing invaluable friendship

were Dr. Jungil Son, Dr. Cihat Tasciglu (now in Turkey), and Mr. Leopold Eisenheld (now in Austria). All in all, I have been fortunate to be surrounded by many wonderful people, and it is not easy to mention each by name here. For these people, I pray for their happiness, and that I can reciprocate their kindness in the future.

I am indebted to Acordis Cellulosic Fibers for donating the lyocell fibers used in this study. I acknowledge the financial support from the USDA/CSREES New England Wood Utilization Research Fund, which funded my Ph.D. study. Also, I appreciate the approval of the Forest Products Society to use two figures from its publications in this dissertation (Figures 4.3 and 4.4).

Last but not least, I would like to thank my parents, who provided me with a decent childhood and fundamental education, laying the foundation of my value and personal development. I am also thankful to my brothers who have been looking out for me, and who believed that I could make it for the Ph.D. degree.

TABLE OF CONTENTS

LIST OF TABLES

LIST OF FIGURES

1. INTRODUCTION

1.1. Potentials and Advantages of Wood-Plastic Composites

Wood-plastic composites (WPC) have made a forceful entry into the wood products market in recent years. In 2001, the WPC market was 320,000 metric tons and it is expected to increase to more than double in 2005 (Mapleston 2001). Of the current WPCs, decking and railing products enjoy the greatest growth in a market that is traditionally dominated by pressure-treated lumber. In 1997, WPCs occupied 2% of the US decking and railing market, but the market share expanded rapidly to 8% of the $3.2 billion market in 2000 (Smith 2001). This market share is projected to grow to 20% by 2005 when the total market for decking and railing in US is expected to increase to $3.9 billion (Smith 2001).

The success of WPCs as an alternative to the conventional wood products primarily lies in its moisture-resistant properties. With WPC decking as an example, wood flour (10-80 mesh size) of up to 70% by weight forms composites with a polyethylene or polypropylene matrix which protects the wood from environmental attack. Hence, fungal resistance and dimensional stability are attained without dependence on preservatives that could leach and post a threat to both human and the environment. Indeed, WPC decking has been partially replacing lumber treated with chromated copper arsenate (CCA) which is to be phased out of residential use as regulated by the Environmental Protection Agency (Clemons 2002).

The desirable properties of wood have made WPC a more favorable building material compared to pure plastics. In WPC, the plastic component transfers external loads to the stiffer wood component, hence sparing the plastics from failure. The addition of wood also reduces the thermal expansion of the plastics. An example of where composite products benefit from the stiffer and more thermally stable wood materials is in window applications. Window profiles have been largely made of poly (vinyl chloride) or PVC for moisture resistance, but recently wood-filled PVC is gaining popularity because of the desirable balance of stiffness, thermal stability, and moisture resistance (Defosse 1999).

Indeed, lignocellulosics have the potential to tap the markets of filler and reinforcement for plastics. The demand for filler and reinforcement in the plastics industry is about 2.5 billion kg annually and the market is currently dominated by talc, calcium carbonate, mica, glass fibers and carbon fibers (Eckert 2000). Compared to these conventional fillers, lignocellulosic materials such as wood have many features that are more favorable -- they are renewable, cheaper, lighter, and less abrasive to processing equipment. Of the lignocellulosics, wood in the form of flour is often preferable primarily because it is free flowing (easy to disperse), more easily available, and less expensive. However, the resultant WPC is usually brittle albeit its stiffness increases. On the other hand, wood fibers or other natural (agricultural) fibers could increase the tensile strength and toughness of the plastics (Clemons 2002). An example

of such advantages is in the reinforcement of polypropylene and polyester polymer using natural fibers for producing automotive door panels where a high impact strength is necessary (Clemons 2002).

1.2. The Bonding Issues

The ability to engineer wood/polymer composites would be enhanced with an improved understanding of the factors that influence the mechanical properties of the composites. It is known that the mechanical properties of fiber/polymer composites depend on (1) the strength and modulus of the fibers, (2) the strength and chemical stability of the matrix polymer, and (3) the effectiveness of the fiber/polymer bond in transferring load across the interphase (Erickson and Plueddemann 1974). The composite properties are also influenced by factors associated with the distribution behavior of the fibers in the matrix polymer; these factors include fiber volume fraction, fiber orientation, and fiber agglomeration. Another influencing factor in the case of discontinuous fiber composites is the fiber aspect ratio (length divided by diameter) – the higher ratio allows a larger percentage of the length of the fiber being fully utilized for transferring load (Hoecker and Karger-Kocsis 1996; Shaler 1993).

While the properties of the bulk fibers and matrix polymers are usually known, the interface region (interphase) is not well understood. An interphase includes the two-dimensional fiber/matrix area of contacts (interface) and the region of some finite thickness extending on both sides of the interface (Drzal 1990). This region is thought

to have properties that are neither those of the fibers nor matrix. Therefore, the fiber/polymer interphase has frequently become the subject of studies for understanding the behavior of composites.

The ability of an interphase to transfer load from one phase to another depends on the fiber/matrix adhesion, which can be physico-chemical or frictional in nature. The frictional contribution to adhesion is primarily a result of the Poisson contraction between the fiber and matrix, differential thermal contraction of the fiber and matrix upon cooling from the processing temperature, and surface roughness of the fiber (Kim and Mai 1998). The physico-chemical contribution, on the other hand, involves molecular interactions between the fibers and matrix, such as intermolecular forces (Brewis and Briggs 1985), transcrystallinity at the interphase, and glass transition of the matrix polymer in the presence of the fibers (Schultz and Nardin 1994). While the frictional contribution dominates in some ceramic matrix composites (Kim and Mai 1998), the physico-chemical contribution is considerably important in polymer matrix composites (Schultz and Nardin 1994).

For a given fiber/matrix system, the physico-chemical interactions at the interphase can be manipulated to enhance the mechanical performance of the composites. Making composites from the polar wood materials and the non-polar or slightly polar thermoplastics frequently violates the requirement of fiber/polymer compatibility, resulting in weak interfacial and composite properties (Rials *et al.* 1998). These problems can be alleviated by treatments that modify the surface physico-

chemical properties of the combining materials to favor interfacial interactions. For example, wood fibers grafted with styrene molecules exhibited an improved tensile strength property in the resulting wood-fiber/polystyrene composites compared to the untreated fibers. This improvement is attributed to the interaction between benzene rings of the induced molecules and the matrix polymer at the interphase (Maldas *et al.* 1988). In another case, cellulose fibers that were treated with the basic aminosilane formed composites of improved tensile strength property with the acidic, plasticized polyvinyl chloride (PVC). Such property enhancement is a consequence of the enhanced acid-base interaction at the interphase (Matuana *et al.* 1998).

Studies of interfacial properties frequently bring up the issue of the definitions of "adhesion". The term "adhesion" refers to the state in which two materials are held together by interfacial forces such that mechanical force or work can be transferred across the interface region (Wu 1982). The intermolecular interactions at the fiber/matrix interphase result in fundamental adhesion. One way to characterize fundamental adhesion is using the thermodynamic or reversible work of adhesion (W_a), which is the amount of work under reversible or equilibrium conditions to disjoin the interface between bonded bodies (Mittal 1975). As opposed to fundamental adhesion, practical adhesion is a measure of mechanical strength associated with irreversibly fracturing the adhesive bond (Mittal 1975). Examples of practical adhesion are peel strength and interfacial shear strength. Although these parameters are normally referred as "adhesion strength" or simply "adhesion", the measured values depend not only on molecular interactions, but also on the bulk fiber and matrix properties discussed earlier,

as well as flaws in the interface region or bulk phases, and the temperature and rate at which the test is performed (Wu 1982). The energy dissipated in the deformation of the test specimen is usually predominant in the measured practical adhesion such that some researchers doubt the ability of the measured values to indicate (fundamental) adhesion.

With the advance of adhesion research, it can be shown that the viscoelastic dissipation in the case of true interfacial failure can be expressed with the work of adhesion as the multiplier (Kinloch 1987). This discovery signifies that the measured practical adhesion can be treated as a relative measure of the (fundamental) adhesion if care is taken to identify the failure path as interfacial. In other word, if the practical bond strength is evaluated under a fixed protocol for a series of bonding systems, the measured values should correlate with (fundamental) adhesion (Miller *et al.* 2000).

Recognizing the confusing terms of adhesion, it is necessary to distinguish between fundamental and practical adhesion. In this dissertation, the practical bond strength will be inferred from the maximum interfacial shear stress, and it will be referred to, from time to time, as "the extent of adhesion" or "the level of adhesion", both of which are a manifestation of practical adhesion. For parameters that characterize fundamental adhesion, such as the work of adhesion and other indicators, which will be discussed in the dissertation, the names of the parameters will be mentioned directly.

1.3. Justification of Studies

Although there have been cases of success in accounting interfacial chemistry for the practical bond strength, the attribute does not seem to apply in every instance even for a given fiber/polymer pair and processing system. For acid-base matching, Beshay and Hoa (1990) formed compression-molded composites using amino-silanated wood fibers and polystyrene which are both basic in Lewis sense, but they observed an improvement in tensile strength property, which implied an enhanced fiber/polymer (practical) adhesion compared to the untreated fibers. Therefore, the contribution of interfacial chemistry to lignocellulosics/polymer practical adhesion is not entirely understood.

If interfacial chemistry can be deduced from the surface chemistry of the composite furnishes, and the role of the interfacial chemistry on the practical adhesion of the resulting lignocellulosics/polymer composites is well understood, one can predict the level of (practical) adhesion by knowing the surface chemistry of the components. From this knowledge, surfaces of a given pair of fibers and matrix polymer can be tailored by surface modification to optimize fiber/matrix (practical) adhesion. Such a privilege, coupled with the existing knowledge of the bulk properties of fibers and matrix polymers, ultimately leads to a better engineering of the properties of the lignocellulosic/polymer.

1.4. Dissertation Objectives and Approach

The overall objective of this dissertation was to gain an understanding of the relationship between interfacial chemistry and the micromechanics of the cellulose-fiber/polymer composites. This research differs from other studies in that it attempted to use a molecular approach in understanding interfacial phenomena – it employed inverse gas chromatography to examine molecular adsorption of the model polymer onto the fibers and it applied Raman spectroscopy to investigate molecular vibration at the fiber/polymer interphase.

Because this study focused on the fundamental knowledge of interfacial phenomena, the selection of samples and experimental procedures was not intended to simulate practical bonding practices. These parameters, however, were chosen for specific reasons. Regenerated cellulose (lyocell) fibers solvent-spun from wood pulps were used as the model fibers because these continuous fibers are easier to handle and more uniform in properties compared to natural fibers. The lyocell fibers also have mechanical properties that are quite similar to mature (Black Spruce) wood fibers (Table 1.1). Silane coupling agents were used for most of the surface modification attempts because these chemicals can be acquired in different terminal functional groups, and the treatment procedures are relatively simple. Polystyrene was used as the matrix polymer because it is a commonly available plastic that is amorphous, hence avoiding interfacial transcrystallinity, which would perturb the investigation of the surface-chemical effects on interfacial properties. Finally, micro-composites were

Table 1.1 Some mechanical properties of regenerated cellulose and wood fibers

	Lyocell fibers [a]	Juvenile wood fibers [b]	Mature wood fibers [c]
Tensile modulus (GPa)	15.2	1.11	9.44
Ultimate tensile strength (GPa)	0.54	0.21	0.48
Strain at failure (%)	7	17 [d]	6 [d]

Note: [a] Data from Eichhorn *et al.* (2001); 20 replicates; 83 μm/s

[b] Data for 10-year old Black Spruce fibers (Egan and Shaler 2000); 18 replicates; 80 μm/s

[c] Data for 55-year old Black Spruce fibers (Egan and Shaler 2000); 34 replicates; 80 μm/s

[d] Data estimated from the stress-strain plots in Egan and Shaler (2000).

tested to separate the interfacial bonding characteristics from the perturbations caused by fiber orientation and volumetric effects which would also influence composite properties in the case of bulk composite testing.

Since the bonding system in this study was between a brittle polymer and a small-diameter, ductile fiber, neither of the two common micromechanical tests, i.e. the micro-debond test and the fiber fragmentation test, was suitable for determining the extent of interfacial adhesion. In the micro-debond test, an interfacial shear strength is determined by shearing a polymer droplet off from the fiber, and so this test requires fibers of high fracture force compared to the droplet pull-off force (Rials *et al.* 1998).

In the fiber fragmentation test, the interfacial shear strength is deduced from the number (or length) of fiber fragments when a fiber-embedding polymer was subjected to a tensile load. Hence this test requires a matrix polymer of high fracture strain compared to the fibers (Rials *et al.* 1998). None of the above-mentioned requirements were satisfied in the bonding system of this research. Therefore, this dissertation was also partially aimed at establishing a novel technique for evaluating a wider range of fiber/polymer systems especially for the combinations involving ductile fibers and brittle polymers.

This dissertation primarily consists of four papers each presented in a chapter of Chapters 2-5. Chapter 2 deals with inverse gas chromatography (IGC) as a tool to quantify the surface chemistry of the fibers induced with different functional groups. It also addresses the issues of predicting fiber/polymer interaction from (1) the surface-chemical properties of the composite constituents and (2) from the direct adsorption studies of the model polymer molecules onto the fibers. Chapter 3 describes a novel Raman technique that examines the point-to-point variation of the vibrational frequency along the fiber/polymer interphase which can be converted into interfacial strain distributions. It also identifies the major factors that would affect the interpretation of the Raman data for manifesting micromechanical properties. Chapter 4 further utilizes the Raman technique for determining the tensile stress distribution at the fiber/polymer interphase. It elaborates the load transfer phenomena from the interfacial tensile stress profiles, and subsequently derives the shear stress distributions for evaluating

fiber/polymer practical adhesion. Chapter 5 finally brings together information from the IGC and Raman studies to discuss the effects of interfacial chemistry on the fiber/polymer interfacial micromechanics.

1.5. References

Beshay, A. and S. V. Hoa. 1990. Reinforcement of polyvinyl chloride (PVC) and polystyrene (PS) with cellulosic fibers treated with silane. Journal of Thermoplastics Composite Materials. 3:264-274.

Brewis, D. M. and D. Briggs. 1985. An overview. Pages 1-14 in D.M. Brewis and D. Briggs, eds. Industrial adhesion problems. John Wiley and Sons, New York.

Clemons, C. 2002. Wood-plastic composites in the United States: The interfacing of two industries. Forest Products Journal. 52(6):10-18.

Defosse, M. 1999. Processors focus on differentiation in window profiles. Modern Plastics. Sept.:74-79.

Drzal, L. T. 1990. The role of the fiber-matrix interphase on composite properties. Vacuum. 41(7-9):1615-1618.

Eckert, C. 2000. Opportunities for natural fibers in plastic composites. In: Proceedings, Progress in Woodfibre-Plastic Composites Conference 2000. University of Toronto, Toronto.

Egan, A. and S. M. Shaler. 2000. Fracture and mechanics of fracture for resin coated single wood fibers. Pages 95-103 in G. Hague, M. McLauchlin, and T. Skinner, eds. Proceedings of the Fourth Panel Products Symposium. The Biocomposites Centre, Bangor, U.K.

Eichhorn, S. J., R. J. Young, and W.–Y. Yeh. 2001. Deformation processes in regenerated cellulose fibers. Textile Research Journal. 71(2):121-129.

Erickson, P. W. and E. P. Plueddemann. 1974. Historical background of the interfaces – Studies and theories. Pages 1-29 in E. P. Plueddemann, ed. Interfaces in polymer matrix composites. Academic Press, New York.

Hoecker, F. and J. Karger-Kocsis. 1996. Surface energetics of carbon fibers and its effects on the mechanical performance of CF/EP composites. Journal of Applied Polymer Science. 59:139-153.

Kim, J. and Y. Mai. 1998. Engineered interfaces in fiber reinforced composites. Elsevier, Oxford, U. K. 401 pp.

Kinloch, A. J. 1987. Adhesion and adhesive science and technology. Chapman and Hall, New York. 441 pp.

Maldas, D., B. V. Kokta, R. G. Raj, and C. Daneault. 1988. Improvement of the mechanical properties of sawdust wood fiber-polystyrene composites by chemical treatment. Polymer. 29:1255-1265.

Mapleston, P. 2001. It's one hot market for profile extruders. Modern Plastics. June:49-52.

Matuana, L. M., R. T. Woodhams, J. J. Balatinecz, and C. B. Park. 1998. Influence of interfacial interactions on the properties of PVC/cellulosic fiber composites. Polymer Composites. 19(4):446-455.

Miller, A. C., M. T. Knowlton, and J. C. Berg. 2000. The use of UNIFAC for the estimation of adhesion enhancement between polymers and mineral surfaces treated with silane coupling agents. Journal of Adhesion Science and Technology. 14(12):1471-1484.

Mittal, K. L. 1975. Surface chemical criteria for maximum adhesion and their verification against the experimentally measured adhesive strength values. Pages 129-171 in L. Lee, ed. Adhesion science and technology. Plenum Press, New York.

Rials, T. G., M. P. Wolcott, and D. J. Gardner. 1998. Characterizing the wood fiber/polymer interface. Pages 31-39 in L. H. Groom and A. G. Zink, eds. Techniques in experimental mechanics applicable to forest products research. USDA Forest Service Southern Research Station, Asheville, NC.

Schultz, J. and M. Nardin. 1994. Some physico-chemical aspects of the fibre-matrix interphase in composite materials. Journal of Adhesion. 45:59-71.

Shaler, S. M. 1993. Mechanics of the interface in discontinuous wood fiber composites. Pages 9-14 in M. P. Wolcott, ed. Wood-fiber/polymer composites: fundamental concepts, processes, and material options. Forest Products Society. Madison, WI., USA.

Smith, P. M. 2001. U.S. woodfiber-plastic composite decking market. Pages 13-17 in Proceedings of the Sixth International Conference on Woodfiber-Plastic Composites. Forest Products Society, Madison, WI, USA.

Wu, S. 1982. Polymer interface and adhesion. Marcel Dekker, New York. 630 pp.

2. INVERSE GAS CHROMATOGRAPHY FOR STUDYING INTERACTION OF MATERIALS USED IN CELLULOSE-FIBER/POLYMER COMPOSITES

2.1. Chapter Summary

The objective of this research was to use inverse gas chromatography (IGC) to examine fiber/matrix interactions for predicting practical adhesion between cellulose-fibers and a non-polyolefin matrix polymer. IGC experiments were performed on polystyrene, untreated, alkyl- and amine-silanated cellulose (Lyocell) fibers. The fiber/matrix acid-base interaction was quantified by (1) matching the acidic parameter (K_A) of a component with the basic parameter (K_B) of another component, and (2) observing the adsorption enthalpy of the polymer building blocks (ethylbenzene) onto the fibers. Results show that the cellulose/polystyrene acid-base interaction inferred from interaction parameters is closely correlated to that evaluated from the specific adsorption of ethylbenzene. This feature indicates that the acid-base interactions, which play an important role in the adhesion between fibers and non-polyolefins, can be conveniently predicted from their respective acid-base parameters (K_A and K_B) prior to composites manufacture. More specifically, treatment with an amine-silane is likely to improve interaction and hence bonding with polystyrene in a composite system. Treatment with alkyl-silane, on the other hand, would result in a weak interaction with polystyrene. These predictions will be verified in future studies which will correlate material interactions with interfacial micromechanics in the resulting micro-composites.

2.2. Introduction

Cellulose fibers, which are high in strength and toughness, low in weight and abrasiveness, offer ample opportunities for filling or reinforcing polymer composites. These opportunities can be better realized with a profound understanding of the interaction between the fibers and the matrix material. Surface modification agents such as silane (Beshay and Hoa 1992), poly(methacrylic) acid copolymer (Liang *et al.* 1994), and maleic anhydride copolymer (Coupas *et al.* 1998) have been found to mitigate the widely-believed incompatibility between cellulose fibers and some common thermoplastics such as polystyrene and polyolefins. To optimize the treatment effects, the interaction between the components in a composite system needs to be better understood so that the desired mechanism can be emphasized to promote bonding. This understanding will allow tailoring of the component surfaces to optimize composite properties for specific applications.

A common approach to predict component interaction in a composite system is to characterize the surface properties of the individual components. Inverse gas chromatography (IGC) has been found to be a practical method to characterize material surfaces for composite applications (Coupas *et al.* 1998). This powerful technique provides information on the dispersive free energy, Lewis acidic parameter (K_A) and Lewis basic parameter (K_B) of the material surfaces. The information obtained allows quantification of surface modification, leading to the prediction of the extent of bonding in composites. For example, it has been recognized that materials having a monofunctional acidic (or basic) surface do not interact strongly with each other (Berg

1993). In essence, surface-chemical information of individual components provides a qualitative prediction of component interaction in composites.

2.3. Literature Review

An increasing amount of research has been carried out to quantify component interactions based on knowledge of surface chemistry of the individual component. Acid-base interaction is an important criterion in developing mechanical properties of composites made of cellulose fibers and polar thermoplastics such as polystyrene (Felix *et al.* 1994). Felix *et al.* (1994) calculated an acid-base interaction parameter (P_{AD}) by matching the K_A of a component and the K_B of another component:

$$P_{AD} = \left(K_{A,f} K_{D,m}\right)^{1/2} + \left(K_{D,f} K_{A,m}\right)^{1/2}, \tag{2.1}$$

where subscripts f and m are, respective, for fibers and matrix, and K_D is the electron donor parameter which has the same meaning as K_B. These researchers found that the interaction parameter correlated strongly with the ductility (strain at failure), elastic modulus, and glass transition temperatures of cellulosic-fiber/polystyrene composites. Park and Donnet (1998) used a similar approach to calculate an acid-base interaction parameter (I_{a-b}):

$$I_{a-b} = K_{A,f} K_{B,m} + K_{B,f} K_{A,m}. \tag{2.2}$$

They discovered that the parameter exhibited a strong linear relationship with the mechanical interfacial properties i.e. the interfacial shear strength of the single-fiber composites and the interlaminar shear strength of the macro composites made of carbon fibers and epoxy resin.

The choice of acid-base scaling for IGC probes has an influence on the units of K_A and K_B values calculated, and therefore it is an important issue when using equations for acid-base interaction parameters. The Lewis basic character for the probe liquids used in IGC experiments is indicated by *DN*, the donor number (Gutmann and Wychera 1966), which is in the unit of energy/mole (refer to Table 2.1). However, the Lewis acid character, indicated by the acceptor number, has at least two versions of scaling: *AN* which is unitless or dimensionless (Mayer *et al.* 1975), and *AN** (Riddle and Fowkes 1990) which is in energy/mole. These acceptor and donor numbers are normally used in IGC experiments to calculate K_A and K_B values for solid samples of interest (Saint Flour and Papirer 1982):

$$-\Delta H_A^{sp} = K_A DN + K_B AN, \tag{2.3}$$

where ΔH_A^{sp} is the specific (or acid-base) enthalpies of adsorption of polar probes on the samples. Referring to Equation 2.3, the specific enthalpy (ΔH_A^{sp}) is in the unit of energy/mole and therefore, the calculated K_A value should be unitless since *DN* is also in energy/mole. Similarly, the K_B value would be unitless when *AN** (in energy/mole)

Table 2.1 Some properties of the probes used in IGC experiments.

Probe	Polarizability index (10^{49} $C^{3/2}m^2V^{-1/2}$)	*DN* (kcal/ mol)	*AN*	*AN** (kcal/ mol)	Specific characteristic
n-hexane	9.2	–	–	–	Non-polar
n-heptane	10.3	–	–	–	Non-polar
n-octane	11.4	–	–	–	Non-polar
n-nonane	12.5	–	–	–	Non-polar
Chloroform	7.8	–	23.1 [a]	4.8 [a]	Acidic
Acetone	5.8	17.0	12.5	2.5	Amphoteric
Ethyl acetate	7.9	17.1	9.3	1.5	Amphoteric
Diethyl ether	7.3	19.2	3.9	1.4	Basic
Tetrahydrofuran	6.8	20.0	8.0	0.5	Basic
Ethylbenzene	10.5 [c]				Weak-polar [b]

Note: Polarizability index from Donnet *et al.* (1991), *DN* from Gutmann (1968), *AN* from Mayer (1979), and *AN** from Riddle and Fowkes (1990).

[a] The *AN* value for chloroform is in accordance with the original work of Mayer *et al.* (1975) as opposed to the 25.1 stated in many references citing the parameter. The *AN** for chloroform was calculated, using 23.1 as *AN*, based on the formulae established by Riddle and Fowkes (1990).

[b] Weak-polar (Donnet *et al.* 1991)

[c] Polarizability index for ethylbenzene was calculated from Equation A4.

is used. When, however, the unitless *AN* is used in Equation 2.3, the calculated K_B value would be in the unit of energy/mole. To facilitate further discussion, we assign calculations using *AN** as Approach 1, and that using *AN* as Approach 2. Table 2.2 shows that the acid-base interaction parameters differ in units depending on the approach used. Approach 1 was used by Felix *et al.* (1994) for determination of P_{AD} (Equation 2.1), while Approach 2 was employed by Park and Donnet (1998) for calculation of I_{a-b} (Equation 2.2). Although Park and Donnet (1998) assigned an arbitrary unit to the calculated I_{a-b}, their choice of calculation approach resulted in a value with energy/mol as the unit (see Table 2.2). When the calculated interaction parameter (I_{a-b}), bears a unit of energy/mole, it was termed, in the research of Pisanova and Mäder (2000), the enthalpy of the acid-base interaction between a fiber and a matrix (ΔH^{AB}).

Table 2.2 Units of quantity involved in the calculations of K_A and K_B (Equation 2.3), and acid-base interaction parameters (Equations 2.1 and 2.2).

Approach	Acceptor number	K_A	K_B	P_{AD}	I_{a-b}
1	Energy/mol (*AN**)	Unitless	Unitless	Unitless	Unitless
2	Unitless (*AN*)	Unitless	Energy/mol	$(\text{Energy/mol})^{1/2}$	Energy/mol

The objective of this research was to examine, using the IGC technique, interactions between cellulose fibers and polystyrene in the perspective of bonding. This research employed interaction parameters to quantify the fiber/matrix interaction using K_A and K_B values, with attention given to the specificity of units reviewed in the previous paragraph. As such, this research differs from previous studies in that it brought together the interaction-parameter calculation approaches proposed in separate publications, to make an evaluation of the calculated parameters. This special feature was presented by explicitly showing all IGC data that are relevant to the calculations, and such an approach compelled the omission of experimental replication which is usually important in research. In addition to the above-mentioned contribution, the present research also attempted to assess cellulose/polymer interaction from the adsorption of the polymer building blocks onto the cellulose fibers. To achieve this purpose, ethylbenzene was used as the model probe for polystyrene (see Figure 2.1).

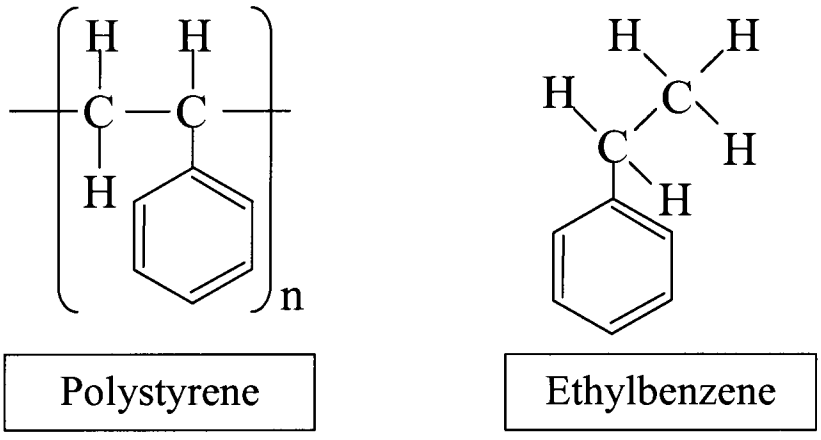

Figure 2.1 Ethylbenzene as the model repeating unit for polystyrene.

2.4. Materials and Methods

2.4.1. Materials and Sample Preparations

Lyocell fibers, regenerated cellulose fibers spun from wood pulp that has been dissolved in N-methylmorpholine-N-oxide, were provided by Acordis Cellulosic Fibers (Tencel^{R}). The atactic polystyrene, acquired from PolySciences Inc., was of 125,000-250,000 weight average molecular weight. The surface modifiers used were of octadecyl [-$(CH_2)_{17}CH_3$] and aminopropyl [-$(CH_2)_3NH_2$] trialkoxysilanes from Aldrich Chemicals.

Lyocell fibers were cleaned by Soxhlet-extraction for 12 hours using HPLC-grade methanol, and subsequently dried in an oven at 70°C until a constant weight was achieved. These fibers became either the control samples or the substrates for chemical treatments in this study.

For surface modification with octadecyl-silane, a 95% methanol aqueous solution (5% water by volume) was first acidified to pH 5 using acetic acid. For amino-silane, the methanol solution was not acidified. In both silane treatments, a dosage of 0.005 M was used. The mixture was allowed to hydrolyze for 5 minutes. Fibers were then soaked into the silane solution for 20 minutes at a temperature of 22°C and a relative humidity between 42-46%. At the end of the treatment time, the residual chemical was rinsed off twice using HPLC-grade methanol. The rinsed fibers were

heated in an oven for 110°C for 10 minutes and subsequently dried at 70°C for 24 hours to complete the crosslinking of the polymerized silane layers. These fibers were extracted again with methanol for 12 hours to remove any silane molecules that were not chemically bonded to the fibers. The extracted fibers were finally dried at 70°C until a constant weight was achieved.

2.4.2. Inverse Gas Chromatography (IGC)

For IGC measurements, dried fibers were packed into a Teflon column having an inner diameter of 2.5 mm and a length of 90 cm. The IGC experiments were carried out using a Hewlett-Packard HP 6850 Gas Chromatograph equipped with an automatic injector. Vapors of analytical-grade alkanes and polar probes (refer to Table 2.1) were individually sampled from the headspace of the vials which contain the probe liquids. An infinite dilute solution of the probe was injected into the IGC column through the inlet port at a temperature of 220°C. The probe was carried through the IGC column by purified helium gas which flowed at a rate of 15 ml/min. The eluted probe was detected by a flame ionization detector near the outlet port which was maintained at 250°C. The resulting chromatogram was integrated using the built-in software to determine the retention time of the probe. The IGC experiments were conducted at three temperatures, i.e. 25°C, 35°C, and 45°C.

The retention time of the probe was used to calculate the net specific retention volume (Conder and Young 1979):

$$V_N = \frac{273.15}{TW} Q(t_r - t_m), \tag{2.4}$$

where V_N is the net specific retention volume per gram of sample (ml/g), T is the column temperature (K), W is the weight (g) of sample packed in the column, Q is the flow rate (ml/min) of carrier gas, t_r is the retention time (min) of the probe and t_m is the retention time (min) of an inert, reference gas (in this study, propane was used) which determined the dead volume of the column.

The net specific retention volumes for a homologous series of n-alkane probes were used to determine the free energy of adsorption of a methylene group on sample surfaces (Dorris and Gray 1980):

$$-\Delta G_{A(-CH_2-)} = \frac{RT}{1000} \ln \frac{V_{N(C_{n+1}H_{2n+4})}}{V_{N(C_nH_{n+2})}}, \tag{2.5}$$

where $[\Delta G_{A(-CH_2-)}]$ is the free energy of adsorption (in kJ/mol) of a methylene group, R is the gas constant (8.3145 J K^{-1} mol^{-1}), n is the number of carbon atoms of the alkane probes which, in this study, ranged from hexane (n = 6) to nonane (n = 9). The factor 1000 in the equation converts the energy unit from J to kJ. Equation 2.5 actually

expresses the difference in ($RT\ln V_N$) for every one increment of carbon atom of the alkane probe. Therefore, [$-\Delta G_{A(-CH_2-)}$] is normally obtained from the slope of plots ($RT\ln V_N$) versus the number of carbon atom of alkane probes.

The [$-\Delta G_{A(-CH_2-)}$] value calculated was used to determine the London dispersive component of the surface free energy of the solid samples (Dorris and Gray 1980):

$$\gamma_S^d = \frac{1}{4}\frac{\Delta G_{A(-CH_2-)}^{\ 2}}{\gamma_{(CH_2)} N^2 a^2} 10^{12}, \qquad (2.6)$$

where γ_S^d is the dispersive free energy (in mJ/m^2) of solid surfaces, [$\gamma_{(CH_2)}$] is the surface free energy of pure methylene groups (35.6 mJ/m^2; assuming a close-packed structure as in polyethylene), N is the Avogadro number (6.0221 x 10^{23} mol^{-1}), a (equals 6 x 10^{-20} m^2 or 6 $Å^2$) is the area of an adsorbed methylene group, and the factor 10^{12} is for converting [$-\Delta G_{A(-CH_2-)}$]^2 from kJ^2/mol^2 to mJ^2/mol^2.

The free energy of specific adsorption (specific interaction) was determined using the probe polarizability approach which was commended adequate for describing interactions between an isolated (gas) molecule and a solid surface (Balard *et al.* 2000). This molecular descriptor has the advantage of not providing, for adsorption of some polar probes, total free energy of adsorption that is seemingly lower than the

corresponding non-polar component. Such a problematic observation could be experienced, especially for solid surfaces of high dispersive free energy (Donnet *et al.* 1991), when using other descriptors involving either probe vapor pressure (Saint-Flour and Papirer 1983) or molecular area (Schultz *et al.* 1987). The use of the polarizability approach in this study therefore, was an attempt to avoid such a difficulty, so that the free energy of specific (acid-base) adsorption could be obtained by subtracting the non-polar component from the total free energy of adsorption.

A detailed account of the equations and data reduction procedure for the polarizability approach is provided in Appendix A. In the nutshell, the specific, or Lewis acid-base, interaction of a polar probe with the solid sample was calculated from the following equation:

$$-\Delta G_A^{sp} = \frac{RT}{1000} \ln \frac{V_N}{V_N^{ref}}, \tag{2.7}$$

where ΔG_A^{sp} is the free energy of specific adsorption (in kJ/mol), V_N is the net specific retention volumes (in ml/g) of a polar probe observed from experiment (calculated from Equation 2.4), and V_N^{ref} is the net specific retention volumes (in ml/g) predicted from the plot of $[\, RT \ln V_N \,]$ versus polarizability index (tabulated in Table 2.1) for a series of n-alkanes (see Figure 2.2).

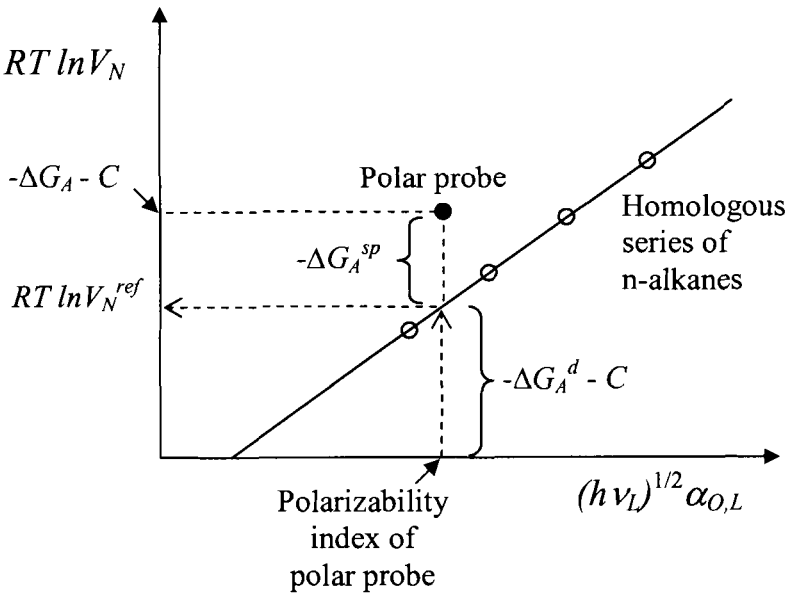

Figure 2.2 A schematic illustration of the estimation of specific interaction (ΔG_A^{sp}) between the solid sample (adsorbent) and the polar probe (adsorbate). Note: The notations are similar to those of Equations 2.7 and A7.

The specific interaction for a polar probe was plotted versus temperature. The enthalpy (ΔH_A^{sp}; in kJ/mol) and entropy (ΔS_A^{sp}; in kJ mol^{-1} K^{-1}) of adsorption of the particular polar probe with fiber samples were determined, respectively, from the intercept and the slope based on the thermodynamic function:

$$-\Delta G_A^{sp} = -\Delta H_A^{sp} + T\Delta S_A^{sp}. \tag{2.8}$$

The specific enthalpies of adsorption of a series of polar probes subsequently allowed determination of acidic and basic parameters (K_A and K_B) of the fiber surfaces using the Gutmann acceptor and donor numbers of the probes (Saint Flour and Papirer 1982) as shown in Equation 2.3. Equation 2.3 can be rewritten as a linear function so that K_A (unitless) and K_B (unitless) for Approach 1 can be obtained respectively from the slope and the intercept of the plots:

$$-\frac{\Delta H_A^{sp}}{4.184AN^*} = \frac{DN}{AN^*}K_A + K_B, \tag{2.9}$$

where the factor 4.184 converts the unit of ΔH_A^{sp} (kJ/mol) to kcal/mol to be in consistence with the unit of the denominator AN^*. When AN is used (Approach 2), the K_A (unitless) and K_B (kJ/mol) values can be obtained respectively from the slope and the intercept of the plots:

$$-\frac{\Delta H_A^{sp}}{AN} = \frac{4.184DN}{AN} K_A + K_B, \qquad (2.10)$$

where the numerator 4.184 converts the unit of *DN* (kcal/mol) to kJ/mol to be in consistence with the unit of ΔH_A^{sp} and K_B.

A similar procedure was performed for polystyrene to obtain the dispersive surface free energy, K_A and K_B values. Acid-base interaction parameters were calculated for each pair of fibers and matrix polymer using Equations 2.1 and 2.2.

The retention time of ethylbenzene on the fibers was also observed for determination of the specific interaction, and the enthalpy and entropy of the acid-base interaction. To enable determination of these parameters, the polarizability index for ethylbenzene, which was not listed in the original work of Donnet *et al.* (1991) was calculated using the equation stated in the same reference (see Appendix A for details). The fiber/ethylbenzene acid-base enthalpy was then compared or correlated to the interaction parameters.

2.5. Results and Discussion

2.5.1. The Dispersive Component of Surface Free Energy

The London dispersive characteristics of the samples are presented in Table 2.3. The Lyocell fibers have a dispersive surface free energy (γ_S^d) of 50 mJ/m^2 when linearly extrapolated to 20°C. This extrapolated value is higher than the IGC experimental result (42 mJ/m^2 at 20°C) of Katz and Gray (1981) for cellophane, a regenerated cellulosic material produced from carbon disulfide treatment of alkali cellulose. The γ_S^d value (50 mJ/m^2) in the present study, however, is closer to the data of Papirer *et al.* (2000) for microfibrous cellulose and microcrystalline cellulose — the values, according to our linear extrapolation of the data (R^2 >0.9), are respectively 47 mJ/m^2 and 56 mJ/m^2 for 20°C (Table 2.4). As such, different cellulose preparations (Luner and Sandell 1969) and different cellulose crystallinity (Papirer *et al.* 2000) affect the value of γ_S^d. Nevertheless, from the perspective of our study, it is more important to detect the relative changes of γ_S^d as a function of surface modification.

The Lyocell fibers have a dispersive surface free energy (γ_S^d) that is higher in value than the silanated fibers at all three temperature levels (Table 2.3). The same trend was observed for $[K(h\nu_S)^{1/2}\alpha_{O,S}]$, a material character which has been demonstrated by Donnet *et al.* (1991) to be positively and linearly related to the value of γ_S^d. The higher γ_S^d value in the control samples indicates that these surfaces,

Table 2.3 The London dispersive characteristics of the surfaces of Lyocell (cellulose) fibers and polystyrene at three column temperatures.

	$[K(h\nu_S)^{1/2}\alpha_{O,S}]$ (10^{49} $V^{3/2}$ $C^{-1/2}$ m^{-2} mol^{-1})			London dispersive component of surface free energy, γ_S^d (mJ/m^2)			
Sample	45°C	35°C	25°C	45°C	35°C	25°C	20°C [b]
Lyocell fiber (control)	2.53	2.60	2.73	41.7	44.3	48.6	50.0
Alkyl-silanated Lyocell fiber	2.28	2.36	2.40	33.9	36.3	37.7	38.8
Amine-silanated Lyocell fiber	2.40	2.50	2.62	37.7	40.6	44.7	46.2
Polystyrene	2.58	2.76	2.86 [a]	43.3	49.9	53.5 [a]	57.1

Note: [a] The IGC experiment was performed at 26°C instead of 25°C.

[b] The values at 20°C were obtained from linear extrapolations.

Table 2.4 The London dispersive characteristics (γ_S^d; in mJ/m^2) of cellulose samples at 20°C extrapolated from the IGC data of Papirer *et al.* (2000) on cellulose samples of different crystallinity.

Cellulose samples	Crystallinity	58°C	49°C	39°C	Extrapolated to 20°C
Microgranular	Low	41.0	43.0	43.2	45.7
Microfibrous	Medium	41.6	43.6	44.3	47.2
Microcrystalline	High	48.1	50.0	52.3	56.5

compared to silanated surfaces, are more inclined to participate in dispersive interactions with any molecule that is brought into contact with them. The alkyl-silanated cellulose exhibited the lowest γ_S^d (39 mJ/m^2) in this study, suggesting the influence of the low-energy alkyl chains deposited. Amine-silane deposition, on the other hand, resulted in a reduction of only 4 mJ/m^2 in the London dispersive surface free energy.

The polystyrene investigated in this study exhibited a higher dispersive surface free energy than cellulose (Table 2.3). The γ_S^d, when linearly extrapolated to 20°C, was found to be 57 mJ/m^2 compared to 50 mJ/m^2 for cellulose. The relativity in γ_S^d values is supported by the results of contact-angle experiments although this technique, probing a larger volume (coverage) of sample surfaces, tends to provide a lower γ_S^d value (Fafard *et al.* 1994). Indeed, polystyrene was reported to have a higher γ_S^d value

(34.8 mJ/m^2) than cellulose (25.5 mJ/m^2) in the contact-angle study of Felix *et al.* (1993). Further supporting the high dispersive free energy of polystyrene surface is the IGC finding of Kontominas *et al.* (1994) who reported 60.8 mJ/m^2 at 30°C. These researchers attributed the high γ_S^d value to the aromatic structure of polystyrene. Such a structure causes an increase in interaction through dispersive London forces.

2.5.2. The Acid-base Characteristics

The specific interactions of polar probes with cellulose fibers or polystyrene are listed in Table 2.5. The alkyl-silanated fibers have the lowest free energy of specific adsorption with all the polar probes, hence indicating a relatively unreactive surface. Notably is the amine-silanated fibers which exhibit $-\Delta G_A^{sp}$ values that are higher for the acidic probe (chloroform) and lower for the basic probe (tetrahydrofuran) when compared to the control sample. This observation implies the basic characteristic of the amine-silanated fibers. Polystyrene has higher values of $-\Delta G_A^{sp}$ compared to all the fiber samples but these values are only slightly affected by temperature, hence exhibiting lower entropy of specific adsorption. The relatively low $-\Delta S_A^{sp}$ value suggests a lower degree of randomness and hence a more energetically homogeneous surface (Kamdem and Riedl 1991) of polystyrene in terms of acid-base interaction sites.

From the K_A and K_B values listed in Table 2.6, cellulose fibers have both acidic and basic sites primarily corresponding to their hydroxyl groups. These hydroxyl groups contain proton-donating hydrogen atoms and lone-paired oxygen atoms

Table 2.5 The free energies, enthalpies, and entropies of specific adsorption.

	$-\Delta G_A^{sp}$ (kJ/mol)			$-\Delta H_A^{sp}$	$-\Delta S_A^{sp}$
	45°C	35°C	25°C	(kJ/mol)	(J mol^{-1} K^{-1})
Lyocell fiber (control)					
Chloroform	5.33	5.60	5.89	14.4	28.4
Acetone	12.4	12.6	13.3	26.7	45.0
Ethyl acetate	8.94	9.43	10.1	27.2	57.5
Tetrahydrofuran	10.8	11.3	12.0	30.7	62.8
Alkyl-silanated Lyocell fiber					
Chloroform	4.61	5.05	5.25	14.7	31.6
Acetone	11.6	12.1	12.5	24.8	41.5
Ethyl acetate	7.44	7.95	8.44	23.3	49.8
Tetrahydrofuran	10.1	10.7	11.2	28.2	56.9
Amine-silanated Lyocell fiber					
Chloroform	5.83	6.18	6.63	18.5	39.8
Acetone	11.7	11.9	12.7	26.5	46.8
Ethyl acetate	7.88	8.35	8.95	24.8	53.2
Tetrahydrofuran	9.98	10.4	11.1	27.8	56.0
Polystyrene					
Chloroform	7.86	7.91	7.96	9.52	5.23
Acetone	16.4	16.9	17.0	27.1	33.6
Diethyl ether	5.29	6.27	6.51	26.0	64.7

Table 2.6 Acid-base characteristics of Lyocell (cellulose) fibers and polystyrene.

Sample	Approach 1		Approach 2	
	K_A	K_B	K_A	K_B (kJ/mol)
Lyocell fiber (control sample)	0.36	0.37	0.31	0.55
Alkyl-silanated Lyocell fiber	0.33	0.30	0.27	0.56
Amine-silanated Lyocell fiber	0.32	0.54	0.25	0.76
Polystyrene	0.29	0.48	0.30	0.43

Note: Approach 1 uses *AN** (Equation 2.9) while Approach 2 uses *AN* (Equation 2.10).

capable of acting as a Lewis acid and a Lewis base, respectively. However, this research did not attempt to compare K_A and K_B values of the same material considering that these parameters actually differ in scale. By comparing K_A or K_B values of different materials, fibers treated with amino silane were found to be more basic than cellulose fibers hence in agreement with the alkaline nature of the amine terminal group introduced. Silane treatments were found to reduce the surface acidity of cellulose fibers. This effect is probably a result of the reduction of surface hydroxyl group when Si-O bonds are formed on cellulose surfaces upon silane deposition. For surface basicity, data from Approach 1 (using *AN**) provide a satisfactory description of the solid surfaces in relation to the cellulose (control) fibers — a lower K_B value for the unreactive alkyl-silanated fibers, and a higher K_B value for polystyrene which has a high electron density (hence a high electron-donating capacity) in its aromatic structure. While recognizing that the *AN* values used in Approach 2 suffer the inclusion of the

London dispersive or non-specific interaction effect (Riddle and Fowkes 1990), the present study does not intend to compare the two approaches; it merely calculates the K_A and K_B values necessary for the evaluation of P_{AD} and I_{a-b}.

2.5.3. Cellulose/Polystyrene Acid-base Interactions

The surface acid-base parameters of the fiber and polymer were used to predict component interactions in the intended cellulose-fiber/polystyrene composites. Two types of interaction parameters, P_{AD} and I_{a-b}, were calculated and their values are presented in Table 2.7. Both the I_{a-b} and P_{AD} parameters exhibited the highest values for the amine-silanated cellulose fibers, hence suggesting that the fibers would have the strongest interaction with polystyrene when compared to other fibers in the present study. On the other hand, the fiber/polystyrene interaction is expected to be lowered with alkyl-silanation, as indicated from the reduced acid-base interaction parameters for the fibers compared to the untreated fibers.

The cellulose/polystyrene interaction was empirically evaluated by observing the specific adsorption of ethylbenzene as the model molecule for polystyrene. Based on the free energy and enthalpy, the specific adsorption of ethylbenzene increased when cellulose fibers were treated with amine-silane (Table 2.8). The interaction expected of the basic aromatic ring in ethylbenzene would be with an acidic groups from fibers. However, amine-silanated cellulose fibers are lower in acidic character (K_A) when compared to the untreated fibers (see Table 2.6). Therefore, the increase in acid-base

Table 2.7 Acid-base interaction parameters of polystyrene with Lyocell (cellulose) fibers of different surfaces.

	P_{AD}	I_{a-b} (kJ/mol)
Calculation approach [a]	1	2
Lyocell fiber (control sample)	0.74	0.28
Alkyl-silanated Lyocell fiber	0.69	0.24
Amine-silanated Lyocell fiber	0.79	0.31

Note: [a] Approach 1 uses AN^* while Approach 2 uses AN to determine K_A and K_B values which are needed for the calculation of the interaction parameters.

Table 2.8 The free energy of specific adsorption of ethylbenzene on Lyocell (cellulose) fibers and the corresponding enthalpy and entropy.

	$-\Delta G_A^{sp}$ (kJ/mol)			$-\Delta H_A^{sp}$	$-\Delta S_A^{sp}$
	45°C	35°C	25°C	(kJ/mol)	(J mol^{-1}K^{-1})
Lyocell fiber (control)	3.46	3.58	3.74	7.88	13.9
Alkyl-silanated Lyocell fiber	3.60	3.73	3.82	7.16	11.2
Amine-silanated Lyocell fiber	3.80	3.88	4.11	8.67	15.4

interaction upon amine-silanation is most likely contributed by the higher basicity of the introduced amine. A possible interaction would be between the highly basic N atoms and the acidic hydrogen atoms from the ethyl CH groups of ethylbenzene. Indeed, the hydrogen bonds formed by C-H/N interactions have received increasing attention in a variety of organic and organometallic systems (Desiraju and Steiner 1999).

The alkyl-silanated fibers, with acidic (K_A) and basic (K_B) parameters (see Table 2.6) lower than the untreated fibers, have a lower enthalpy of specific interaction with ethylbenzene as expected. Despite having a lower $-\Delta H_A^{sp}$ with ethylbenzene, the alkyl-silanated fibers have $-\Delta G_A^{sp}$ values that are higher than the untreated fibers at the temperature tested in this study (Table 2.8). This phenomenon is a consequence of low entropy where specific adsorptions are less dependent on temperature compared to the untreated fibers (Figure 2.3). The relatively low entropy of specific interaction with ethylbenzene suggests that the acid-base interaction sites in alkyl-silanated fiber are more energetically homogeneous than the untreated fibers (and amine-silanated fibers). This argument is supported by the fact that long-chain silanes, like the 18-carbon chain used in this study, tend to coat the substrates more uniformly for self-assembled monolayer deposition (Cave and Kinloch 1992). The acid-base interaction with ethylbenzene is most likely an SiO-H/π interactions where the Lewis acidic hydrogen atoms of the silanol groups interact with the π-electrons of the aromatic ring in ethylbenzene. The presence of uncondensed silanol groups after silane deposition is well known (Matuana *et al.* 1999), and this phenomenon was evidenced in the present study from the considerably high K_A values (0.32) of the fibers even though treated with the non-polar alkane groups.

The cellulose/polystyrene acid-base interactions inferred from interaction parameters are closely correlated to that evaluated from the specific adsorption of

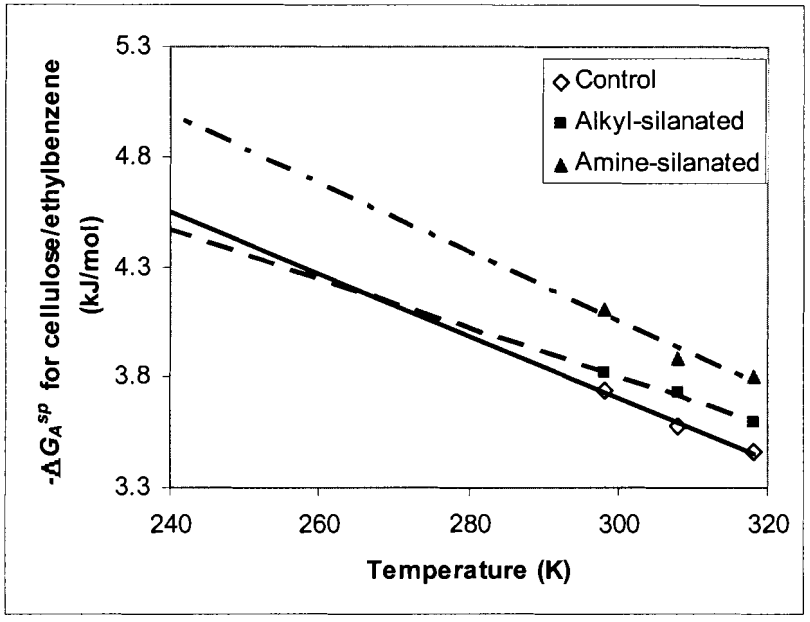

Figure 2.3 Temperature dependence of $-\Delta G_A^{sp}$ for interaction between ethylbenzene and surfaces of different fiber samples.

ethylbenzene (Figure 2.4). If I_{a-b} can be regarded as the acid-base enthalpy of fiber/matrix interaction, then this enthalpy value ($-\Delta H^{AB}$) is consistently 30 times (i.e. 1/slope or 1/0.03) lower than the enthalpy of specific adsorption for cellulose/ethylbenzene ($-\Delta H_A^{sp}$). This observation is reasonable as the calculated parameters (I_{a-b} or $-\Delta H^{AB}$) refer to solid-solid interaction while the empirically-determined $-\Delta H_A^{sp}$ refers to the interaction between a solid and a vapor which has a higher mobility. Without being pre-occupied with absolute values, the close correlation depicted in Figure 2.4 suggests that either P_{AD} or I_{a-b} can be used to predict the cellulose/polystyrene acid-base interaction. This feature favorably indicates that the

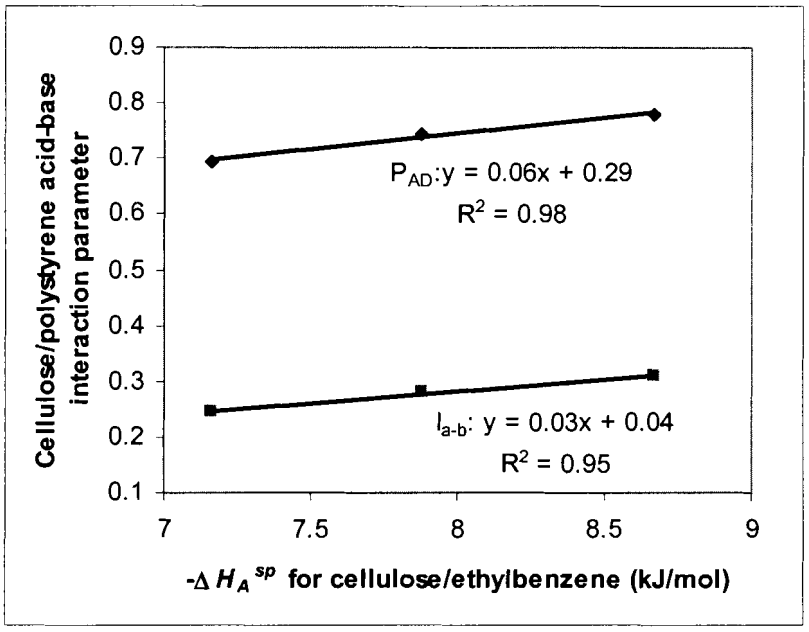

Figure 2.4 The relationship between the calculated interaction parameters (for cellulose/polystyrene system) and the observed $-\Delta H_A^{sp}$ (for celluolose/ ethylbenzene system).

acid-base interactions, which play an important role in the adhesion between fibers and a non-polyolefin matrix, can be conveniently predicted from the respective acid-base parameters (K_A and K_B) of the materials.

2.6. Conclusions

The surface chemistry of polystyrene, untreated, alkyl- and amine-silanated cellulose (Lyocell) fibers was studied using IGC. The free energy and enthalpy of specific adsorption of ethylbenzene suggest that treatment with amine-silane is likely to improve interaction and hence bonding with polystyrene in a composite system. From

the acid-base enthalpy of ethylbenzene adsorption, treatment with alkyl-silane is likely to result in a weak interaction with polystyrene. The same predictions can be made from the acid-base interaction parameter calculated from the K_A or K_B values of both the fibers and the polymer matrix. These predictions will be verified in future studies which will correlate the quantified material interaction with interfacial micromechanics in cellulose-fiber polymer composites.

2.7. References

Balard, H., E. Brendle, and E. Papirer. 2000. Determination of the acid-base properties of solid surfaces using inverse gas chromatography: advantages and limitations. Pages 299-316 in K. L. Mital, ed. Acid-base interactions: Relevance to adhesion science and technology. Vol. 2. VSP, Zeist, The Netherlands.

Berg, J. C. 1993. The importance of acid-base interactions in wetting, coating, adhesion, and related phenomena. Nordic Pulp and Paper Research Journal. 1:75-85.

Beshay, A. and S. V. Hoa. 1992. Improved interface bonding between cellulosic fibers and thermoplastics. Science and Engineering of Composite Materials. 2(2):85-97.

Cave, N. G. and A. J. Kinloch. 1992. Self-assembling monolayer silane films as adhesion promoters. Polymer. 33(6):1162-1170.

Conder, J. R. and C. L. Young. 1979. Physicochemical measurements by gas chromatography. Wiley-Interscience, New York. 632 pp.

Coupas, A. –C., H. Gauthier, and R. Gauthier. 1998. Inverse gas chromatography as a tool to characterize ligno-cellulosic fibers modified for composite applications. Polymer Composites. 19(3):280-286.

Desiraju, G. R. and T. Steiner. 1999. The weak hydrogen bond in structural chemistry and biology. Oxford University Press, Oxford. 508 pp.

Donnet, J. B., S. J. Park, and H. Balard. 1991. Evaluation of specific interactions of solid surfaces by inverse gas chromatography. Chromatographia. 31(9/10):434-440.

Dorris, G. M. and D. G. Gray. 1980. Adsorption of n-alkanes at zero surface coverage on cellulose paper and wood fibers. Journal of Colloids and Interface Science. 77(2):353-362.

Fafard, M., M. El-Kindi, H. P. Schreiber, G. Dipaola-Baranyi, and A. M. Hor. 1994. Estimating surface energy variations of solid by inverse gas chromatography. Journal of Adhesion Science and Technology. 8(12):1383-1394.

Felix, J. M., P. Gatenholm, and H. P. Schreiber. 1993. Control interactions in cellulose-polymer composites: I. Effect on mechanical properties. Polymer Composites. 14(6):449-457.

Felix, J. M., P. Gatenholm, and H. P. Schreiber. 1994. Plasma modification of cellulose fibers: effects on some polymer composite properties. Journal of Applied Polymer Science. 51:285-295.

Gutmann, V. and E. Wychera. 1966. Coordination reactions in non aqueous solutions – The role of the donor strength. Inorganic and Nuclear Chemistry Letters. 2:257-260.

Gutmann, V. 1968. Coordination chemistry in non-aqueous solutions. Springer-Verlag, New York. 174 pp.

Kamdem, D. P. and B. Riedl. 1991. IGC characterization of PMMA grafted onto CTMP fiber. Journal of Wood Chemistry and Technology. 11(1):57-91.

Katz, S. and D. G. Gray. 1981. The adsorption of hydrocarbons on cellophane. I. Zero coverage limit. Journal of Colloid and Interface Science. 82:318-325.

Kontominas, M. G., R. Gavara, and J. R. Giacin. 1994. The adsorption of hydrocarbons on polystyrene by inverse gas chromatography: infinite dilution concentration region. European Polymer Journal. 30(2):265-269.

Liang, B., L. Mott, S. M. Shaler, and G. T. Caneba. 1994. Properties of transfer-molded wood-fiber/polystyrene composites. Wood and Fiber Science. 26(3):382-389.

Luner, P. and M. Sandell. 1969. The wetting of cellulose and wood hemicellulose. Journal of Polymer Science: Part C. 28:115-142.

Matuana, L. M., J. J. Balatinecz, C. B. Park, and R. N. S. Sodhi. 1999. X-ray photoelectron spectroscopy study of silane-treated newsprint-fibers. Wood Science and Technology. 33:259-270.

Mayer, U., V. Gutmann, and W. Gerger. 1975. The acceptor number – a qualitative empirical parameter for the electrophilic properties of solvents. Monatshefte für Chemie. 106:1235-1257.

Mayer, U. 1979. A semiempirical model for the description of solvent effects on chemical reactions. Pure and Applied Chemistry. 51:1697-1712.

Papirer, E., E. Brendle, H. Balard, and C. Vergelati. 2000. Inverse gas chromatography investigation of the surface properties of cellulose. Journal of Adhesion Science and Technology. 14(3):321-337.

Park, S. J. and J. B. Donnet. 1998. Anodic surface treatment on carbon fibers: Determination of acid-base interaction parameter between two unidentical solid surfaces in a composite system. Journal of Colloid and Interface Science. 206:29-32.

Pisanova, E. and E. Mäder. 2000. Acid-base interactions and covalent bonding at a fiber-matrix interface: contribution to the work of adhesion and measured adhesion strength. Journal of Adhesion Science and Technology. 14(3):415-436.

Riddle, F. L. Jr. and F. M. Fowkes. 1990. Spectra shifts in acid-base chemistry. 1. van der Waals contributions to acceptor numbers. Journal of the American Chemical Society. 112(9):3259-3264.

Saint Flour, C. and E. Papirer. 1982. Gas-solid chromatography: a method of measuring surface free energy characteristics of short glass fibers. 2. Through retention volumes measured near zero surface coverage. Industrial & Engineering Chemistry: Product Research and Development. 21(4):666-669.

Saint Flour, C. and E. Papirer. 1983. Gas-solid chromatography: A quick method of estimating surface free energy variations induced by the treatment of short glass fibers. Journal of Colloid and Interface Science. 91:69-75.

Schultz, J., L. Lavielle, and C. Martin. 1987. The role of the interface in carbon-fiber epoxy composites. Journal of Adhesion. 23(1):45-60.

3. DETERMINATION OF STRAIN DISTRIBUTIONS AT THE CELLULOSE-FIBER/POLYMER INTERPHASE USING A RAMAN MICRO-SPECTROSCOPIC TECHNIQUE

3.1. Chapter Summary

The objective of this research was to use a Raman micro-spectroscopic technique to identify strain distributions along cellulose fibers at the fiber/polymer interface. A single fiber, with an attached microdroplet of polystyrene, was strained in tension. Raman spectra were collected at five-micrometer intervals along the fiber axis at the fiber/polymer interface. The Raman band for cellulose at 895 cm^{-1} has been found to shift in frequency with applied strain, and therefore the strain-band frequency relationship can be used to map the local tensile strain at the interface region. Results showed that the local tensile strain of the fiber at the interface region was highest at the edge of the droplet, and declined from the edge region to the middle region of the drop. With progressive stretching of the fiber, the strain values at the middle region of the drop also increased, presumably when a strain concentrator such as local flaws were present in the polymer or interphase. The maximum value of these local strains corresponds to the location of a strain-control fracture of the matrix polymer. These findings show that the Raman technique provides a non-invasive approach to determine strain distributions at the fiber/polymer interphase. This technique should be applicable to studying composites involving lignocellulosic fibers which also contain cellulose.

3.2. Introduction

Wood fibers have great potential to be utilized for filling or reinforcing synthetic composites. Compared to the conventional fillers (such as glass fibers) for polymer composites, wood fibers have many features that are more favorable -- they are cheaper, lighter, and less abrasive to the processing equipments. Wood fibers have added advantages over synthetic fibers in that they are renewable and recyclable, hence responding more positively to increasing environmental concerns.

The use of wood fibers in polymer composites, though constrained by the poor interaction between the polar wood materials and the non-polar or slightly polar thermoplastics, can be remedied using surface modification treatments. Two examples of such treatments are coupling with silane (Maldas *et al.* 1988) and grafting with maleic anhydride (Gauthier *et al.* 1998). The formulations and procedures of surface treatments can be optimized if the fiber/polymer interface region can be adequately understood. Such knowledge will provide an opportunity to tailor fiber surfaces to achieve the adhesion-related properties of the composite, and eventually lead to a more efficient use of wood resources.

3.3. Literature Review

An interface in a fiber/polymer composite is originally defined as the region of contact between the fiber and matrix. This concept has been expanded to the three-dimensional interphase, which includes the two-dimensional fiber/matrix interface and

the region of some finite thickness extending on both sides of the interface (Drzal 1990). The interface region (or interphase) is thought to have properties that are neither those of the fibers nor matrix.

An important method used in evaluating fiber/matrix interfacial properties involves micromechanical studies of single-fiber composites. These micro-composite tests characterize interface qualities whose information can otherwise be perturbed by fiber volumetric and orientation effects in bulk mechanical tests (Fan *et al.* 1991). Micromechanical tests characterize the integrity of a fiber/polymer interphase by inferring the ability of load transfer between fibers and matrix polymers – a better load transfer means a stronger interphase. For example, in the micro-debond test, the load required to shear a polymer droplet off from a fiber is measured (Gaur and Miller 1989). A larger load value measured in the micro-debond test means that more load can be transferred from the polymer to the fiber. In the fiber fragmentation test, a dogbone-shape polymer containing an embedded single fiber is subjected to a tensile load (Herrera-Franco and Drzal 1992). In this case, a higher number of fiber-breaks indicates a better load transfer ability between the polymer and the embedded fiber.

The load transfer ability inferred by most micro-composite tests may not accurately reflect the fiber/polymer interfacial properties. In the micro-debond test, for example, the maximum load to shear-off the droplet is averaged over the area of contact between the fiber and the matrix (Gaur and Miller 1989). The distribution of stress (or strain) in an interface, however, is not uniform due to stress (strain) concentrations.

Because failures occur at locations of maximum stress or strain, depending upon the controlling failure criteria, the average state of the interphase may not accurately characterize the integrity of the interphase. The consequence of such a problem is commonly observed in the micro-debond tests – the calculated values of interfacial shear strength tend to be smaller with a larger droplet embedment (Gu and Young 1997). This problem is partially remedied by linearly extrapolating the acquired interfacial shear strength to zero embedment length. However, the information of the locations of the critical stress or strain values is still lacking.

An attempt to determine the strain distributions of wood fibers has yielded information on strain concentration and fiber failure mechanisms, which are invaluable in the understanding of wood cell walls as a natural polymer composite. Mott *et al.* (1996) strained single wood pulp fibers under the environmental scanning electron microscope (ESEM), and subsequently applied digital image correlation to compare sequential images for surface displacement, which could be converted to microstrain distributions on the fiber surfaces. They detected strain concentrations on locations of strain risers such as pit apertures and pit borders of the cell walls. They also observed blunt crack tips initializing from these cell-wall defects, allowing them to categorize the cracking mechanism as the quasi-ductile fracture. The advantage of this powerful technique, however, may not be fully utilized in fiber/polymer systems when the visibility of the fiber underlying the matrix polymer is greatly reduced.

Raman micro-spectroscopy is a novel technique to collect molecular information of fibers at the fiber/polymer interphase. When using the Raman technique for interphase studies, a laser beam is focused onto the fiber embedded in a matrix polymer. The induced dipole results in inelastic scattered light, giving rise to a unique frequency pattern (Raman spectra) that is specific to the molecular compound and local environment of the sample (Banwell 1972). When a compound is strained, the local environment in the molecules is altered thereby, giving rise to a shift in Raman frequency that depends on the extent of stretching (Tuinstra and Koenig 1970). If these Raman bands are collected at different locations of the fiber along the fiber/polymer interphase, the point-to-point variation (or spatial distribution) of strain can thus be determined for the interface region.

The Raman spectroscopic technique has been proven successful to study the interphase of a carbon-fiber/thermosetting polymer system. Gu and Young (1997) collected Raman spectra along the fiber/polymer interphase while shearing off a cured epoxy droplet from a carbon fiber. They found that the local strain of the fiber was highest at the droplet edge where it was restrained by the microvise, and the strain decreased continuously towards the other edge of the droplet.

The Raman micro-spectroscopic technique, when applied to cellulose fibers, revealed two Raman bands that shifted in frequency upon tensile loading. Eichhorn *et al.* (2001) collected Raman spectra while stretching regenerated (lyocell) cellulose fibers. They found two strain-sensitive cellulose bands: one at 895 cm^{-1} and the other

one at 1095 cm^{-1}. The 895 cm^{-1} band corresponds to the angle bending mode of the CCC, COC, and OCC atoms in the ring structure (Figure 3.1), while the 1095 cm^{-1} band corresponds to the ring and C-O stretching mode (Atalla and Dimick 1975). Eichhorn *et al.* (2001) reported that both of these bands shift to lower frequencies with a rate of 0.18 cm^{-1} for every one percent increase in tensile strain. However, this work was not extended to study polymer bonding with the cellulose fibers.

Raman spectroscopy is expected to complement numerical analyses of the wood-fiber/polymer system. Egan and Shaler (2000) performed finite element analysis of a wood-fiber/phenol-formaldehyde system with the fiber undergoing a tensile loading condition. Their finite model consisted of a half symmetric solid (resin droplet) on a fiber. They found high stress intensities near the fiber/polymer interface where the fiber entered and exited the polymer droplet. Empirically, a similar strain profile should also be discernable when applying the Raman micro-spectroscopic technique on a stretched fiber with a polymer droplet attached. Such an empirical approach has the advantage of not requiring mathematic models involving assumptions on sample geometry and boundary conditions.

The objective of this research was to identify strain distributions along the cellulose-fiber/polymer interphase. This research employed Raman micro-spectroscopy to collect spectra of the fiber along the fiber/polymer interface as a function of applied (global) strain. Raman bands that are strain-sensitive were then analyzed to deduce local strain of the fiber at the interface region.

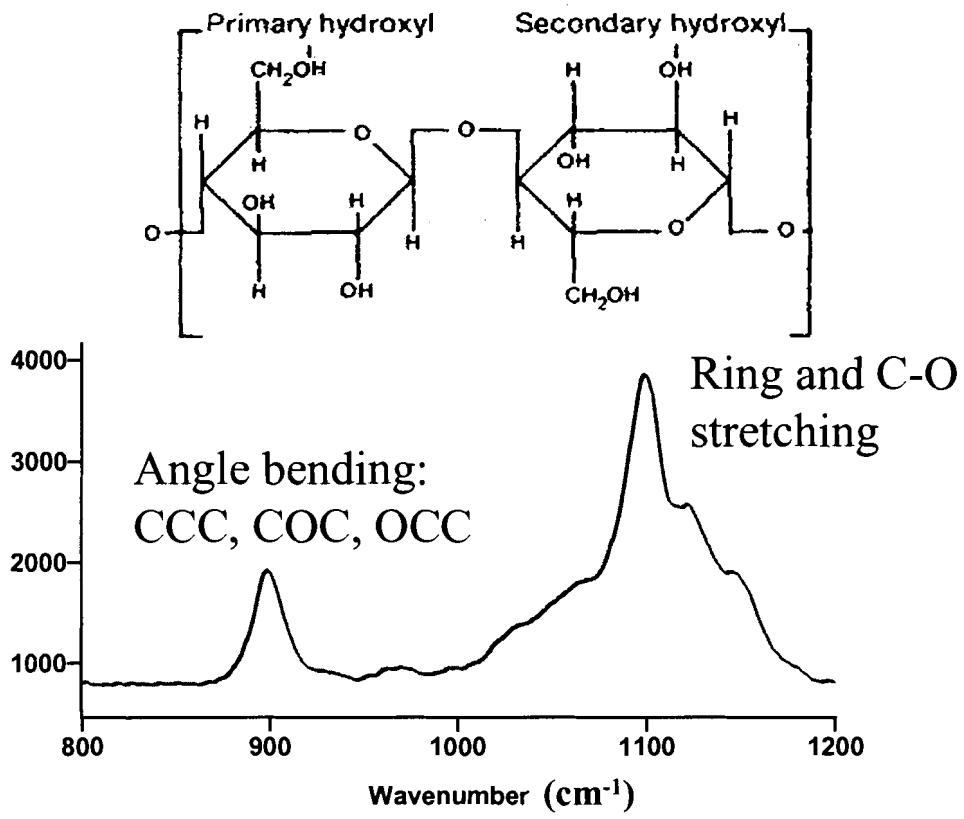

Figure 3.1 Two strain-dependent cellulose bands and the corresponding molecular vibration modes. Note: The y-axis is the intensity of the bands in arbitrary unit.

3.4. Materials and Methods

3.4.1. Testing Materials and Equipment

The fibers used in this study were regenerated cellulose fibers solvent-spun from wood pulp. These Lyocell fibers, 12 micrometers in diameter, were provided by Acordis Cellulosic Fibers (Tencel^{R}). These fibers have mechanical properties that are quite similar to mature (Black Spruce) wood fibers (Table 3.1). The atactic polystyrene, acquired from PolySciences Inc., was of 125,000-250,000 weight average molecular weight.

The Raman spectrometer (Renishaw system) used a diode laser operating at 785 nanometers (Figure 3.2). The spectrometer was equipped with a microscope which could focus the laser beam to a spot size of 2 micrometers using a 50x objective lens (0.25 numerical aperture). A microtensile apparatus was placed under the microscope to hold or stretch a single fiber, and expose the fiber to the laser beam for collection of Raman spectra. The fiber holder of the apparatus had a moving arm at one side, and a stationary arm at the other side. The moving arm was actuated by a stepper motor via a leadscrew/nut system and gearhead, providing a linear motion of 0.1 micrometer repeatability. The motion was computer-controlled to attain a desired distance and speed for stretching the fiber. The stationary arm of the fiber holder was equipped with a strain-gage load cell of $\pm$ 0.15% error (250 gram-force full scale). The stationary arm

Table 3.1 Some mechanical properties of regenerated cellulose and wood fibers

	Lyocell fibers [a]	Juvenile wood fibers [b]	Mature wood fibers [c]
Tensile modulus (GPa)	15.2	1.11	9.44
Ultimate tensile strength (GPa)	0.54	0.21	0.48
Strain at failure (%)	7	17 [d]	6 [d]

Note: [a] Data from Eichhorn *et al.* (2001); 20 replicates; 83 μm/s

[b] Data for 10-year old Black Spruce fibers (Egan and Shaler 2000); 18 replicates; 80 μm/s

[c] Data for 55-year old Black Spruce fibers (Egan and Shaler 2000); 34 replicates; 80 μm/s

[d] Data estimated from the stress-strain plots in Egan and Shaler (2000).

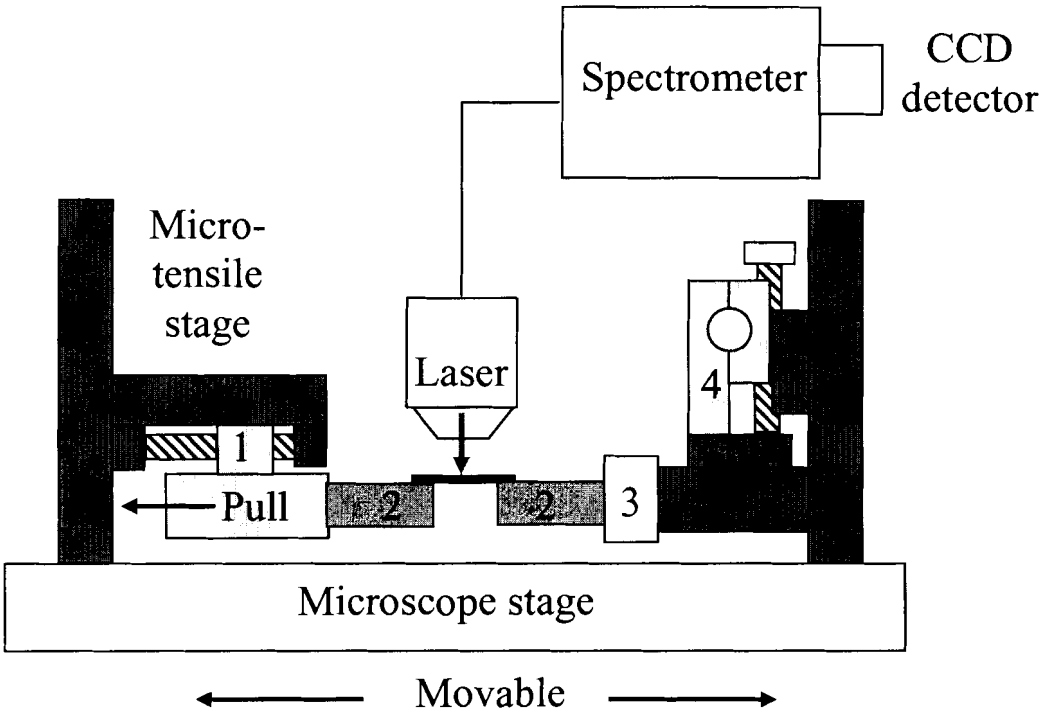

Figure 3.2 The micro-Raman tensile test apparatus. Note: 1 = moving arm; 2 = fiber mounting arm; 3 = load cell; 4 = fiber aligning XY stage.

was also connected to a mini XY stage to position the fiber both horizontally and vertically prior to stretching. The microscope stage that held the tensile apparatus was another XY stage which could be computer-programmed to position and move the tensile apparatus, and hence also the fiber, to allow spatial mapping at fixed intervals.

3.4.2. Sample Preparation

Lyocell fibers were cleaned by Soxhlet-extraction for 12 hours using HPLC-grade methanol, and subsequently dried in an oven at 70°C until a constant weight was achieved.

For depositing polymer droplets onto the fibers, polystyrene beads were dissolved in toluene to form a 20 weight-% solution. A stiff fiber optic strand was used to transfer a drop of the polymer solution to the fiber, with an embedment length of 70-90 micrometers. The solvent was then evaporated from the droplet at room temperature for 18 h. No heating was attempted so that thermal residual stresses in the fiber/polymer system could be avoided.

A single fiber was mounted onto the tensile stage with a gage length of 10 mm. The fiber was fixed at both ends, using an epoxy adhesive, onto metal surfaces just at the edge of the adjusted 10-mm gap. Although a fast-curing (five-minute) epoxy was used, the epoxy block was allowed to stand for 18 hours at room temperature to maximize curing so that fiber slippage could be minimized during tensile displacement.

As such, this study assumed no fiber slippage and the fiber strain was considered similar to the nominal strain calculated from the displacement and gage length.

3.4.3. Raman Scanning

To establish the correlation between tensile strain and frequency shift, a single fiber was subjected to a tensile displacement, and held in position to allow collection of Raman spectra. A typical Raman spectrum required 30 seconds to record. The fibers were then further stretched and Raman spectra were subsequently collected after each stretch. The resulting spectra were analyzed for frequency (position) of the 895 cm^{-1} band by curve fitting using a Laurentian:Gaussian ratio of 75:25. This band has been reported to shift with applied strain (Eichhorn *et al.* 2001). A calibration curve was then established to relate frequency shift of this band to the applied tensile strain. All the calibration tests and the subsequent Raman mapping experiments were carried out at $22\pm1^{\circ}C$ and $40\pm3\%$ relative humidity.

To perform spatial mapping of the interphase, the same procedure for stretching and spectra collection was performed on a single fiber with a polymer droplet attached. For each applied strain, Raman spectra were collected at a five-micrometer interval along the fiber axis at the fiber/polymer interface. The 895 cm^{-1} band of cellulose was analyzed for frequency which was then converted to the fiber axial strain using the correlation curves previously established.

It is noteworthy that in Raman scanning of the cellulose fibers, the laser probe depth was not determined. Consequently, the Raman information obtained from fibers underneath a polymer droplet should also include a certain depth beneath the fiber surfaces. Therefore, the spectra information obtained was not interpreted as strain on the fiber surface (interface) but rather, strain at the interface region (interphase), which, fortunately, was the entity of interest. Another important issue is that this study only considered axial strain of the fiber, and it assumed a negligible transverse (Poisson-effect induced) fiber strain.

3.5. Results and Discussion

3.5.1. Raman Scanning of Bare Fibers: Frequency Shift Resulted from Straining

Two Raman bands of cellulose, one at 895 cm^{-1} and the other at 1095 cm^{-1}, have been reported to be strain dependent (Eichhorn *et al.* 2001). The 1095 cm^{-1} band is superimposed on top of several other bands (see Figure 3.1) in the same region, while the 895 cm^{-1} band is a single peak. In our work, we used the 895 cm^{-1} band for strain calibration because it was simpler to analyze.

A typical correlation plot between tensile strain and Raman frequency for the 895 cm^{-1} band of cellulose is shown in Figure 3.3. Overall, the band exhibited a frequency reduction of 2.0 cm^{-1} for the entire 5%-straining. More specifically, the

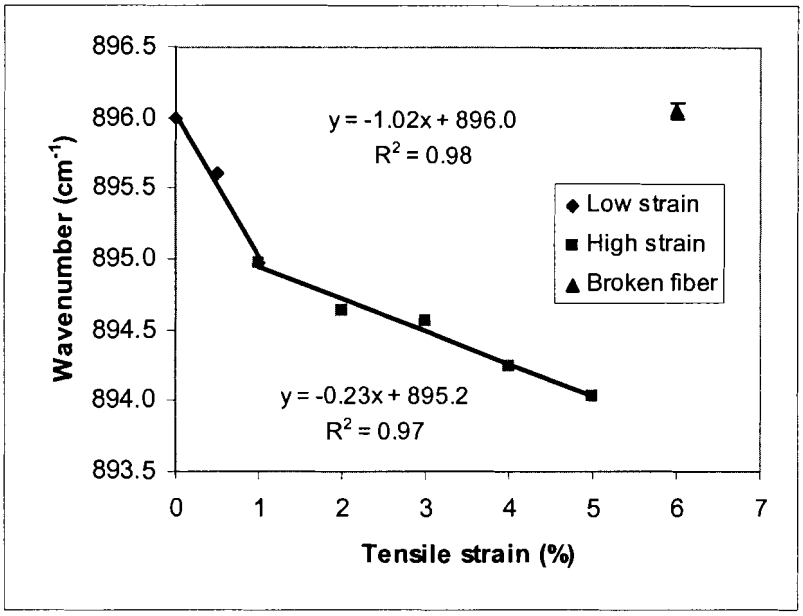

Figure 3.3 A typical plot of the relationship between Raman wavenumber and tensile strain for the 895 cm^{-1} band.

strain dependence of the Raman wavenumber can be approximated with two linear relationships – one at the low strain level (0-1%), and the other one at the high strain level (>1%). The average values of the strain dependence, obtained from six sets of calibration tests, are listed in Table 3.2. The low strain region exhibited a 1.09 ± 0.12 cm^{-1} frequency reduction for 1% strain, while the high strain region (>1%) displayed a 0.22 ± 0.04 cm^{-1} reduction for every 1% strain increment. Such a two-curve strain-dependent behavior contradicts the finding of Eicchorn *et al.* (2001) who found a common relationship of 0.18 ± 0.05 cm^{-1}/% strain, a value somewhat similar to the high strain region in the present study (0.22 cm^{-1}/%).

Table 3.2 The sensitivity and variability of frequency shift of the 895 cm^{-1} band of lyocell fibers.

Mechanical perturbation	Elapse time after perturbation	Frequency shift [a]
Tensile strain (1%)	Immediate	-1.09 ± 0.12 cm^{-1} / %
Tensile strain (> 1%)	Immediate	-0.22 ± 0.04 cm^{-1} / %
Tensile stress	Immediate	-4.42 ± 0.7 cm^{-1} / GPa
Tensile strain (1%)	After 5 minutes	-0.92 ± 0.08 cm^{-1} / %
Tensile strain (> 1%)	After 5 minutes	-0.23 ± 0.04 cm^{-1} / %

Note: [a] Six sets of calibration test were carried out for each tabulated frequency shift. The variability refers to 99% confidence interval.

To further validate our two-curvilinear relationship between the Raman frequency and applied strain, the frequency was also plotted as a function of the tensile stress resulting from fiber straining (Figure 3.4). Regardless of low or high strain level, the frequency of the 895 cm^{-1} band decreases in a single trend line with an increase in tensile stress. The average stress-dependence of the band is -0.44 cm^{-1}/0.1 GPa (Table 3.2). This result implies that the band frequency shift is a direct consequence of tensile stress which relates to strain through a curve of linear and non-linear regions (Figure 3.5). Another simple evident for showing that the frequency shift is directly related to stress was to observe the wavenumber of a broken fiber (Figure 3.3). A fiber that is strained to failure has exceeded its linear elasticity limit, and Figure 3.3 shows that the frequency returned to the value of the unstrained fiber indicating zero stress rather than zero strain.

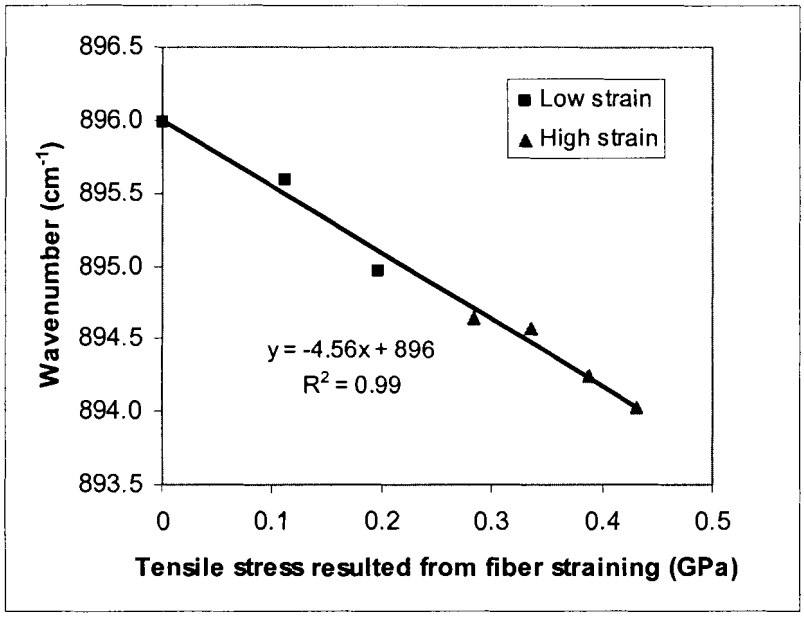

Figure 3.4 A typical plot of the relationship between Raman wavenumber and tensile stress for the 895 cm^{-1} band.

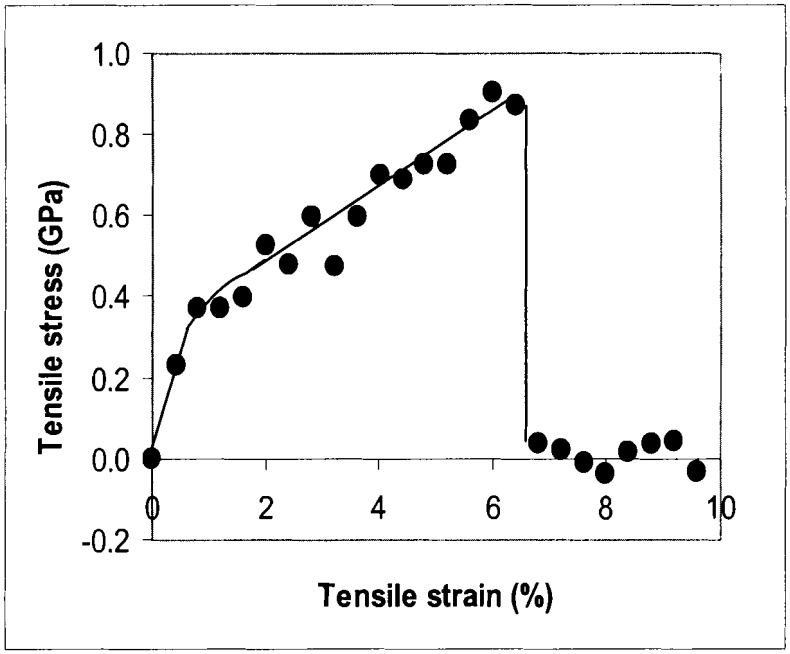

Figure 3.5 A typical stress-strain curve in tensile loading of lyocell fiber.

3.5.2. Raman Scanning of Bare Fibers: Frequency Shift Resulted from Factors Other Than Straining

The next attempt of this study was to investigate other factors that may also influence the band frequency shift. In the eventual mapping of the fiber/droplet interphase, the polymer droplet would be deposited with solvent, and the Raman mapping would involve prolonged exposure to laser, collection of spectra from one location to another during which time, the fibers would be held in position under strain. Each of these situations was simulated on bare fibers in the following sets of experiments.

To ascertain fiber degradation due to prolonged laser exposure, cellulose fibers were irradiated with the laser beam of the Raman spectroscope at maximum power for 55 minutes, and a spectrum was subsequently collected from the same spot. The frequencies of three initial spectra collected consecutively were: 895.99, 896.03, and 895.96 cm^{-1}, showing a good repeatability of the Raman readings. At the end of the laser exposure, the frequency of the band became 895.87 cm^{-1}. The effects of instrumental drift were eliminated by checking the spectra of silicon which showed a negligible shift of 0.04 cm^{-1} from the initial 520 cm^{-1}. Therefore, a general reduction of 0.12 cm^{-1} was primarily a consequence of the prolonged laser exposure. This reduction, nevertheless, was small compared to the calibrated 1.09 cm^{-1} or 0.22 cm^{-1} shift per 1% strain. Furthermore, such a deviation was the worst-case scenario because a Raman

spectrum in this study only required a sampling spot to be exposed to the laser beam for 30 seconds, while the entire spatial scanning across the polymer droplet only took about 14 minutes.

The axial variation of the fiber was examined by taking Raman spectra along the entire gauge length (10 mm) of the fiber (Figure 3.6). The strain-dependent cellulose band under the unstretched condition was lowest at both ends near the epoxy-glue fixtures, indicating edge effects. However, in the middle 4 mm of the gauge length (positions between 3 mm and 7 mm) where the polymer droplet was to be deposited, the frequency was $\pm$ 0.10 cm^{-1} around the average value of 896.01 cm^{-1}. As such, the frequency shift at the high strain region, (0.22 cm^{-1} / % strain), even though small, is clearly above the spot to spot variation across the fiber.

To ascertain whether solvent affects the strain-dependence of Raman band, fibers were soaked in toluene for 30 seconds, and subsequently evaporated in the environment similar to that for polymer droplet. A single fiber was then teased out, and subsequently stretched under the Raman spectroscope. Plots of Raman-band versus strain show that the strain dependence of the Raman frequency appears to be similar between the untreated and toluene-soaked fibers (Figure 3.7). The slight differences in the strain dependence (or the values of slopes) at the low-strain levels (–1.14 from Figure 3.7 versus -1.09 from Table 3.2) and the high strain levels (-0.25 from Figure 3.7 versus -0.22 from Table 3.2) fall within the respective variabilities of $\pm$ 0.12 cm^{-1} and $\pm$ 0.04 cm^{-1} (Table 3.2). Statistical comparisons, by examining the residual variations

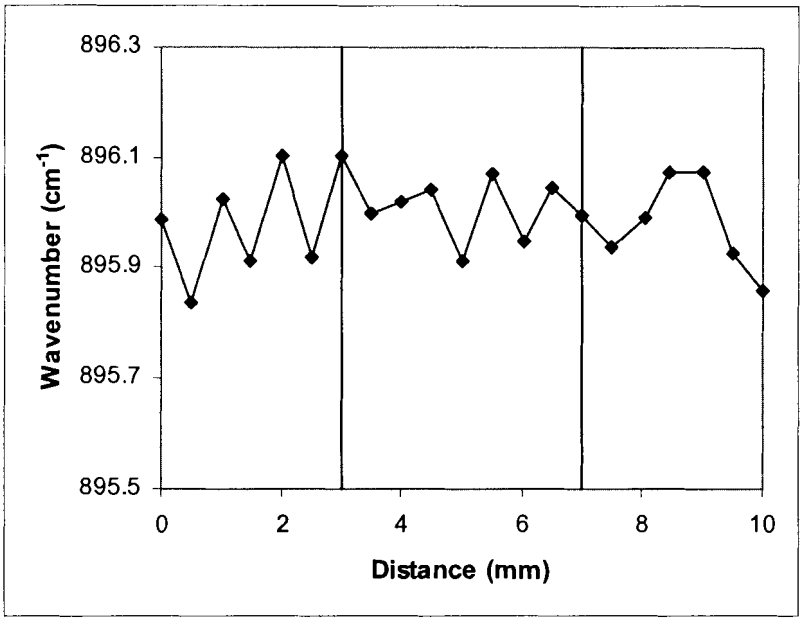

Figure 3.6 The variation in the strain-sensitive cellulose band along the axis of the fiber. Note: The variability for the 4-mm region in the middle of the span is $\pm$ 0.10 cm^{-1}.

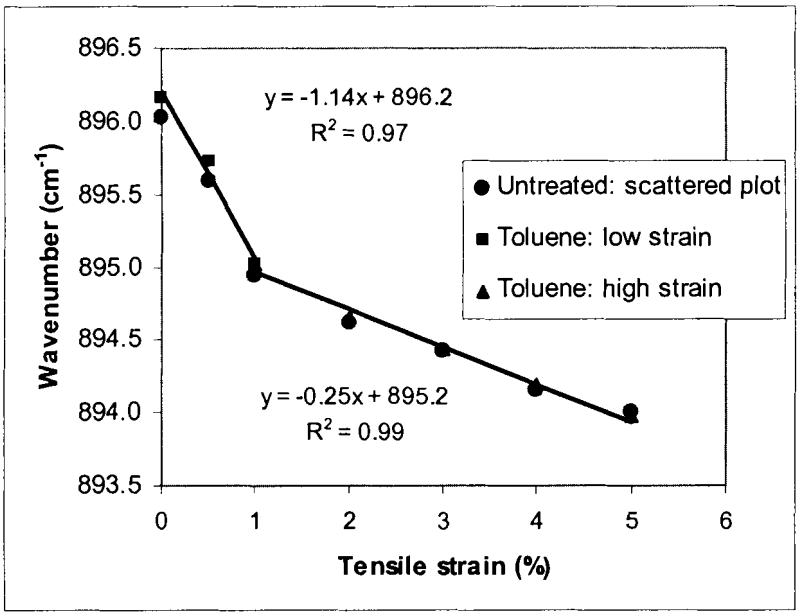

Figure 3.7 The effects of toluene on the strain-dependence of the 895 cm^{-1} band. Note: Each data point of the scattered plot is the mean for six replicates.

about individual regression fits versus a single-line fit (Mead *et al.* 1993), revealed that the slope values were not significantly different at a probability level of 0.05. Therefore, toluene, in the context of this study, does not affect the strain-dependence of the Raman band.

The time-dependent response of cellulose fibers to the applied strain was also examined. A single cellulose fiber was stretched and held in position for 20 minutes during which Raman spectra were collected from a single point at 5-minute intervals with an additional scan taken for the first minute. The fiber was then stretched to a higher stain level, and the Raman measurements were repeated. The laser beam was cut off in between scanning to avoid laser degradation. The results of this experiment are shown in Figure 3.8. The 895 cm^{-1} band exhibited an abrupt shift to lower frequencies when the fiber was stretched. Corresponding to stress relaxation (see the load data in Figure 3.8), the band frequency had an instant snap-back, and became more or less constant after about 5 minutes.

Based on the time-dependence in band frequency, Raman spectra were collected five minutes after each applied strain. This approach ensured that the point-to-point variation of the local strain in subsequent interphase mapping was not due to stress relaxation (time effect) but to strain concentration (spatial effect). For implementing this new approach, another set of frequency-strain calibrations was performed, and the Raman spectra were collected five minutes after each of the fiber straining levels.

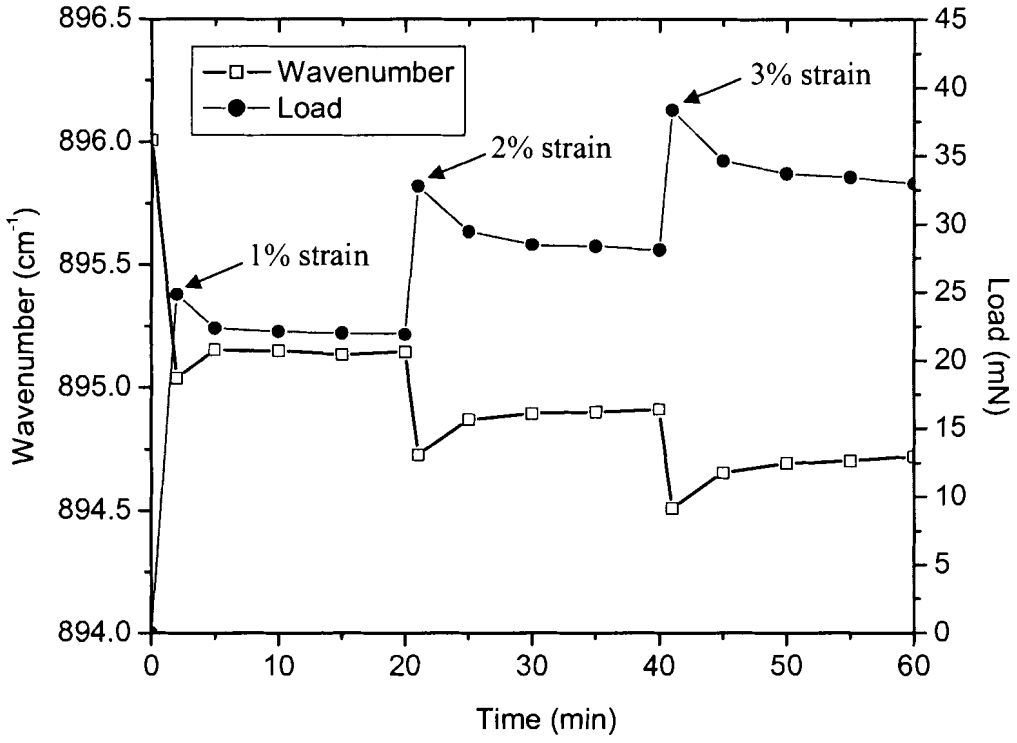

Figure 3.8 The time dependence of the 895 cm^{-1} band during fiber straining.

A typical plot for such calibrations is shown in Figure 3.9, which clearly shows that the frequencies of the 895 cm^{-1} band (collected at the same location on the fiber) at the high-strain region were approximately 0.1 cm^{-1} higher than the immediate scans because of the stress relaxation phenomenon. Results of six calibration tests revealed a frequency reduction of 0.92 cm^{-1} for every 1% strain increase at the low strain region (Table 3.2). This value is beyond the variability ($\pm$ 0.12) of the -1.09 cm^{-1}/% strain obtained for immediate scanning (Table 3.2), and a statistical comparison using t-test also revealed that the two calibration values are significantly different

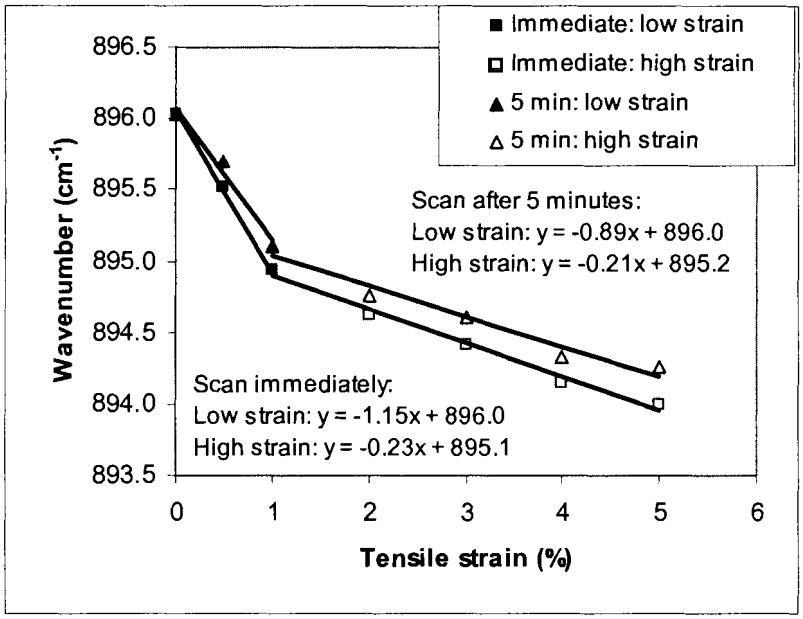

Figure 3.9 A typical frequency-strain calibration curve for spectra collected both immediately and 5 minutes after fiber straining.

($p = 0.049$ for one-tail test). For the high-strain region, the strain dependence (0.23 cm^{-1}/% strain; Table 3.2) remained unchanged compared to immediate scanning (0.22 cm^{-1}/% strain; Table 3.2).

Following the preceding observations, a procedure was set for analyzing the Raman spectra which were collected starting from minute five after the fiber straining. The frequency of the acquired 895 cm^{-1} band was first compared to the frequency value for the zero-strain condition. Any frequency shifts that were below or at 0.9 cm^{-1} were converted to strain by dividing with 0.9 cm^{-1} / %strain, while frequency shifts that were more than 0.9 cm^{-1} were divided with 0.23 cm^{-1} / % strain (Table 3.2). The established

procedures were successfully applied to obtain fiber strain distribution profiles at progressive stretching of the fiber (Figure 3.10). The determined local strain values were in close correspondence with the levels of applied strain. Noteworthy is the lower variability at the low strain levels (0% and 1% applied strain) compared to the case of high strain levels. Such a distinction originated from the greater dependence of the frequency to strain at the low strain levels (0.90 cm^{-1} / % strain) compared to the high stain levels (0.23 cm^{-1} / % strain). For elaboration, the point-to-point variability of the fiber was about $\pm$ 0.1 cm^{-1}, which translates to a variability of about $\pm$ 0.1% strain (0.1/0.90) at low strain levels but $\pm$0.5% (0.1/0.23) at high strain levels.

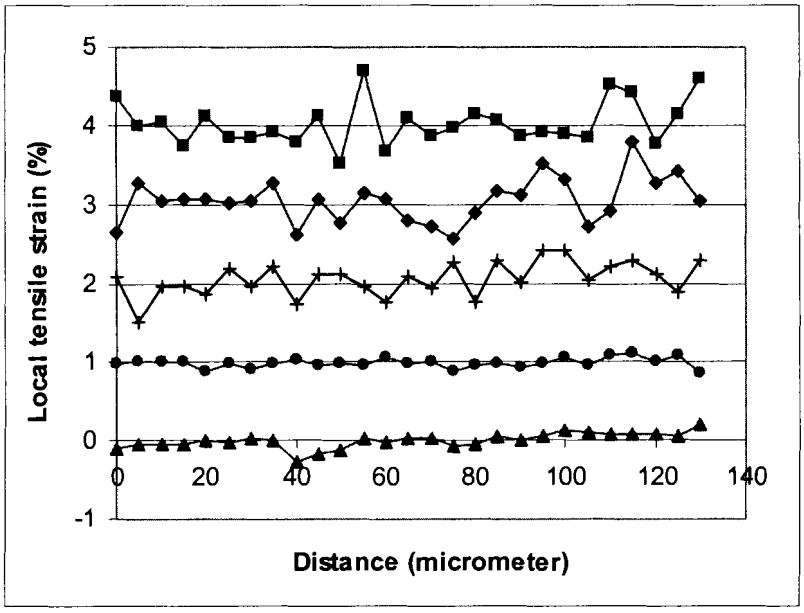

Figure 3.10 Strain distributions in a bare fiber determined from Raman mapping at increasing strain levels.

3.5.3. Spatial Mapping of the Fiber/Polymer Interphase

For spatial mapping of the fiber/polymer interphase, Raman bands were collected of cellulose fibers that were embedded in the polymer droplet. The collected spectra consisted of cellulose and polystyrene bands (Figure 3.11), and therefore these spectra were subtracted with the spectrum of solid polystyrene (without cellulose) prior to frequency analyses.

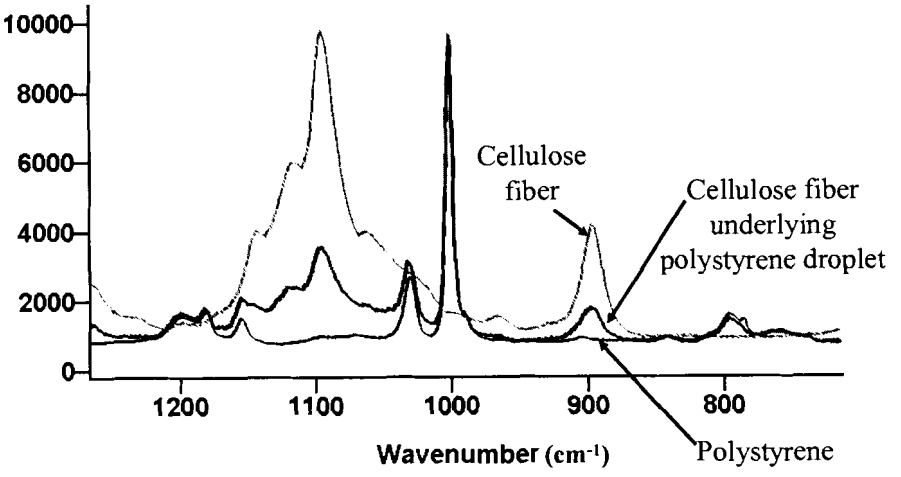

Figure 3.11 The Raman bands of cellulose-fiber/polystyrene system and the individual components.

The variation of wavenumber along the cellulose-fiber/polystyrene interphase is plotted in Figure 3.12. In the stretched condition, the wavenumber of cellulose bands in the droplet was higher than those outside the drop, and these wavenumbers

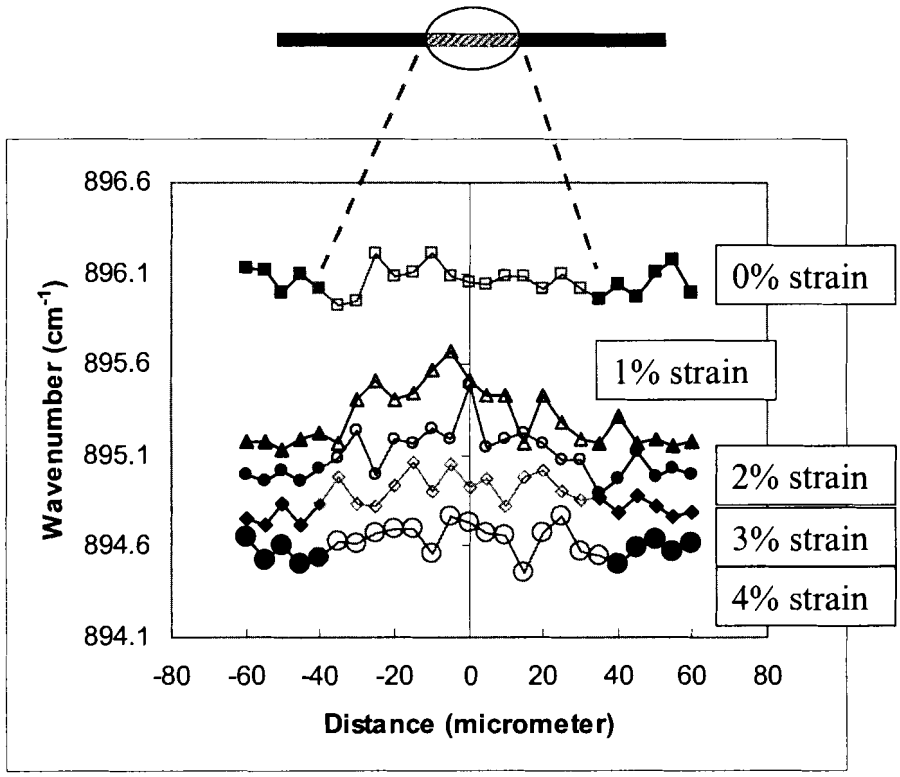

Figure 3.12 The wavenumber variation of the 895 cm^{-1} band of cellulose fibers along the fiber/polystyrene interphase.

increased from the edge of the droplet to the middle region of the drop. Such a spatial distribution pattern was not observed at 0% strain or for cellulose fibers embedded in the droplet of silicon fluid (Figure 3.13). Therefore, the observation of the fiber/polystyrene interphase in this study was not an artifact originating from the droplet curvature which could deviate the passage of light.

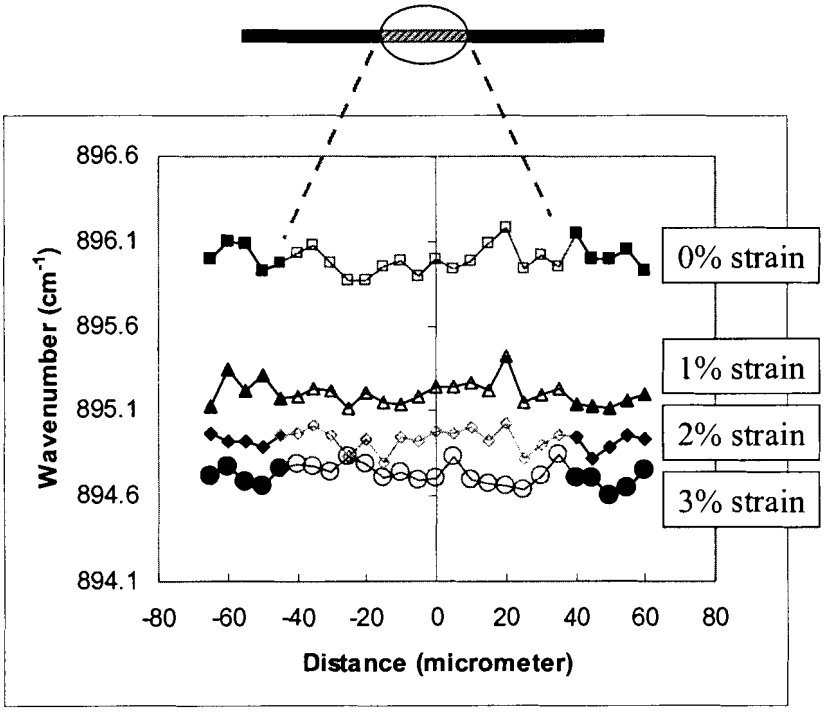

Figure 3.13 The wavenumber variation of the 895 cm^{-1} band of cellulose fibers along the fiber/silicon-fluid interphase.

The converted local strain values were plotted as a function of distance in Figure 3.14. Compared to the unstretched fiber, the stretched fiber had a more distinct local strain distribution profile at the interphase. At 1% applied stain, the fiber strain profile

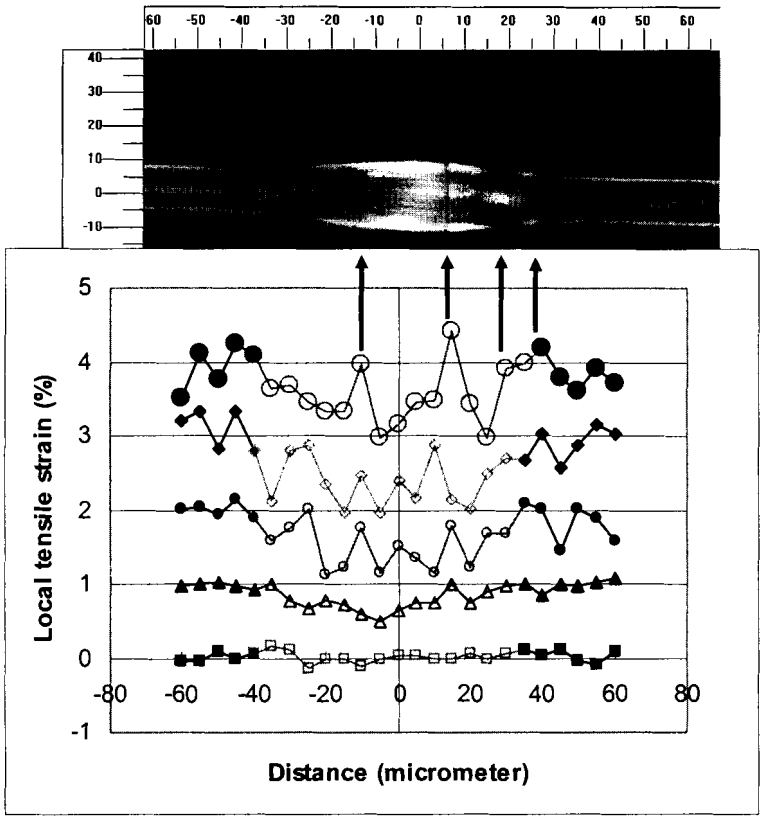

Figure 3.14 The variation of fiber local strain along the fiber/polymer interphase and the corresponding polymer fractures in the sample.

exhibited a maximum value at both edges of the droplet with the strain declining towards the mid-length region of the embedment. This observation agrees with the finite element analysis study of Egan and Shaler (2000). The low fiber strain at the droplet middle is a consequence of the thicker matrix material (polystyrene) that takes up more tensile load from the fibers, sparing them from experiencing an excessive strain. The maximum local strain at the edge of the droplet also suggests that this region is a potential fracture location for the fiber/polymer composites.

The fiber strain distribution profile shifted to a higher value when a higher global strain was applied to the fiber. The shift indicates that the fiber/polymer system underwent a more severe strain at the interface region when a higher global strain was applied onto the fiber. When the resultant local strain exceeded the ultimate strain capacity of polystyrene (2-3%), the polymer droplet fractured at its weakest regions which included the predicted droplet edge and two other locations (Figure 3.14). These two other locations of failure were possibly local flaws in the polymer or interphase. Interestingly, the strain profile at the applied strain level of 3% also showed a peak (high local strain) at each of the observed polystyrene fracture positions. Therefore, the Raman technique is able to provide information of locally induced strain failures which are not detected in numerical analyses.

Figure 3.15 shows the local strain distribution of cellulose fibers embedded in silicon fluid. Silicon fluid is an inert compound which does not interact with cellulose, and it is not load-sustaining, hence forming a fiber/droplet interphase that did not

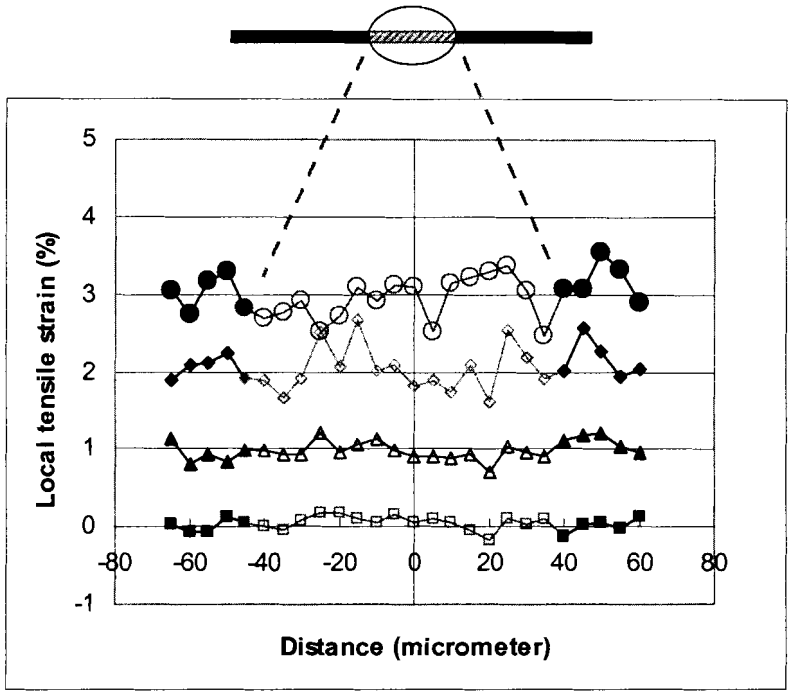

Figure 3.15 The variation of fiber local strain along the fiber/silicon-fluid interphase.

transfer load. The resultant strain profile did not exhibit a strain reduction behavior at the fiber/droplet interphase at all levels of applied strain. This observation reinstates that the strain reduction at the fiber/polystyrene interphase is a phenomenon of load transfer. The observation also verifies that the local strain distributions for fiber/polystyrene interphase have been successfully determined.

3.6. Conclusions

Micro-Raman spectroscopy has been applied to study the interphase between a polystyrene droplet and a single cellulose fiber. The fiber was stretched, and the point-to-point mapping of the local strain was performed along the fiber/polymer interface. The tensile strain profile agrees with the finite element study of the wood-fiber/polymer system reported in the literature. The highest tensile strain was found near the edge of the droplet where the fiber enters and exits the polymer droplet. The local fiber strain declined from the droplet edge region to the middle region of the drop. In addition, the strain values at the middle region of the drop could also increase, presumably when a strain concentrator was present. The maximum of these local strains corresponded to a strain-control fracture of the matrix polymer.

Overall, this study concludes that micromechanics of the cellulose-fiber/polymer interphase can be studied using a chemical tool. The Raman technique also distinctly provides a non-perturbing approach to determine strain distributions at the fiber/polymer interphase. This technique should be applicable to studying composites involving lignocellulosic fibers which also contain cellulose.

3.7. References

Atalla, R. and B. E. Dimick. 1975. Raman-spectral evidence for differences between the conformations of cellulose I and cellulose II. Carbohydrate Research. 39:C1-C3.

Banwell, C. N. 1972. Fundamentals of molecular spectroscopy. 2nd edition. McGraw-Hill, London. 348 pp.

Drzal, L. T. 1990. The role of the fiber-matrix interphase on composite properties. Vacuum. 41(7-9):1615-1618.

Egan, A. and S. M. Shaler. 2000. Fracture and mechanics of fracture for resin coated single wood fibers. Pages 95-103 in G. Hague, M. McLauchlin, and T. Skinner, eds. Proceedings of the Fourth Panel Products Symposium. The Biocomposites Centre, Bangor, U.K.

Eichhorn, S. J., R. J. Young, and W.–Y. Yeh. 2001. Deformation processes in regenerated cellulose fibers. Textile Research Journal. 71(2):121-129.

Fan, C. F., D. A. Waldman, and S. L. Hsu. 1991. Interfacial effects on stress distribution in model composites. Journal of Polymer Science: Part B: Polymer Physics. 29:235-246.

Gaur, U. and B. Miller. 1989. Microbond method for determination of the shear strength of a fiber/resin interface: Evaluation of experimental parameters. Composites Science and Technology. 34:35-51.

Gauthier, R., C. Joly, A. C. Coupas, H. Gauthier, and M. Escoubes. 1998. Interfaces in polyolefin/cellulosic fiber composites: chemical coupling, morphology, correlation with adhesion and aging in moisture. Polymer Composites. 19(3):287-300.

Gu, X. and R. J. Young 1997. Deformation micromechanics in model carbon fiber reinforced composites. Part II. The microbond test. Textile Research Journal. 67(2):93-100.

Herrera-Franco, P. J. and L. T. Drzal. 1992. Comparison of methods for the measurement of fiber/matrix adhesion in composites. Composites. 23:2-27.

Maldas, D., B. V. Kokta, R. G. Raj, and C. Daneault. 1988. Improvement of the mechanical properties of sawdust wood fiber-polystyrene composites by chemical treatment. Polymer. 29:1255-1265.

Mead, R., R. N. Curnow, and A. M. Hasted. 1993. Statistical methods in agriculture and experimental biology. 2nd edition. Chapman and Hall, London. 415 pp.

Mott, L., S. M. Shaler, and L. H. Groom. 1996. A technique to measure strain distributions in single wood pulp fibers. Wood and Fiber Science. 28(4):429-437.

Tuinstra, T. and J. L. Koenig. 1970. Characterization of graphite fiber surfaces with Raman spectroscopy. Journal of Composite Materials. 4:492-499.

4. EVALUATION OF LOAD TRANSFER AT THE CELLULOSE-FIBER/POLYMER INTERPHASE USING A MICRO-RAMAN TENSILE TEST

4.1. Chapter Summary

The objectives of this research were (1) to use a Raman micro-spectroscopic technique to determine the tensile stress distributions of a cellulose-fiber/polymer droplet interphase, and (2) to examine if the stress profile could be applied to evaluate fiber/polymer interfacial bonding. Lyocell (regenerated cellulose) fibers were treated with styrene-maleic anhydride copolymer (SMA). A single fiber, with an attached polystyrene droplet in the mid-length region of the fiber, was strained in tension. Raman spectra were collected at five-micrometer intervals along the embedded region of the fiber. The stress-dependent peak of cellulose (895 cm^{-1}) was analyzed for frequency shift so that the local tensile stress at the interface region could be determined. Results show that the local tensile stresses of the strained fiber were lower in the embedded region compared to the exposed region, suggesting a transfer of load from the fiber to the matrix polymer. A deeper and sharper decline of the stress profile was observed when the fiber/droplet interaction is enhanced (in cellulose-SMA/polystyrene system). The depth and slope of the tensile stress profile along the interface region allows for an estimation of the load transfer ability and an inference for the practical bond strength of the composite system. As such, the Raman technique provides a novel approach to evaluate the practical adhesion between a ductile fiber and a brittle polymer, which is difficult to measure using common micro-mechanical tests.

4.2. Introduction

Wood plastic composites (WPC) have been increasingly favored over the traditional wood products and the unfilled plastics for applications where structural requirements are low. Two examples of such applications are decking and window profiles. For railings and decking, WPCs, being more environmental friendly, are partially replacing lumber treated with chromated copper arsenate (Smith 2001). In window applications, wood-filled poly (vinyl chloride) composites are gaining wide acceptance because they are more moisture resistant compared to wood products, and are stiffer and more thermally stable compared to the unfilled plastics (Defosse 1999).

Recently, high-purity, stiff cellulose fibers are receiving much attention for producing engineered wood-plastic composites that have an enhanced structural performance. Chemical pulp fibers (≥ 95% alpha-cellulose content) have been used to reinforce engineered plastics such as nylon 6 at a fiber loading of 30-33% (Sears *et al.* 2002). The resulting composites exhibited properties that are intermediate between the wollastonite-reinforced nylon and the glass fiber-reinforced nylon. Apart from natural fibers, continuous regenerated cellulose (lyocell) fibers solvent-spun from wood pulp have also been used as a reinforcing agent for plastics. When combined with cellulose acetate butyrates, a naturally-derived plastic, the resulting lyocell/polymer composites attained a stiffness modulus that exceeded 20 GPa (Franko *et al.* 2001). In brief, as the WPC applications shift to end-uses of higher performance, the need for a better engineering of the composites is increasingly justified.

The ability to engineer wood/polymer composites would be enhanced with an improved understanding of the factors that influence the mechanical properties of the composites. It is known that the mechanical properties of fiber/polymer composites depend on (1) the strength and modulus of the fibers, (2) the strength and chemical stability of the matrix polymer, and (3) the effectiveness of the fiber/polymer bond in transferring load across the interphase (Erickson and Plueddemann 1974). The composite properties are also influenced by factors associated with the distribution behavior of the fibers in the matrix polymer; these factors include fiber volume fraction, fiber orientation, and fiber agglomeration. Another influencing factor in the case of discontinuous fiber composites is the fiber aspect ratio (length divided by diameter) – the higher ratio allows a larger percentage of the length of the fiber being fully utilized for transferring load (Hoecker and Karger-Kocsis 1996; Shaler 1993).

While the mechanical properties of bulk fibers and matrix polymers are usually well known, the interface region (interphase), whose properties are neither of the combining constituents, are not well understood. Therefore, much effort has been placed on studying the mechanical properties of the fiber/polymer interphase, and relating these properties to the composite performance. A crucial tool for achieving such aims is an effective characterization technique for the fiber/polymer interphase.

4.3. Literature Review

Micromechanical tests are commonly used to infer load transfer at the fiber/polymer interphase, but the currently employed test methods suffer particular limitations. In the micro-debond test, the interfacial shear strength is determined by shearing a polymer droplet off from the fiber (Gaur and Miller 1989). However, this test is of limited use when the fiber is either too thin or too weak, or the interphase is too strong thereby, causing the fiber to break before shear removal of the droplet. In the fiber fragmentation test, the interfacial shear strength is deduced from the number (or length) of fiber fragments when a fiber-embedded polymer sample is subjected to a tensile load (Herrera-Franco and Drzal 1992). Unfortunately, this test cannot be applied for a brittle matrix polymer because it will fracture before fiber fragmentation is observed.

Evaluation of interphases that are formed between cellulosic fibers and brittle polymers continually presents a challenging task. Liu *et al.* (1996) performed micro-debond tests on wood-fiber/polystyrene interphases of 50-100 micrometers in embedding length. They reported that 55% and 5% of the total samples tested in their study failed of fiber breakage and matrix cracking, respectively. Trejo-O'Reilly *et al.* (2000), on the other hand, employed fiber fragmentation tests for their lyocell-fiber/polystyrene system. They carried out the tests at 94°C, which is near the glass-transition temperature of polystyrene, presumably aiming to reduce the brittleness of the matrix polymer by transforming it from the glassy to rubbery state. These researchers

successfully obtained the interfacial shear strength values, but forfeited the information of the fiber/polymer interactions at the glassy state of the matrix, which may be of interest in the normal service condition of the composites.

For interphases involving cellulosic fibers and polymers of higher ductility, the common micromechanical tests can be performed in conjunction with photoelastic measurements to determine the distributions of stresses at the interphase. This photoelastic technique specifically applies to transparent, birefringent materials, which are doubly refracting because of their ability to rotate the plane of polarized light (Van Krevelen 1990). Polarized light passes through a birefringent material at different intensities depending on the stresses within the materials, thereby providing information of the stress fields in response to mechanical loading. Mercado (1992) loaded a wood fiber-containing polyurethane samples in tension under a polarized microscope, and subsequently recorded the image. He then performed image analyses to quantify the light intensity in the birefringent pattern, which can be converted to stresses within the matrix polymer around the region of the fiber/polymer interphase. This technique allowed the researcher to observe matrix stress distributions, which were distinguishable between two types of embedded fibers that were generated under different processing conditions (steam pressure or temperature). The technique, however, has been primarily limited to transparent and birefringent polymers (such as epoxy, polycarbonate, and polyester).

Raman micro-spectroscopy is a novel technique that provides a robust approach in identifying interfacial stress distributions for a potentially wide range of cellulose-fiber/polymer combinations. This technique relies on identifying the stress-dependent vibrational frequency, establishing the stress-frequency calibration curve, and directly converting the frequency of a spectrum of interest to local stresses (Figure 4.1). The stress-dependent Raman bands of cellulose have been identified by Eichhorn *et al.* (2001b) to be at 895 cm^{-1} and 1095 cm^{-1}. The 895 cm^{-1} band shifts 0.41 cm^{-1}, while the 1095 cm^{-1} band shifts 0.44 cm^{-1} to lower frequencies for every 100 MPa increase in tensile stress. Therefore, if Raman bands are collected at different locations of the fiber along the fiber/polymer interphase, the point-to-point variation (or spatial distribution) of stress can thus be determined for the interface region.

The Raman technique has been applied to study microdeformation of natural cellulose (flax and hemp) fibers (Eichhorn *et al.* 2000) and to monitor the deformation process in regenerated cellulose (viscose and Lyocell) fibers (Eichhorn *et al.* 2001b). None of these studies dealt with interaction of cellulose fibers with a polymer. In another study, Eichhorn *et al.* (2001a) investigated the deformation mechanism in fiber composites systems; but these systems, namely paper and wood, form in-situ bonding and do not involve interaction with an applied matrix polymer. On the issue of using synthetic polymers, Eichhorn and Young (2001) mixed microcrystalline cellulose powder with epoxy. However, their purpose was to hold the powder together for

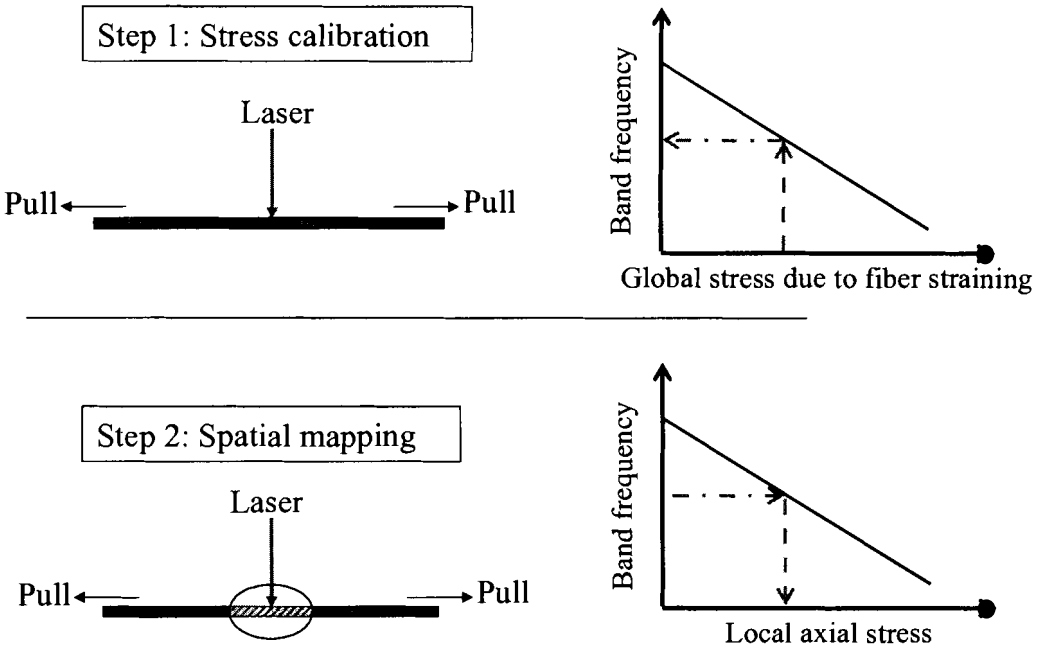

Figure 4.1 A schematic approach of using Raman micro-spectroscopy for mapping tensile stress at the fiber/polymer interphase.

bending tests so that the Young's modulus of the microcrystalline cellulose could be determined. With this objective in mind, these researchers did not attempt to study interphase or interactions between the particulates (or fibers) and polymer.

In the previous Chapter, Raman spectroscopic studies were conducted for the first time on the cellulose-fiber/polymer interphase. In the studies, single cellulose fibers with an attached microdroplet of polystyrene were strained in tension, while Raman mapping was performed along the fiber/polymer interface to determine strain

distributions. It was found that the local tensile strain at the interphase declined from the edge to the mid-length regions of the embedment, suggesting a transfer of load from the fiber to the matrix polymer. Additionally, fractures of polystyrene were observed at the edge of the embedding region where the local tensile strain was the highest. These findings led to the conclusion that the Raman technique is a useful tool to study micromechanics of the fiber/polymer interphase in a non-invasive manner.

In this Chapter, the Raman micro-tensile technique was used to determine stress distributions at the cellulose-fiber/polymer interphase of the micro-droplet composite samples. The stress profiles were further analyzed to deduce load transfers at the interphase, and to examine their applicability in evaluating fiber/polymer interfacial bonding.

4.4. Materials and Methods

The fibers used in this study were regenerated cellulose fibers solvent-spun from wood pulp to a diameter of 12 micrometer. These Lyocell fibers were provided by Acordis Cellulosic Fibers (Tencel^{R}). The atactic polystyrene was of 125,000-250,000 weight average molecular weight, and it was acquired from PolySciences Inc. The surface modifier used in this study was styrene-maleic anhydride random diblock copolymer of 50/50 styrene and anhydride content based on percent weight (Polyscience Inc.). The copolymer had a number average molecular weight of 1600 g/mol and an acid number of 480.

Lyocell fibers were cleaned by Soxhlet-extraction, as described in Chapter 3, prior to the experiments. The fibers were grafted with styrene-maleic anhydride (SMA) copolymer according to the procedure adopted by Liu (1994). First, 3.5 grams of copolymer were dissolved in 20 mL of N,N-dimethylformamide (DMF) with 0.07 grams (0.2% of copolymer weight) of 4-dimethylaminopyridine (DMAP) as the catalyst. Then, about 0.5 grams of cellulose fibers were added into the solution for the esterification reaction at 100°C for five hours. At the end of the reaction time, the fibers were rinsed twice using acetone, and subsequently extracted with acetone by Soxhlet extraction for six hours. The extracted fibers were then dried at 70°C to evaporate the solvent.

Polystyrene was deposited from a 20 weight-% solution (in toluene) onto single fibers, and the polymer droplet embedded a length of 70-90 micrometers on the fiber. The fiber was strained in tension at a rate of 10 micrometer/second and subsequently, an elapse time of five minutes was allowed for the instantaneous stress relaxation to occur. The embedded region of the fiber was then scanned, using a Raman micro-spectrometer, at a five-micrometer interval along the fiber axis. The detailed procedure and the description of the micro-Raman tensile test apparatus was reported in Chapter 3. The resulting spectra were subtracted with the spectrum of polystyrene (without cellulose) to produce cellulose spectra. The 895 cm^{-1} band of the cellulose spectra was analyzed for frequency shift. A frequency shift of 0.44 cm^{-1} was found to correspond to 100 MPa in tensile stress (Table 3.2). This frequency shift could thus be converted to local axial stress.

4.5. Results and Discussion

4.5.1. Tensile Stress Distribution at the Fiber/Polymer Interphase

Figure 4.2 plots tensile stresses of the fiber as a function of distance from the center of embedment. When the fiber was unstrained, the tensile stresses along the fiber/polymer interphase did not differ from the local stresses of the fiber outside the droplet. When the fiber was stretched at 1% strain level, the local tensile stresses became lower in the embedded region compared to the exposed region, suggesting a transfer of load from the fiber to the embedding polymer. The fiber stresses declined from regions at both edges of the polymer droplet, and attained a minimum value near the mid-region of the embedment (Figure 4.2). The occurrence of a minimum fiber stress at the droplet middle can be attributed to two phenomena: (1) the further away a region of interphase from the far-field stress (tensile loading point), the less tensile load it has to sustain, and (2) a thicker matrix material (at the center of the droplet) takes up more tensile load from the fiber.

The tensile stress distribution profile shifted to a higher stress value when the fiber stretching was increased from 1% to a higher strain level (Figure 4.2). However, the increase in tensile stresses was not as large as the increase observed for the initial stretching (from zero to 1% strain). This contrast can be attributed to the fact that fiber attained its linear elasticity limit at 1% strain level after which a high strain input only resulted in a low stress value (refer to Figure 3.5).

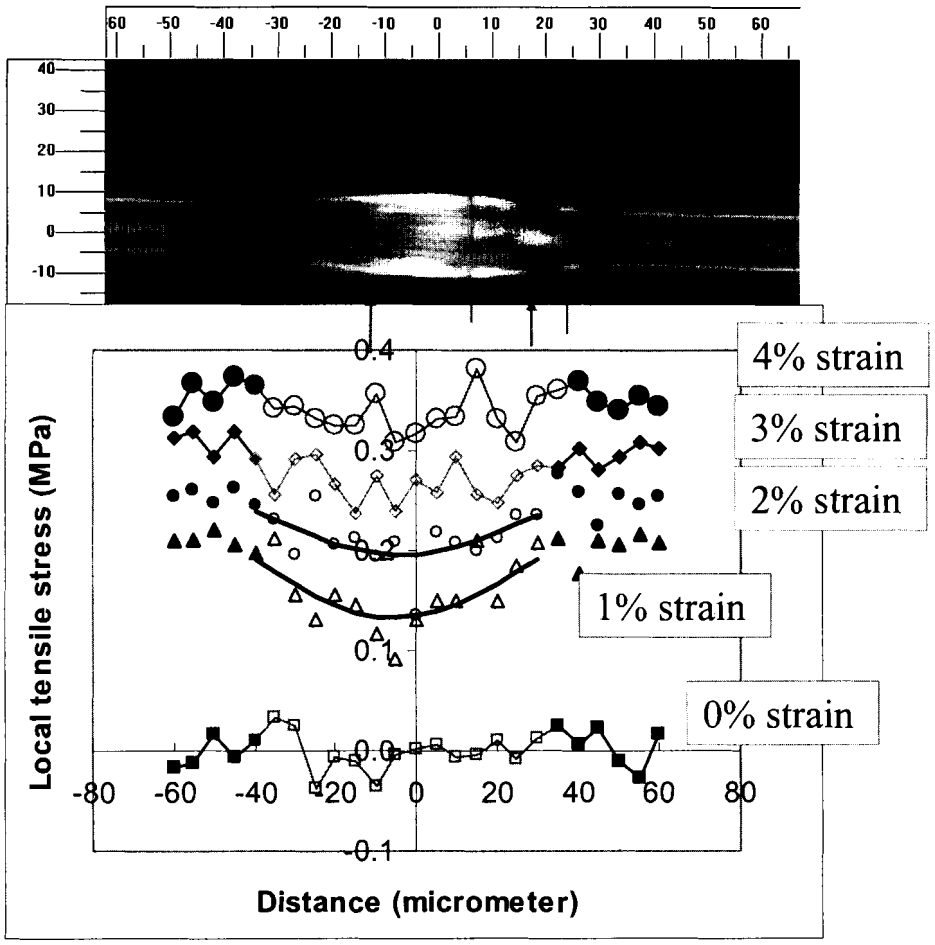

Figure 4.2 The variation of fiber local tensile stress along the fiber/polymer interphase.

The tensile stress as a function of distance along the fiber/polymer interphase can be fitted using a fourth order polynomial relationship. Such equations were satisfactory (r-square not less than 0.80) for stress distribution profiles at 1% and 2% strain levels. For stretching at a higher strain level, the tensile stress distribution, in addition to the general trend of stress dissipation towards the mid-region of the embedment, exhibited local variations. The local tensile peak values corresponded to locations of polystyrene fractures (Figure 4.2) that were observed to begin at 2% global strain level when the ultimate strain of polystyrene was attained. To ensure that the load dissipated in the embedded fiber was solely transferred to the load-sustaining matrix polymer but not consumed to fracture the polymer, the subsequent discussions will be focused on stress distribution profile at 1 % global strain level, when there were no polymer fractures.

4.5.2. Load Transfer at the Fiber/Polymer Interphase

In the earlier section, it was shown that the tensile stress distribution along the fiber/polymer interface declined from both edges of the polymer droplet to the center of the drop (Figure 4.2). Here, the results are compared with a typical tensile stress distribution in the fiber fragmentation test (Figure 4.3) which is normally used to demonstrate the shear-lag analysis proposed by Cox (1952). The stress profile of a fiber embedded in a continuous matrix exhibits a minimum value near both ends of the fiber, and the stress increases abruptly toward the center of the fiber length to attain a maximum value at most part of the region along the fiber. In the same fragmentation

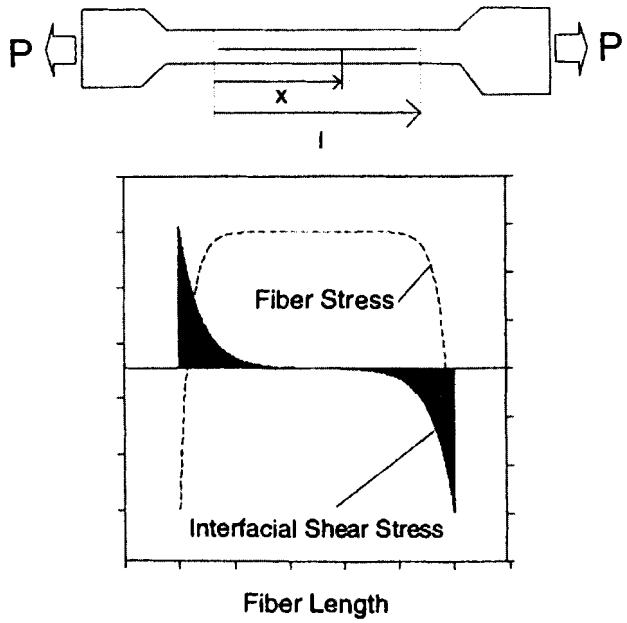

Figure 4.3 Stresses along a fiber embedded in a continuous matrix when the matrix is subjected to a tensile load in the longitudinal direction of the fiber. Figure from Liu *et al.* (1996).

test, when the fiber is (or fragmented to a length) shorter than the effective length (l_e) required to transfer load, the fiber axial stress is maximum at the mid-length region of the fiber, while the stress remains the lowest at the fiber ends (Figure 4.4: profiles 3 and 4). Under this condition, the fiber tensile stress profile exhibits a trend opposite to the stress profile obtained from this study. Such an opposite trend is reasonable because the fiber fragmentation test involves straining the matrix polymer and measuring fiber fracture due to stress transferred to the embedded fiber, while the approach presented here is the opposite – the fiber is strained and the stress remaining in the fiber is determined, i.e. after load is transferred to the polymer droplet. Nevertheless, both approaches show that the maximum transfer of load occurs at the mid-length region of the embedded fiber where it is furthest away from the far-field stress.

The next attempt of the study was to verify the load transfer phenomenon in the cellulose-fiber/polystyrene system. To demonstrate a case where no load transfer occurs, a micro-droplet of silicon fluid was applied onto single cellulose fibers. Silicon fluid is an inert compound which does not interact with cellulose, hence it presents a fiber/polymer system where the interphase is not strong enough to transfer load and the matrix (droplet) is not load sustaining. To demonstrate a case where the load transfer ability is improved, cellulose fibers were treated with styrene-maleic anhydride (SMA) copolymer prior to forming a micro-bond with polystyrene. The copolymer has anhydride groups at one end to bond to cellulose through ester (covalent) linkages and it has styrene groups at the other end to interact with polystyrene. The SMA copolymer

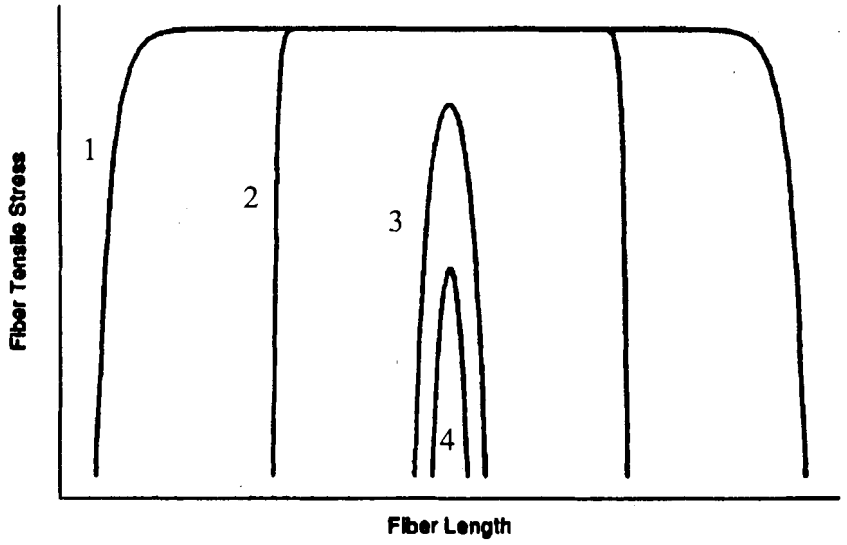

Figure 4.4 Effect of fiber length on the fiber tensile stress distributions at the fiber/polymer interphase as predicted by Cox. Figure from Shaler 1993. Note: Profiles 1 and 2 refer to fiber lengths longer than the effective length (l_e), while profiles 3 and 4 for fiber lengths shorter than l_e.

was reported to improve the interfacial shear strength of the lignocellulosic (wood) fiber/polystyrene composites (Liu 1994), hence also improving the load transfer ability at the interphase.

Figure 4.5 depicts the stress distribution profiles for cellulose/silicon-fluid, cellulose/polystyrene, and cellulose-SMA/polystyrene systems at 1% applied strain. When no load was transferred from the fiber to the droplet (in cellulose/silicon-fluid system), the tensile stress profile did not show a noticeable decline along the fiber length. When the fiber/droplet interaction was enhanced (in cellulose-SMA/polystyrene system), the tensile stress profile exhibited a deeper decline towards the center of

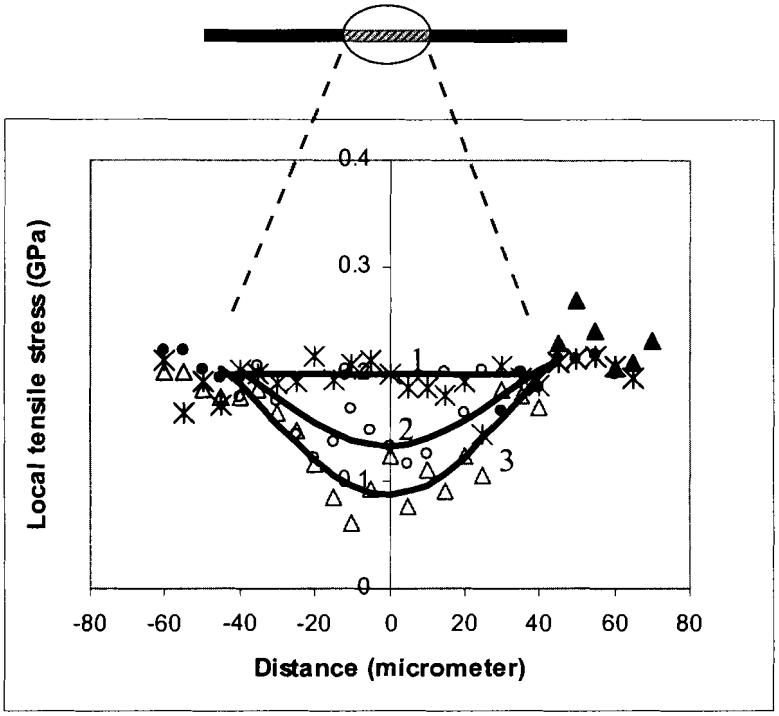

Figure 4.5 Tensile stress distributions at three interphases at 1% global strain. Note: 1 = cellulose-fiber/silicon-fluid; 2 = cellulose-fiber/polystyrene, 3 = SMA-treated cellulose/ polystyrene. SMA refers to grafting with styrene-maleic anhydride copolymer.

the droplet. For elaboration, in the mid-length of the embedment, the (minimum) tensile stress values are estimated, from the regressed curves, to be 0.13 GPa for untreated-cellulose/polystyrene interphase and 0.09 GPa for cellulose-SMA/polystyrene interphase (Figure 4.5). At a variability of $\pm$ 0.7 cm^{-1} for the calibrated stress dependence (Table 3.2), the fiber tensile stress, calculated from a frequency shift of Δf, has a lower limit of $\frac{\Delta f}{4.42 + 0.7}$, and a higher limit of $\frac{\Delta f}{4.42 - 0.7}$. Correspondingly, the tensile stress values lie within a lower limit of 86% $\left(i.e., \frac{\frac{\Delta f}{4.42 + 0.7}}{\frac{\Delta f}{4.42}} \; x \; 100\% \right)$ and an upper limit of 119% $\left(i.e., \frac{\frac{\Delta f}{4.42 - 0.7}}{\frac{\Delta f}{4.42}} x \; 100\% \right)$ of the nominal value $\left(i.e., \frac{\Delta f}{4.42} \right)$. Based on this information, the fiber tensile stress value in the droplet center could range from 0.11 GPa (0.13 GPa x 0.86) to 0.15 GPa. (0.13 GPa x 1.19) for the untreated-cellulose/polystyrene interphase. For the cellulose-SMA/polystyrene system, these values span from 0.08 GPa to 0.10 GPa. Hence, the fiber tensile stress value in the mid-length of the embedment is significantly lower for the cellulose-SMA/polystyrene system when compared to the interphase where fibers were not treated. Correspondingly, a deeper and sharper decline of the stress profile was observed in the cellulose-SMA/polystyrene interphase.

To summarize the preceding discussions, the tensile stress profiles determined from the micro-Raman tensile test are manifestations of load transfer phenomena in fiber/polymer composites. Although the transfer of loads from the fiber to the matrix was studied, as opposed to the matrix-to-fiber load transfer in practical applications of fiber-reinforced composites, it is anticipated that either case reflects the integrity of a bonding system because an interphase should allow load to transfer equally well in either direction.

4.5.3. Quantifying Fiber/Polymer Interfacial Bonding

It has been established that the tensile stress profiles at the fiber/polymer interphase exhibit a deeper and sharper decline when there is a larger load transfer within the interphase. The following efforts aim at quantifying the depth and slope of the stress profile so that fiber/polymer interfacial bonding can be evaluated.

For studying the depth of the decline at the center of the embedment, a simple arithmetic relationship was employed to describe the maximum fraction of load dissipated from the fiber (into the matrix). Thus an estimation of load transfer ability (LTA) at an applied strain level was defined:

$$LTA = 1 - \left(\frac{\sigma_L}{\sigma_{F,avg}} \right), \tag{4.1}$$

where σ_L refers to the local tensile stress of an embedded fiber, and $\sigma_{F,avg}$ refers to the far-field stress or tensile stress of the fiber outside the embedment. Note that $\frac{\sigma_L}{\sigma_{F,avg}}$ is the stress intensity of the embedded fiber. Referring to Figure 4.5, the maximum *LTA* attainable is estimated to be 0.35, i.e., 1-(0.13GPa/0.2GPa) for the cellulose/polystyrene interphase at 1% strain level. The value implies that up to 35% of the load in the fiber was transferred to the matrix. In the stronger bonding system (cellulose-SMA/polystyrene), the maximum load transfer ability is estimated to be 0.55, hence an additional 20% load can be transferred through the improved interphase.

For analyzing the slope of the tensile stress profile, the rate of change in tensile stress at any point along the fiber/polymer interphase was calculated. Indeed, the slope of a stress profile has been related to interfacial shear strength for micro-debond samples where polymer droplets are sheared off from single fibers (Gu and Young 1997). Under this approach, the change in tensile force in the fiber is balanced by the change in shear force at the interface (Figure 4.6).

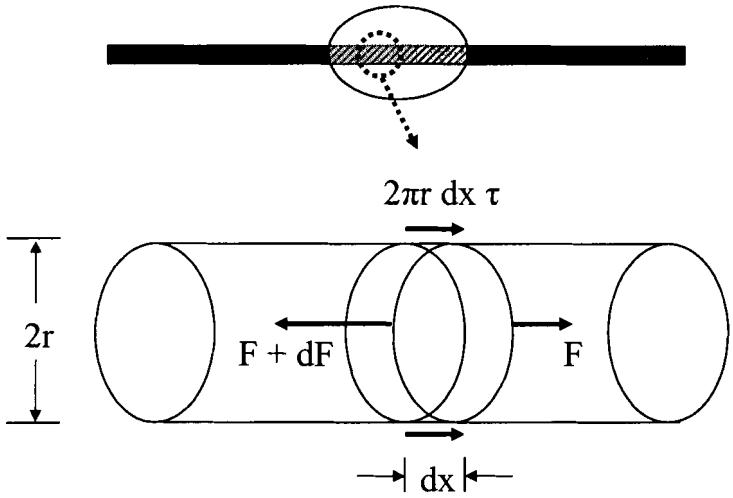

Figure 4.6 Balance of tensile and shear forces on an element of the fiber embedded in the polymer.

Figure 4.6 can be numerically represented by:

$$dF = 2\pi r \tau dx, \tag{4.2}$$

where F, r, τ, and x, respectively, refers to the tensile force on the fiber, the fiber radius, the shear stress at the fiber/polymer interface, and the position along the fiber in the embedded region. Equation 4.2 can be simplified in terms of interfacial shear stress (τ):

$$\tau = \frac{1}{2\pi r}\frac{dF}{dx}. \tag{4.3}$$

Because fiber stress (σ_f) is the amount of force (F) acting on a unit of fiber cross-sectional area (πr^2):

$$dF = \pi r^2 d\sigma_f, \text{ hence} \tag{4.4}$$

$$\tau = \frac{1}{2\pi r}\frac{\pi r^2 d\sigma_f}{dx}, \text{ or}$$

$$\tau = \frac{r}{2}\frac{d\sigma_f}{dx}, \tag{4.5}$$

where σ_f is the tensile stress on the fiber, and $\frac{d\sigma_f}{dx}$ is the slope of tensile stress distribution curve at any point along the fiber.

Figure 4.7 shows the shear stress distribution curves determined using Equation 4.5. The values of $\frac{d\sigma_f}{dx}$, which are required to calculate shear stresses, were determined from the slope of the regressed line of the tensile stress profile. From the plots, it was observed that the shear stress is not uniform along the fiber/polymer interphase. The interfacial shear stress (τ) is maximum near regions where the fiber entered and exited the polymer droplet, and minimum at the mid-length of the embedment.

Referring to Figure 4.7, the maximum shear stresses (τ_{max}) at 1% strain level are 8.7 MPa and 12.1 MPa, respectively, for cellulose/polystyrene and cellulose-SMA/polystyrene systems, implying that the improvement of interfacial bonding is significant. This improvement is comparable with the study of Liu (1994) where

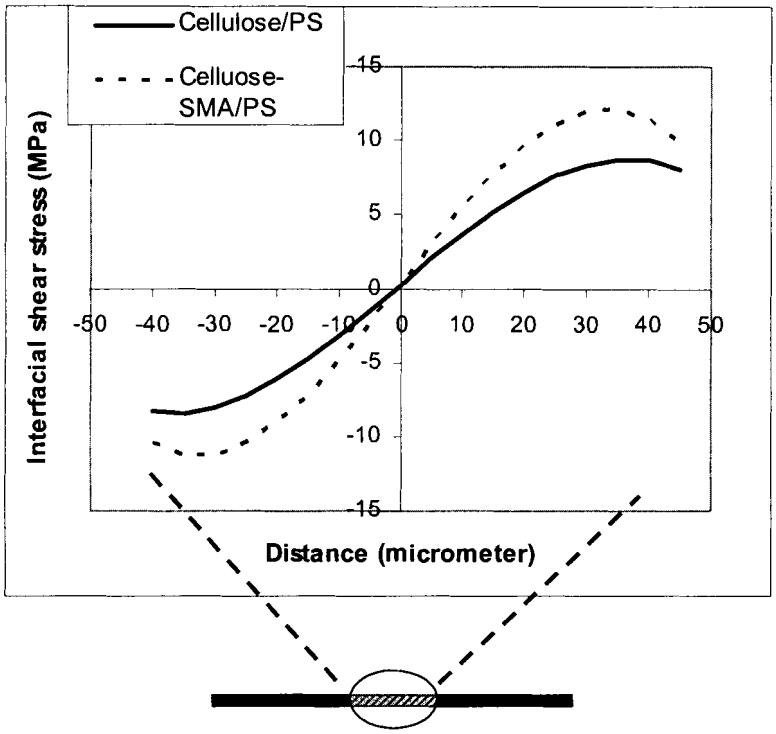

Figure 4.7 Distributions of shear stress at the cellulose-fiber/polystyrene interphase for two systems of different fiber/matrix interactions at 1% global strain.

macerated wood fibers were grafted with styrene-maleic anhydride copolymer using the same procedure and recipe conducted in this study. Based on the micro-debond test data, Liu (1994) found an improvement in the fiber/polystyrene interfacial shear strength from 5.6 MPa to 10.0 MPa, both of which values could be higher if the researcher had, conventionally, performed extrapolation to zero-embedment to eliminate the influence of embedding length. The estimated maximum shear stress for cellulose-fiber/polystyrene interphase in this study also approximates the value of 10.2 MPa in the study of Trejo-O'Reilly *et al.* (2000) although they employed fiber

fragmentation tests at 94°C for their lyocell-fiber/polystyrene system. In the same study, these researchers also grafted styrene-maleic anhydride copolymer of 25 mol-% anhydride onto lyocell fibers and they obtained an interfacial shear strength of 11.0 MPa.

To ensure that the droplet size variation did not affect the evaluations of load transfer, the micro-deformation of two extreme embedded lengths in this study (69 micron versus 89 micron) were compared. Figure 4.8 shows the stress intensity ($\frac{\sigma_L}{\sigma_{F,avg}}$) distributions of the fibers embedded in droplets of two different sizes. The figure shows that, at 1% global strain, the fiber with the longer embedded length (89 micron) experienced lower stress intensity ($\frac{\sigma_L}{\sigma_{F,avg}}$) or higher *LTA*, i.e., ($1-\frac{\sigma_L}{\sigma_{F,avg}}$). Clearly, the embedded lengths (69-89 microns) examined in this study are synergetic to fiber lengths that are shorter than the effective length (l_e) in the fiber fragmentation test, where the longer embedded length allows more load-transfer, as evidenced from the larger maximum at the mid-length region of the fiber (profiles 3 versus 4 in Figure 4.4). Nevertheless, the difference in the fiber stress intensity profile in droplets of two sizes in the present study implies that the *LTA* (Equation 4.1) should be compared among samples of similar droplet size.

The slopes of the regressed lines of the tensile stress profiles in Figure 4.8 were used to determine the shear stress profiles at the fiber/polymer interphase (Figure 4.9). The fiber embedded in a smaller droplet exhibits a maximum shear stress of 9.4 MPa

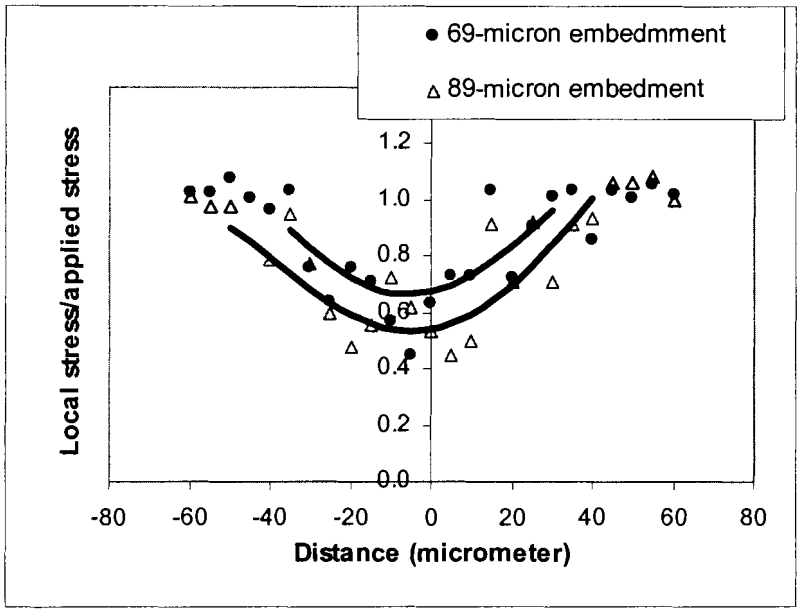

Figure 4.8 Load transfer in the fiber/polymer system at two different embedded lengths at 1% global strain.

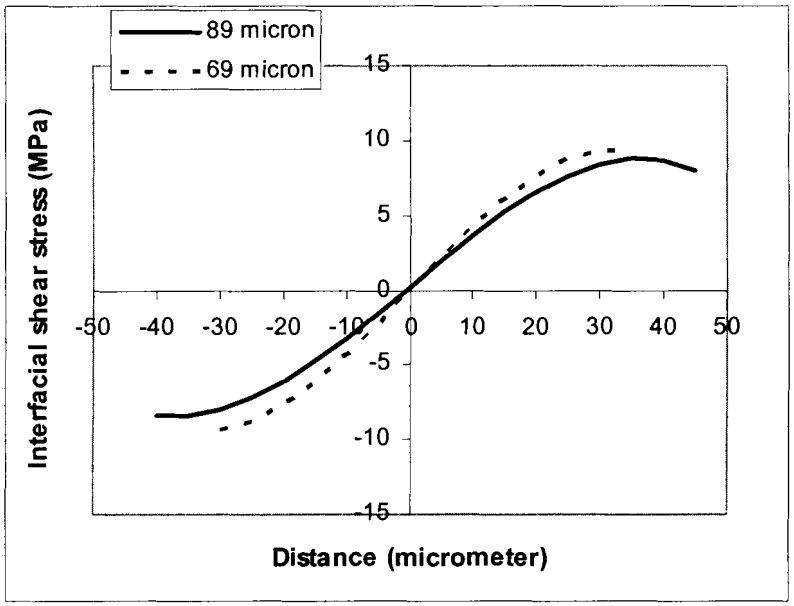

Figure 4.9 Distributions of shear stress at the cellulose-fiber/polystyrene interphase for two embedded lengths at 1% global strain.

as opposed to 8.7 MPa for a larger droplet. Therefore, this finding suggests that the maximum interfacial shear stress calculated from the slope of the tensile stress distribution profile is independent of droplet size.

To further gain insights of the variability of the maximum interfacial shear stress determined using the approach presented in this study, four more fiber/droplet systems were examined. The maximum interfacial shear stress values of the six replicates have an average of 9.3 MPa, with a variability of $\pm$ 2.3 MPa at 99% confidence interval. The variability is anticipated to include instrumental, experimental, and data reduction errors, as well as fiber-to-fiber variability.

4.6. Conclusions

Micro-Raman spectroscopy was applied to determine tensile stresses of lyocell fibers as a function of distance along the fiber/polystyrene interphase. The fiber stress distribution profile exhibited a decline from the edge to the middle of the embedment. Such a load decline was not observed on fibers embedded in silicon fluid where no load transfer occurs between the fiber and the droplet. On the other hand, the load decline was deeper and sharper for embedment of fibers pre-treated with styrene-maleic anhydride copolymer where a strong interphase is anticipated. Further analysis proved that the depth of the stress profile demonstrates the phenomenon of load transfer where the load in the embedded fiber is dissipated to the matrix polymer. The slope of the stress profile, on the other hand, allows the calculation of the interfacial shear stress.

As such, the Raman technique provides a novel approach for evaluating fiber/polymer interfacial shear stress in micro-composites. Its applicability is even more notable in bonding systems involving a ductile fiber and a brittle polymer, as in lyocell-fiber/polystyrene bonding, which is difficult to study using common micro-mechanical tests. Therefore, this technique expands the research possibilities in the field of cellulose-based composites, which also include wood-fiber/plastic composites. The success of the Raman technique also demonstrates the unique approach of applying chemistry (molecular vibration information) to the understanding of mechanical properties of a fiber/polymer composite system.

4.7. References

Cox, H. L. 1952. The elasticity and strength of paper and other fibrous materials. British Journal of Applied Physics. 3:72-79.

Defosse, M. 1999. Processors focus on differentiation in window profiles. Modern Plastics. Sept.:74-79.

Eichhorn, S. J., M. Hughes, R. Snell, and L. Mott. 2000. Strain induced shifts in the Raman spectra of natural cellulose fibers. Journal of Materials Science Letters. 19:721-723.

Eichhorn, S. J. and R. J. Young. 2001. The Young's modulus of a crystalline cellulose. Cellulose. 8:197-207.

Eichhorn, S. J., J. Sirichaisit, and R. J. Young. 2001a. Deformation mechanisms in cellulose fibres, paper and wood. Journal of Materials Science. 36:3129-3135.

Eichhorn, S. J., R. J. Young, and W.–Y. Yeh. 2001b. Deformation processes in regenerated cellulose fibers. Textile Research Journal. 71(2):121-129.

Erickson, P. W. and E. P. Plueddemann. 1974. Historical background of the interfaces – Studies and theories. Pages 1-29 in E. P. Plueddemann, ed. Interfaces in polymer matrix composites. Academic Press, New York.

Franko, A., K. C. Seavey, J. Gumaer, and W. G. Glasser. 2001. Continuous cellulose fiber-reinforced cellulose ester composites III. Commercial matrix and fiber option. Cellulose. 8:171-179.

Gaur, U. and B. Miller. 1989. Microbond method for determination of the shear strength of a fiber/resin interface: Evaluation of experimental parameters. Composites Science and Technology. 34:35-51.

Gu, X. and R. J. Young 1997. Deformation micromechanics in model carbon fiber reinforced composites. Part II. The microbond test. Textile Research Journal. 67(2):93-100.

Herrera-Franco, P. J. and L. T. Drzal. 1992. Comparison of methods for the measurement of fiber/matrix adhesion in composites. Composites. 23:2-27.

Hoecker, F. and J. Karger-Kocsis. 1996. Surface energetics of carbon fibers and its effects on the mechanical performance of CF/EP composites. Journal of Applied Polymer Science. 59:139-153.

Liu, P. F. 1994. Characterizing interfacial adhesion between wood fibers and a thermoplastic matrix. Ph.D. dissertation. West Virginia University. Morgantown, WV., USA. 170 pp.

Liu, P. F., T. G. Rials, M. P. Wolcott, and D. J. Gardner. 1996. Interactions between wood fibers and amorphous polymers. Pages 74-81 in Woodfiber-plastic composites: Virgin and recycled wood fiber and polymers for composites. Forest Products Society, Madison, WI., USA.

Mercado, J. 1992. Using digital image analysis to determine the reinforcement of wood fiber polyurethane composites. M.S. thesis. Michigan Technological University, Houghton, MI, USA. 71 pp.

Sears, K. D., R. Jacobson, D. F. Caulfield, and J. Underwood. 2002. Reinforcement of engineering thermoplastics with high purity wood cellulose fibers. Pages 27-34 in Proceedings of the Sixth International Conference on Woodfiber-Plastic Composites. Forest Products Society, Madison WI., USA.

Shaler, S. M. 1993. Mechanics of the interface in discontinuous wood fiber composites. Pages 9-14 in M. P. Wolcott, ed. Wood-fiber/polymer composites: fundamental concepts, processes, and material options. Forest Products Society. Madison, WI., USA.

Smith, P. M. 2001. U.S. woodfiber-plastic composite decking market. Pages 13-17 in Proceedings of the Sixth International Conference on Woodfiber-Plastic Composites. Forest Products Society, Madison, WI, USA.

Trejo-O'Reilly, J. A., J. Y. Cavaillé, M. Paillet, A. Gandini, P. Herrera-Franco, and J. Cauich. 2000. Interfacial properties of regenerated cellulose fiber/polystyrene composite materials. Effect of the coupling agent's structure on the micromechanical behavior. Polymer Composites. 21(1):65-71.

Van Krevelen, D. W. 1990. Properties of polymers – Their correlation with chemical structure; their numerical estimation and prediction from additive group contributions. Elsevier, Amsterdam. 875 pp.

5. DEFORMATION MICROMECHANICS OF THE FIBER/ MATRIX INTERPHASE IN CELLULOSE-FIBER/POLYMER COMPOSITES: CONTRIBUTIONS OF INTERFACIAL CHEMISTRY

5.1. Chapter Summary

This study was conducted to examine the effects of fiber/polymer interfacial chemistry on the interfacial micromechanics of cellulose-fiber/polystyrene composites. Different interfacial chemistries were created by bonding polystyrene (a common amorphous polymer) to fibers whose surfaces contained different functional groups. The chemical compatibility within the interphase was evaluated by matching the solubility parameters (δ) between the polymer and the induced functional groups. The physico-chemical interactions within the interphase were determined using the Lifshitz-van der Waals work of adhesion (W_a^{LW}) and the acid-base interaction parameter (I_{a-b}). The micromechanical properties of the fiber/polymer interphase were evaluated using a novel micro-Raman tensile test. The results show that the maximum interfacial shear stress, a manifestation of practical adhesion, can be increased by increasing the (I_{a-b}) or reducing chemical incompatibility ($\overline{\Delta\delta}$) between the fibers and polymer. A modified diffusion model was employed to predict, with considerable success, the contribution of interfacial chemistry to the practical adhesion of cellulose-based fibers and amorphous polymers. Such achievements, coupled with the existing knowledge of the bulk properties of fibers and matrix polymer, ultimately leads to a better engineering of composite properties.

5.2. Introduction

Lignocellulosic-fiber/polymer composites have gained increasing attention because of the many advantageous features of these products. From the standpoint of polymer utilization, inclusion of tough and light-weight lignocellulosic fibers improves the strength-to-weight ratio of the composites. Moreover, addition of such renewable and biodegradable fibrous materials enhances the environmental-friendliness of the composite products. From the perspective of wood or biomaterial utilization, combining fibers with a less biodegradable polymer reduces the dependence on certain environmentally hazardous preservatives such as copper chrome arsenate (CCA). Additionally, the enormous opportunities in matching lignocellulosic fibers with a wide variety of polymers expand the range of end-uses for the resulting wood-hybrid products.

The integrity of fiber/polymer composites is of utmost importance in ensuring that the intended functions of the composites can be realized. For example, once a fiber/matrix system is chosen to design a composite of desired modulus, the interfacial bonding ensures that these two phases stay intact. That the fiber/matrix interphase provides fiber/polymer composites their structural integrity is well recognized (Chamis 1974). The fiber/matrix interphase allows the load to transfer from the matrix to the embedded fibers which sustain the load, sparing the composites from failure. Indeed, the transverse tensile strength (carbon-fiber/epoxy composites; Hoecker and Karger-Kocsis 1996) and the flexural strength (glass-fiber/polypropylene composites; Thomason and Schoolenberg 1994) of the composites have been reported to increase

with an increase of the micromechanical interfacial shear strength, a manifestation of the load transfer ability at the interphase.

The ability of an interphase to transfer load from one phase to another depends on the fiber/matrix adhesion, which can be physico-chemical or frictional in nature. The frictional contribution to adhesion is primarily a result of the Poisson contraction between the fiber and matrix, differential thermal contraction of the fiber and matrix upon cooling from the processing temperature, and surface roughness of the fiber (Kim and Mai 1998). The physico-chemical contribution, on the other hand, involves molecular interactions between the fibers and matrix, such as intermolecular forces (Brewis and Briggs 1985), transcrystallinity at the interphase, and glass transition of the matrix polymer in the presence of the fibers (Schultz and Nardin 1994). While the frictional contribution dominates in some ceramic matrix composites (Kim and Mai 1998), the physico-chemical contribution is considerably important in polymer matrix composites (Schultz and Nardin 1994).

For a given fiber/matrix system, the physico-chemical interactions at the interphase can be manipulated to enhance the mechanical performance of the composites. For example, wood fibers grafted with styrene molecules exhibited an improved tensile strength property in the resulting wood-fiber/polystyrene composites compared to the untreated fibers. This improvement is attributed to the interaction between benzene rings of the induced molecules and the matrix polymer at the interphase (Maldas *et al.* 1988). In another case, cellulose fibers that were treated with

the basic aminosilane formed composites of improved tensile strength property with the acidic, plasticized polyvinyl chloride (PVC). Such property enhancement is a consequence of the enhanced acid-base interaction at the interphase (Matuana *et al.* 1998).

5.3. Literature Review

5.3.1. Fundamental and Practical Adhesion

The term "adhesion" refers to the state in which two materials are held together by interfacial forces such that mechanical force or work can be transferred across the interface region (Wu 1982). The intermolecular interactions at the fiber/matrix interphase result in fundamental adhesion. Fundamental adhesion can be characterized using the thermodynamic or reversible work of adhesion (W_a), which is the amount of work under reversible or equilibrium conditions to disjoin the interface between bonded bodies (Mittal 1975). The basic relation between the interfacial interaction and fundamental adhesion is expressed by the Young-Dupré equation (Berg 1993):

$$W_a = \gamma_l (1 + \cos\theta), \tag{5.1}$$

where γ_l is the surface tension of the matrix polymer and θ is the contact angle of a liquid (or polymer) on the adherend.

As opposed to fundamental adhesion, practical adhesion is a measure of mechanical strength associated with irreversibly fracturing the adhesive bond (Mittal 1975). Examples of practical adhesion are peel strength and interfacial shear strength. Although these parameters are normally referred as "adhesion strength" or simply "adhesion", the measured values depend not only on molecular interaction, but also on other factors such that some researchers doubt the ability of the measured values to indicate (fundamental) adhesion (Dutschk *et al.* 1998). For a simple illustration, the Griffith criterion for linear-elastic materials in plane stress is used to express interfacial fracture:

$$f = \left(\frac{E_{12} G_a}{\pi \, a} \right)^{1/2}, \tag{5.2}$$

where the symbols f, G_a, and a, respectively refer to the fracture stress, the interfacial fracture energy, and the half-length of the central interfacial crack. The symbol E_{12} is a composite elastic modulus expressed as:

$$E_{12} = \frac{E_1 E_2}{\phi_1 E_2 + \phi_2 E_1}, \tag{5.3}$$

where E_1 and E_2 are the respective elastic modulus of the fiber and matrix polymer, while ϕ_1 and ϕ_2 are the respective fractional lengths of the fiber phase and matrix

phase. Equations 5.2 and 5.3 clearly show that the measured (practical) adhesion strength (f) is influenced by the interfacial bonding (fracture energy) and also the flaw size and viscoelestic properties of the two phases. Furthermore, for interfacial failure, the fracture energy (G_a) consists of two major components: the reversible work of adhesion (W_a) and the irreversible plastic work (W_p) or viscoelastic dissipation due to plastic yielding (Wu 1982):

$$G_a = W_a + W_p . \tag{5.4}$$

The plastic work is highly rate- and temperature-dependent, and it is usually several orders of magnitude greater than the reversible work of adhesion. Therefore, the measured practical adhesion, in either interfacial fracture energy or fracture stress (strength), is dominated by the viscoeleastic dissipation thereby, obscuring any manifestation of (fundamental) adhesion.

The credential of the measured (practical) bond strength in indicating (fundamental) adhesion was partially restored with the demonstration that interfacial fracture energy can be expressed in the form of product (Kinloch 1987):

$$G_a = W_a \, \Phi_v(\dot{a}T\varepsilon), \tag{5.5}$$

where $\Phi_v(\dot{a}T\varepsilon)$ is the mechanical loss function that depends on the crack growth rate ($\dot{a}$), temperature (T), and the strain level in the adhesive (ε). Therefore, if composite

preparation and mechanical testing are performed in a constant manner and condition to attain constant $\dot{a}$, T, and ε, and care is taken to identify the failure path as interfacial, the measured fracture energy (G_a) for a set of bonding systems should be indicative of (fundamental) adhesion (Harding and Berg 1997). Likewise, the practical bond strength (such as interfacial shear strength and peel strength) should also provide information on (fundamental) adhesion. Indeed, Wu (1982) demonstrated, using one adhesive (epoxy) on a series of polymer solids, that the (practical) adhesion bond strength (σ) is (linearly) related to the work of adhesion:

$$\sigma = k_1 W_a - k_2, \tag{5.6}$$

where k_1 and k_2 are constants that are a function of the composite elastic modulus (E_{12}), the fracture energy (G_a) of the system, and the size of unwetted interfacial defects at zero spreading coefficient.

To sum up the review of this section, fundamental and practical adhesion cannot be compared but if the practical bond strength is evaluated under a fixed protocol for a series of bonding systems, the measured values should correlate with (fundamental) adhesion. In addition, fundamental and practical adhesion should be distinguished to avoid confusions. In this paper, the practical bond strength will be inferred from the maximum interfacial shear stress, and it will be referred to, from time to time, as "the extent of adhesion" or "the level of adhesion", both of which are a manifestation of

practical adhesion. For parameters that characterize fundamental adhesion, such as the work of adhesion and other indicators, which will be reviewed in the next section, the names of the parameters will be mentioned directly.

5.3.2. Various Thermodynamic Indicators of (Fundamental) Adhesion

As an alternative to fiber/polymer contact angles whose measurement can be tedious and subjective, the work of adhesion can also be expressed as the sum of the dispersive (LW or Lifshitz-van der Waals) and Lewis acid-base (AB) components (Fowkes 1962 and Fowkes 1983):

$$W_a = W_a^{LW} + W_a^{AB}. \tag{5.7}$$

The parameter W_a^{LW} in Equation 5.7 can be calculated from the respective Lifshitz-van der Waals component of the surface free energy of the polymer adhesive (γ_l^{LW}) and the solid adherend (γ_s^{LW}) based on Fowkes (1962):

$$W_a^{LW} = 2\sqrt{\gamma_s^{LW}\gamma_l^{LW}}. \tag{5.8}$$

On the other hand, W_a^{AB} in Equation 5.7 can be estimated from ΔH^{AB}, the enthalpy of acid-base adduct formation at the interface (Fowkes and Mostafa 1978):

$$W_a^{AB} = fN\left(-\Delta H^{AB}\right), \tag{5.9}$$

if the number of moles (N) of accessible acid-base sites per interfacial area and the factor (f) that converts the $N\left(-\Delta H^{AB}\right)$ enthalpy quantity to the free energy value are known.

Because of the uncertainties in determining f and N in Equation 5.9, many researchers bypassed the measurement of W_a^{AB} and instead, used an acid-base interaction parameter (I_{a-b}; Park and Donnet 1998):

$$I_{a-b} = K_{A,f}K_{B,m} + K_{B,f}K_{A,m}, \tag{5.10}$$

where the subscripts f and m are, respectively, for fibers and matrix, while K_A and K_B are the Lewis acid parameter and the Lewis basic parameter determined from inverse gas chromatography. These researchers discovered that the parameter exhibited a strong linear relationship with the interfacial shear strength and the interlaminar shear strength of carbon-fiber/epoxy composites. In Chapter 2, cellulose/polystyrene acid-base interactions were examined by observing the specific adsorption of the polymer building block (ethylbenzene) onto fibers of different surface chemistry. The resulting values ($-\Delta H^{AB}$) were found to be closely correlated to I_{a-b} (Figure 2.4):

$$I_{a-b} = 0.03\left(-\Delta H^{AB}\right) + 0.04, \text{ or}$$

$$-\Delta H^{AB} = 33.3 I_{a-b} - 1.3, \text{ or}$$

$$-\Delta H^{AB} = k_3 I_{a-b} - k_4, \tag{5.11}$$

where k_3 and k_4 are empirical constants. Based on Equations 5.9 and 5.11, a general relationship among W_a^{AB}, $-\Delta H^{AB}$, and I_{a-b} can be summarized as follows:

$$W_a^{AB} \alpha \; -\Delta H^{AB} \alpha \; I_{a-b}. \tag{5.12}$$

Therefore, the strong correlation between the interfacial shear strength and I_{a-b} reported in the published literature is an implication of a strong dependence of the practical adhesion strength to W_a^{AB} (see Equation 5.12).

Diffusion is another interaction that may take place at the fiber/polymer interphase. The diffusion process is based on the thermodynamics of mixing which requires a negative value of the free energy of mixing (ΔG_m) for molecular mixing to occur:

$$\Delta G_m = \Delta H_m - T\Delta S_m, \tag{5.13}$$

where ΔS_m is the entropy of mixing which is generally positive, and ΔH_m is the enthalpy of mixing. A condition that ensures $\Delta G_m < 0$ is to have ΔH_m approaching 0

which can be attained when the respective solubility parameters (δ) of the two substances are close to each other (Hildebrand and Scott 1950):

$$\Delta H_m = V\phi_1\phi_2(\delta_1 - \delta_2)^2, \tag{5.14}$$

where V is the total volume of the system, ϕ is the volume fractions, while the subscripts 1 and 2 refer to components 1 and 2.

The solubility parameter concept was refined by Hansen (1969) to alleviate the poor ability of $(\delta_1 - \delta_2)^2$ in accounting for specific interactions between molecules. An improved version of the chemical incompatibility ($\overline{\Delta\delta}$) is as follows:

$$\overline{\Delta\delta} = \sqrt{(\delta_{d,1} - \delta_{d,2})^2 + (\delta_{p,1} - \delta_{p,2})^2 + (\delta_{h,1} - \delta_{h,2})^2}, \tag{5.15}$$

where δ_d, δ_p, and δ_h, respectively, refer to the dispersion, polar, and hydrogen-bonding contributions to the solubility parameters. Therefore, Equation 5.14 becomes:

$$\Delta H_m = V\phi_1\phi_2(\overline{\Delta\delta})^2. \tag{5.16}$$

The solubility parameter approach was qualitatively applied by Liu (1994) to explain the effects of weight percent gain (WPG) of wood fibers, grafted with styrene-maleic anhydride (SMA) copolymer, on the interfacial shear strength of the resulting

wood-fiber/polystyrene composites. In the study of Liu (1994), the (fundamental) adhesion mechanism was considered to consist of two processes: (1) interfacial adsorption of the matrix polymer onto the fibers, and (2) interdiffusion across the fiber/matrix interface. With a few assumptions, which were summarized in Appendix B, the following equation for the free energy of adhesion (ΔG_{adh}) was established:

$$-\Delta G_{adh} = -V\phi_1\phi_2(\delta_1 - \delta_2)^2 - \Delta H^{AB}. \qquad (5.17)$$

In short, the (fundamental) adhesion should increase by increasing ($-\Delta G_{adh}$), and this can be achieved, according to Equation 5.17, by either increasing the chemical compatibility (decreasing the difference in δ) or increasing the acid-base interactions ($-\Delta H^{AB}$) between the fibers and the polymer.

A quantitative application of the solubility parameter concept to filler/polymer adhesion was demonstrated by Miller *et al.* (2000) who estimated the enhancement of bonding between poly(butyral) and glass bead surfaces treated with ten different silane coupling agents. These researchers performed detailed computations of the free energy of mixing (ΔG_m) based on the solubility parameters and the effective molar volumes of the polymer repeating unit and silane organofunctional groups in the interfacial layer. They found a positive linear relationship between the computed $-\Delta G_m$ and the practical adhesion strength for bonding systems that are capable of engaging in acid-base, van der Waals, and oriented dipole interactions. However, the concept of thermodynamic mixing seemed to underestimate the practical adhesion in the bonding

systems that were, considered by the researchers, to be capable of forming an interpenetrating network (for phenylamino- and triamino-silanated fillers) or covalent bonds (for methacryloxy-silanated fillers).

Although there have been cases of success in accounting interfacial chemistry for the practical bond strength, the attribute does not seem to apply in every instance even for a given fiber/polymer pair and processing system. For acid-base matching, Beshay and Hoa (1990) formed compression-molded composites using amino-silanated wood fibers and polystyrene which are both basic in Lewis sense, but they observed an improvement in tensile strength property, which implied an enhanced fiber/polymer (practical) adhesion compared to the untreated fibers. Therefore, the contribution of interfacial chemistry to lignocellulosics/polymer practical adhesion is not entirely understood. If such understanding can be improved, one can better predict (practical) adhesion strength based on component surface chemistry. From this knowledge, surfaces of a given pair of fibers and matrix polymer can be tailored by surface modification to optimize fiber/matrix (practical) adhesion. Such a privilege, coupled with the existing knowledge of the bulk properties of fibers and matrix polymers, ultimately leads to a better engineering of the properties of the lignocellulosic/polymer composites.

This study was intended to examine the effects of interfacial chemistry on the interfacial micromechanics of cellulose-fiber/polymer composites. Polystyrene was chosen as the matrix because it is a common amorphous polymer, and its atactic

configuration was used in order to avoid interfacial transcrystallinity which would also affect the micromechanics of the fiber/polymer interphase. The interfacial chemistry was represented by chemical compatibility (solubility parameters) and physico-chemical interactions (Lifshitz-van der Waals work of adhesion and the acid-base interaction parameter). The interfacial micromechanics were manifested by the maximum shear stress identified from the stress distribution profile along the fiber/polymer interphase.

5.4. Materials and Methods

5.4.1. Materials and Sample Preparation

The fibers used in this study were regenerated cellulose fibers solvent-spun from wood pulp. These Lyocell fibers, 12 micrometers in diameter, were provided by Acordis Cellulosic Fibers (Tencel^{R}). The polystyrene, acquired from PolySciences Inc., was of 125,000-250,000 weight average molecular weight. The styrene-maleic anhydride block copolymer, also obtained from PolySciences Inc., was of 50 weight-% styrene content, 1600 g/mol number average molecular weight, and 480 acid number. The trialkoxysilanes used for fiber surface modification were of phenyl [$-C_6H_5$], phenylamine [$-(CH_2)_3NHC_6H_5$], amine [$-(CH_2)_3NH_2$], and octadecyl [$-(CH_2)_{17}CH_3$] functionalities, and they were acquired from Gelest, Inc.

Fibers were cleaned by Soxhlet-extraction for 12 hours using HPLC-grade methanol. For silane deposition, a dosage of 0.005 M was pre-hydrolyzed in methanol of 95 volume-% after which fibers were soaked for 20 minutes. The detailed experimental procedures were described in a previous study (Chapter 2). For grafting with styrene-maleic anhydride (SMA) copolymer, the reaction was conducted at 100°C for five hours, as described in detail in another paper (Chapter 4).

5.4.2. Calculations of Solubility Parameters

The solubility parameters of the induced functional groups were calculated based on Hoy (1985)'s method that assigned contributions of structural groups to the increment of molar attractions and molar volumes of amorphous polymers (Table 5.1). The organofunctional group of each coupling agent in this study was divided into several structural groups (Table 5.2). The group contribution for each of these structural groups was summed up to calculate for the solubility parameter and its components. An example of such calculations was included in Appendix C.

For SMA-grafted fibers, it was assumed that the interacting anhydride group in the copolymer forms an ester linkage with the fiber at the underlayer of the grafted molecules, and a free carboxylic group (Figure 5.1). The formation of such a mono-ester was reported in the grafting of maleated polypropylene on lignocellulosic fibers (Matuana *et al.* 2001). It was further assumed that the anhydride groups away from the fibers are converted to two carboxylic groups, and these groups, together with the

Table 5.1 Group contributions to the molar attraction function for calculating solubility parameters (Hoy 1985).

	F_t (J cm^3)$^{1/2}$/mol	F_p (J cm^3)$^{1/2}$/mol	V (cm^3/mol)	$\Delta_T^{(P)}$
$-CH_3$	303.5	0	21.55	0.022
$-CH_2-$	269	0	15.55	0.020
$-\overset{\vert}{C}H-$	176	0	9.56	0.013
CH_{aromatic}	241	62.5	13.42	0.018
C_{aromatic}	201	65	7.42	0.015
$-NH_2$	464	464	17	0.035
-NH-	368	368	11	0.0275
-COOH	565	415	26.1	0.039

Note: from Van Krevelen (1990), where constants in SI units were tabulated.

F_t = molar attraction function

F_p = polar component of the molar attraction function

V = molar volume

$\Delta_T^{(P)}$ = Lyderson correction for non-ideality for an amorphous polymer

Table 5.2 Functional groups used for the calculation of solubility parameters of the composite materials in the experiments.

.Composite material	Functional group
Polystyrene	1 CH_2, 1 CH, 5 $CH_{aromatic}$, and 1 $C_{aromatic}$
Cellulose:	
Aminopropyl-silanated	3 CH_2 and 1 NH_2
Phenylaminopropyl-silanated	3 CH_2, 5$CH_{aromatic}$, 1 $C_{aromatic}$, and 1 NH
Phenyl-silanated	5$CH_{aromatic}$ and 1 $C_{aromatic}$
Octadecyl-silanated	1 CH_3 and 17 CH_2
SMA-grafted	1 CH_2, 3 CH, 5 $CH_{aromatic}$, 1 $C_{aromatic}$, and 2 COOH

Note: SMA is the acronym for styrene-maleic anhydride copolymer; see text for the justification of using such a group combination for calculating the solubility parameter components of the SMA-grafted fibers.

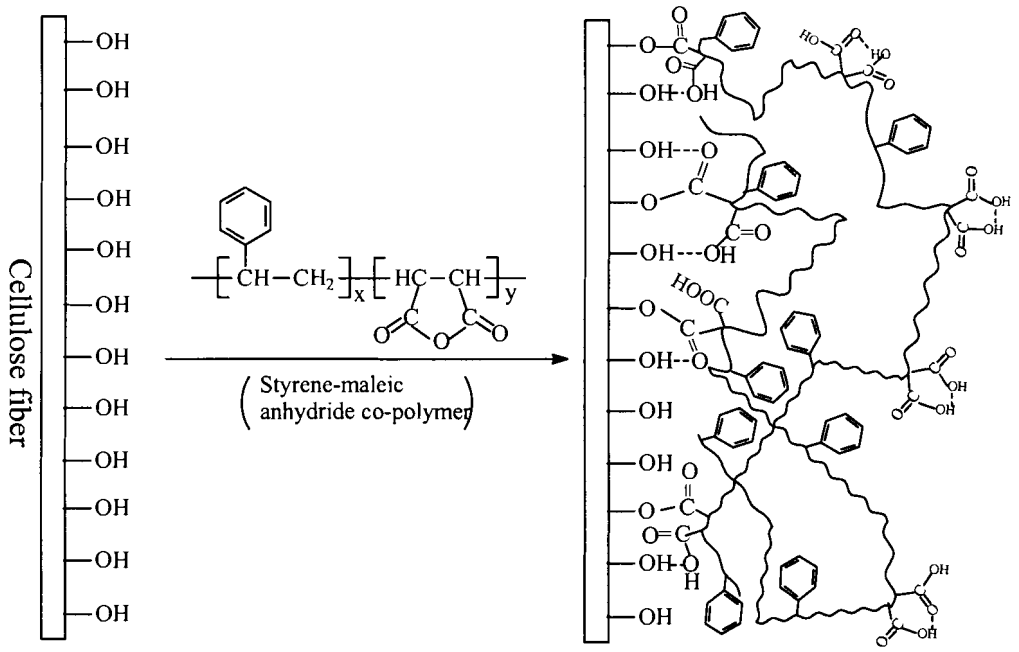

Figure 5.1 A schematic reaction for the grafting of styrene molecules onto cellulose fibers.

styrene molecules, were the effective species influencing the solubility parameter at the fiber/matrix interphase. These groups were taken into consideration in the calculation of the solubility parameter of the SMA-grafted fibers (Table 5.2).

5.4.3. Inverse Gas Chromatography (IGC)

The fiber or polymer samples were packed into a Teflon column for IGC measurements, which were performed at a temperature range of 25°C and 45°C. From the retention data of non-polar and acid-base probes, the London dispersive component

of the surface free energy ($\gamma^d \approx \gamma^{LW}$) was determined, and using the probe polarizability as the molecular descriptor, the free energies and enthalpies of specific adsorption were calculated. The acidic and basic parameters (K_A and K_B) of the fiber surfaces could then be determined by matching K_A with the donor number (*DN*; in kJ/mol), and K_B with the acceptor number (*AN**; in kJ/mol) of the probes. The Lifshitz-van der Waals work of adhesion (W_a^{LW}) and acid-base interaction parameter (I_{a-b}) were then calculated for each pair of fibers and polymer matrix (Equations 5.8 and 5.10). A detailed account of the experimental procedures and calculations was described in Chapter 2.

5.4.4. Micro-Raman Tensile Test

This technique was described in detail in Chapters 3 and 4. In brief, polystyrene was deposited from solution onto single fibers. These samples were scanned, using a Raman micro-spectrometer, at a five-micrometer interval along the axis of the fiber in the embedded region. The 895 cm^{-1} band of the cellulose spectra was analyzed for frequency shift. A frequency shift of 0.44 cm^{-1} was found to correspond to 100 MPa in tensile stress (Chapter 3). This frequency shift could thus be converted to local axial stress. The slope of the tensile stress profile at any point ($\frac{d\sigma_f}{dx}$) along the fiber/polymer interphase was then calculated to determine the distribution of shear stress (τ):

$$\tau = \frac{r}{2}\frac{d\sigma_f}{dx}, \tag{5.18}$$

where r is the fiber radius and σ_f is the tensile stress on the fiber. The maximum shear stress (τ_{max}) was identified from the stress distribution profile along the fiber/polymer interphase. Previous studies (Chapter 4) showed that the maximum shear stress corresponding to 1% applied strain level, i.e. prior to matrix fracture, can be used as a measure of fiber/polymer (practical) adhesion.

5.5. Results and Discussion

5.5.1. Solubility Parameters and the Fiber/Polymer Interfacial Compatibility

Table 5.3 lists the solubility parameter components of fibers calculated based on the contributions of the functional groups induced upon chemical treatments. The functionalilties were considered the effective species interacting with the matrix polymer, and therefore the calculated solubility parameters reflect the interfacial compatibility when matched against the solubility parameters of the matrix polymer (polystyrene). Although these solubility parameters were calculated under the ideal assumption that the fiber surfaces were completely covered with the coupling agents or grafted molecules, no efforts were made in this study to provide for evidence of

Table 5.3 Solubility parameter (in $J^{1/2}/cm^{3/2}$) of the organofunctional groups induced onto cellulose surfaces and their comparisons with the matrix polymer.

	Total, δ_t	Dispersive, δ_d	Polar, δ_p	Hydrogen bonding, δ_h	Incompatibility [b], $\overline{\Delta\delta}_{polystyrene-cellulose}$
Polystyrene	19.3	16.7	8.25	5.15	--
Cellulose:					
Untreated [a]	38.6	24.3	19.9	22.5	22
Amino-silanated	20.8	15.6	11.4	7.72	4.2
Phenylamino-silanated	20.3	16.2	10.1	6.94	2.6
Phenyl-silanated	19.6	16.2	9.53	5.78	1.5
Octadecyl-silanated	17.8	17.8	0	0	9.8
SMA-grafted	20.3	15.6	11.4	6.11	3.5

Note: [a] Data from Hansen and Björkman (1998) who used dextran as a model for cellulose.

[b] Calculated based on $\overline{\Delta\delta} = \sqrt{(\delta_{d,1} - \delta_{d,2})^2 + (\delta_{p,1} - \delta_{p,2})^2 + (\delta_{h,1} - \delta_{h,2})^2}$ from Equation 5.15, where the subscripts 1 and 2, respectively, refer to polystyrene and cellulose fibers.

complete coverage. Instead, the calculated solubility parameters were merely used as relative values, which should allow us to compare the chemical compatibility between different fiber/polymer systems.

The incompatibility between cellulose and polystyrene is clearly shown from their respective solubility parameter values: 38.6 $J^{1/2}/cm^{3/2}$ for cellulose (Hansen and Björkman 1998) and 19.3 $J^{1/2}/cm^{3/2}$ for polystyrene (Table 5.3). The cellulose/polystyrene compatibility can be increased by reducing the solubility parameter of the cellulose surface to match that of polystyrene. Indeed, all coupling agents or copolymers containing phenyl molecules in this study display an improved compatibility, with $\overline{\Delta\delta}$ less than 4 $J^{1/2}/cm^{3/2}$. Notable is the aminopropyl silane which is anticipated to provide polar sites for acid-base interactions, also simultaneously provides cellulose a favorable compatibility with polystyrene ($\overline{\Delta\delta}$ < 5 $J^{1/2}/cm^{3/2}$). On the other hand, silanation with the non-polar octadecyl functionality is expected to reduce the solubility parameter of cellulose excessively, rendering a compatibility improvement that is not as good as other groups introduced in this study.

5.5.2. Surface Chemistry of Fibers and Polymer

The London dispersive characteristics of the samples, determined using inverse gas chromatography (IGC), are presented in Table 5.4. The Lyocell fibers have a dispersive surface free energy (γ_S^d) of 49 mJ/m^2 when linearly extrapolated to 20°C. This value is close to that of microfibrous cellulose (47 mJ/m^2; extrapolated to 20°C)

Table 5.4 The London dispersive component of the surface free energy (in mJ/m^2) of polystyrene and cellulose fibers.

	This study		Published literature [b]	
	γ_S^d at 20°C [a]	Rel. γ_S^d	γ_S^d from DCA	Rel. γ_S^d
Polystyrene	55.8 ± 1.3	1.14	34.8	1.36
Cellulose:				
Untreated	49.0 ± 1.0	--	25.5	--
Amino-silanated	45.5 ± 0.8	0.93		
Phenylamino-silanated	41.4 ± 0.8	0.84		
Phenyl-silanated	40.6 ± 0.6	0.83		
Octadecyl-silanated	38.2 ± 0.7	0.78		
SMA-grafted	47.7 ± 0.7	0.97		

Note: [a] Extrapolated value from IGC data obtained at 45°C, 35°C, and 25°C; average of two replicates.

[b] Data from Felix *et al.* (1993); the cellulose was 99% alpha-cellulose from bleached kraft pulp.

Rel. γ_S^d is the ratio between the mean γ_S^d of a material and the mean γ_S^d of the untreated cellulose.

DCA refers to dynamic contact angle analyses conducted at ambient temperature with diiodomethane as the non-polar probe liquid.

reported by Papirer *et al.* (2000). The dispersive surface free energy of polystyrene is 56 mJ/m^2, and such a high value (55 mJ/m^2) was also reported by Kontominas *et al.* (1994).

To facilitate comparisons to published literature that also investigated the γ_S^d values of both cellulose and polystyrene, we used the term relative γ_S^d, which is the ratio between γ_S^d of a material and the γ_S^d of the untreated cellulose (Table 5.4). Table 5.4 also shows the relative γ_S^d values of polystyrene based on dynamic contact angle analyses (Felix *et al.* 1993), which are normally performed at ambient temperature (~20°C) and commonly known to provide a smaller γ_S^d value (Fafard *et al.* 1994) compared to the IGC experiments. Despite the disagreement between IGC and DCA for the absolute values of γ_S^d, the DCA studies of Felix *et al.* (1993) revealed a relative γ_S^d value of 1.36 for polystyrene, which is close to the value obtained from the present study (1.14). For chemically modified fibers, the relative γ_S^d values were less than 1, indicating a reduction in the dispersive component of the surface free energy of cellulose fibers upon chemical modification. The alkyl-silane treatment, as expected, decreased γ_S^d values the most (lowest relative γ_S^d) because of the low-energy alkyl chains.

Table 5.5 lists the Lewis acid (K_A) and basic parameters (K_B) calculated from IGC data. Regenerated cellulose fibers have average K_A and K_B values of 0.36 and 0.39, respectively. Polystyrene was found to be less acidic (K_A = 0.28) but slightly

Table 5.5 Lewis acid-base characteristics of polystyrene and cellulose fiber surfaces.

Composite material	This study				Published literature	
	K_A	K_B	Rel. K_A	Rel. K_B	K_A	K_B
Polystyrene	0.28 ± 0.01	0.46 ± 0.03	0.79	1.18	0.09[a]	0.34[a]
Cellulose:						
Untreated	0.36 ± 0.01	0.39 ± 0.02	--	--	0.31[a]	0.24[a]
Amino-silanated	0.33 ± 0.01	0.52 ± 0.03	0.93	1.34	0.05 [a]	0.35 [a]
Phenylamino-silanated	0.32 ± 0.00	0.42 ± 0.02	0.90	1.08		
Phenyl-silanated	0.34 ± 0.01	0.43 ± 0.02	0.94	1.12		
Octadecyl-silanated	0.33 ± 0.01	0.27 ± 0.04	0.92	0.70		
SMA-grafted	0.42 ± 0.02	0.57 ± 0.04	1.17	1.48	0.39[b]	1.29[b]

Note: [a] Data from Felix *et al.* (1993); the cellulose was 99% alpha-cellulose from bleached kraft pulp.

[b] Data from Mukhopadhyay and Schreiber (1994); the SMA copolymer was of 26 weight percent maleic anhydride; no coating was performed on cellulose fibers.

The K_A and K_B values were averages of two replicates.

Rel. K_A or K_B are values relative to the mean K_A or mean K_B of the untreated cellulose.

more basic (K_B = 0.46) than cellulose fibers. The higher Lewis basicity for polystyrene is an indication of a higher tendency for donating electrons, and it can be attributed to its electron-rich, nucleophilic aromatic ring. Such an observation was supported by Felix *et al.* (1993), who reported a K_B value for polystyrene which was 1.4 times (in this study, 1.2; Table 5.5) the K_B value of the untreated fibers (Table 5.5). On the other hand, polystyrene is lower in Lewis acidity scale compared to cellulose because cellulose contains hydroxyl groups that carry proton-donating hydrogen atoms.

Fibers treated with silanes exhibited very similar K_A values (0.32-0.34; Table 5.5), and this was attributed to the acidic silicon atom (Harding and Berg 1997) or the uncondensed silanols (Si-OH). The relative K_B value of the fibers silanated with amino functional groups was larger than 1, hence suggesting an increase in Lewis basicity. Fibers deposited with phenyl-silane displayed surfaces of increased basicity, once again supporting that aromatic rings are relatively Lewis basic. For fibers that were silanated with the non-polar alkyl chains, a decrease in basicity is observed as expected.

Perhaps, more striking is the high acidity and basicity of the fibers grafted with styrene-maleic anhydride (SMA) copolymer (Table 5.5). The increased acidity can be attributed to the acidic carboxylic groups when the initial anhydride groups of the copolymer reacted (Figure 5.1). The largely increased basicity, on the other hand, is ascribed to the lone-paired electrons of the oxygen atoms in the carboxylic groups and the ester linkages on the grafted surface. A similar observation was reported by Coupas

et al. (1998) who found an excessive increase in Lewis basicity after grafting maleic-anhydride functionalized polypropylene onto lignocellulosic fibers. Other supporting evidence for the largely increased basicity of the SMA-grafted fibers is the high basicity of the copolymer itself (Table 5.5) as reported by Mukhopadhyay and Schreiber (1994) based on IGC studies.

5.5.3. Shear Stress Distribution and Maximum at the Fiber/Polymer Interphase

Figures 5.2 and 5.3 show the shear stress distributions, determined using the micro-Raman tensile tests, at the interphases between polystyrene and fibers treated with different surface modifying agents. The shear stress is not uniform along the fiber/polymer interphase. The maximum shear stress (τ_{max}) occurs near locations where the fiber entered and exited the polymer droplet.

Treatments of fibers with a silane of non-polar functionality (octadecyl) resulted in a fiber/polystyrene interphase of reduced interfacial shear stress (Figure 5.2), suggesting a reduction in practical adhesion. On the other hand, treatment with a silane of polar functionality (amine) having a reduced solubility parameter (from the initial 38.6 $J^{1/2}/cm^{3/2}$ to 20.8 $J^{1/2}/cm^{3/2}$; Table 5.3) resulted in an increased shear stress (load transfer) or (practical) adhesion between fibers and polystyrene (solubility parameter 19.3 $J^{1/2}/cm^{3/2}$). For fibers with induced phenyl groups, i.e. the phenylamino-silanated, phenyl-silanated, and styrene copolymer esterified fibers, the resulting interphases exhibited an almost similar distribution of shear stress which is larger than the

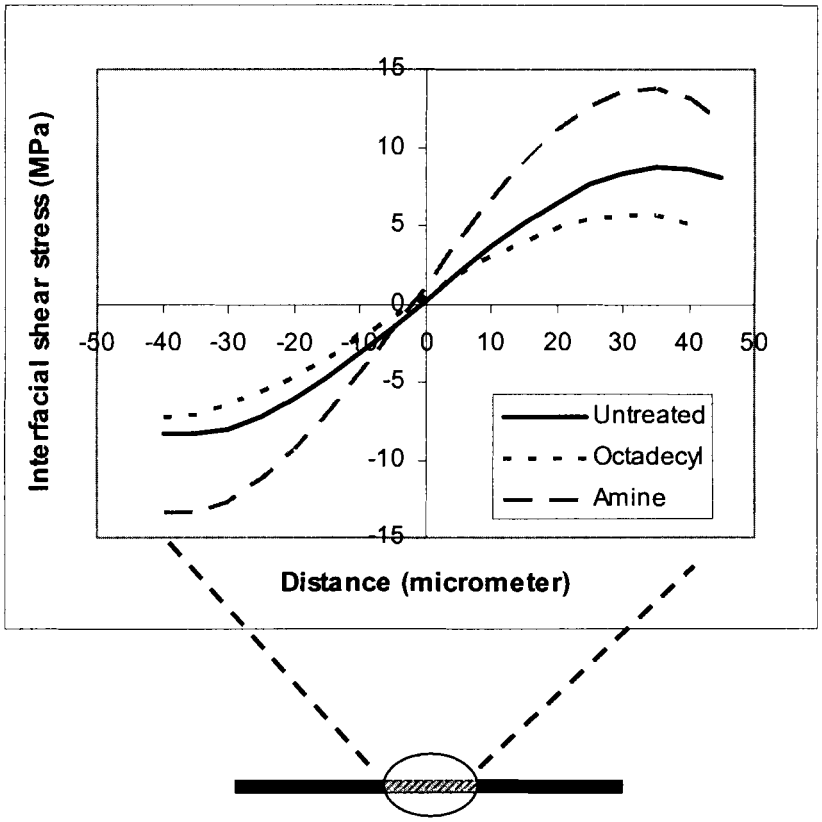

Figure 5.2 Shear stress along the interphases (at 1% global strain) between polystyrene and cellulose fibers treated with either non-polar (octadecyl-) or polar (amine-) functional silanes. Note: The data for untreated fibers were also plotted for comparisons.

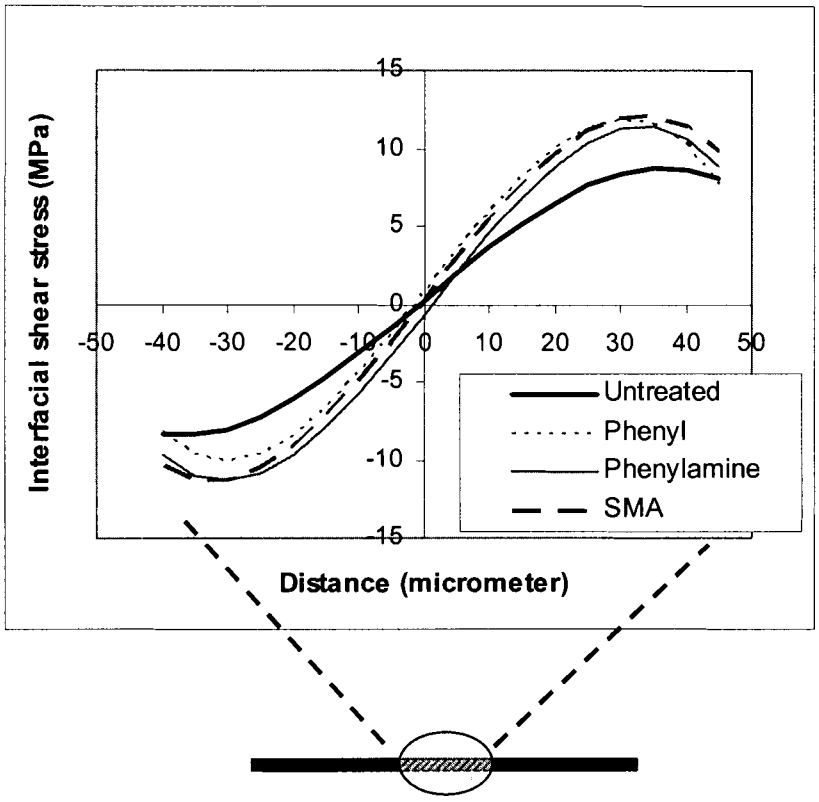

Figure 5.3 Shear stress along the interphases (at 1% global strain) between polystyrene and cellulose fibers treated with surface modifying agents that carry styrene molecules. Note: The data for untreated fibers were also plotted for comparisons.

shear stress in the case of untreated fibers (Figure 5.3). Therefore, the introduced phenyl group is the active group that interacts with polystyrene which also carries phenyl functionalities.

The maximum interfacial shear stress (τ_{max}) values of each bonding system are presented in Table 5.6. An immediate observation is the highest local stress transfer rate at the interphase involving polystyrene and amine-silanated fibers, suggesting the superior fiber/polystyrene (practical) adhesion. With this observation, it is interesting that the amine group in the phenylamino-silanated fibers did not appear to contribute to (practical) adhesion since these fibers demonstrated interfacial shear stress values that are similar to the phenyl-silanated fibers (Table 5.6). A possible explanation for this phenomenon is that in a phenylamino-silane molecule, the lone-paired electrons of the nitrogen atom interacts in resonance with the electron-rich phenyl ring. These electron-rich resonant structures, much like the phenyl groups in phenyl-silanes, are dominant in the interaction with polystyrene.

5.5.4. Effects of Interfacial Chemistry on the Maximum Shear Stress at the Fiber/Polymer Interphase

Correlation analyses were carried out to preliminarily examine whether the increase or decrease in the maximum interfacial shear stress (τ_{max}) was associated with the Lifshitz-van der Waals work of adhesion (W_a^{LW}), the acid-base interaction

Table 5.6 Maximum interfacial shear stress (at 1% applied strain) and the fiber/ matrix non-polar and polar interaction parameters.

Cellulose (Lyocell) fiber	Lifshitz-van der Waals work of adhesion, W_a^{LW} (mJ/m^2)	Lewis acid-base interaction parameter, I_{a-b}	Maximum interfacial shear stress, τ_{max} (MPa)
Untreated	105	0.27	9.3 (0.8) C
Amino-silanated	101	0.29	13.8 (1.2) A
Phenylamino-silanated	96	0.26	11.0 (1.2) B
Phenyl-silanated	95	0.27	11.8 (1.0) B
Octadecyl-silanated	92	0.22	8.0 (0.9) D
SMA-grafted	103	0.35	12.1 (1.0) B

Note: The W_a^{LW} and I_{a-b} values were calculated from γ_S^d, K_A, and K_B values (Tables 5.4 and 5.5). Their variabilities were $\pm$ 2.0 mJ/m^2 (for W_a^{LW}) and $\pm$ 0.01 (for I_{a-b}).

The τ_{max} averages were obtained from six replicates. Values in parenthesis are the standard deviations of the averages. The average values assigned with the same letters (i.e., A, B, C, or D) are not significantly different from one another at 95% confidence level, as tested based on the Student-Newman-Keul method using SigmaStat software. An exception is the statistical difference between the untreated and octadecyl-silanated fibers, whose confidence level is at 90%.

parameter (I_{a-b}), or the chemical incompatibility ($\overline{\Delta\delta}$) at the fiber/polymer interphase. Results of the analyses are expressed as the coefficient of correlations whose absolute values are between zero and one – the larger the value, the stronger the association .between two sets of data. The coefficients of correlation were 0.34 for W_a^{LW}, 0.69 for I_{a-b}, and -0.62 for the absolute values of ($\overline{\Delta\delta}$). The positive coefficient for I_{a-b} indicates that the maximum interfacial shear stress increased when the acid-base interaction was increased. The negative coefficient for ($\overline{\Delta\delta}$) implies that the maximum interfacial shear stress increased when the chemical incompatibility was reduced. The low value of the coefficient for W_a^{LW} suggests that the changes in the maximum interfacial shear stress are weakly correlated with the Lifshitz-van der Waals work of adhesion.

The interpretations from the correlation analyses do not imply that van-der Waals interactions are not important in the fiber/polymer adhesion. Instead, it is more reasonable that such interactions (92-105 mJ/m^2 in this study) contribute to the basic level of (fundamental) adhesion, which practically is more or less similar regardless of the interacting materials (Pisanova and Mäder 2000). Indeed, the differences in the level of adhesion in different fiber/polymer systems are a result of acid-base interactions. For example, Mangipudi *et al.* (1994) employed a surface forces apparatus to directly measure the work of adhesion of polyethylene (PE), a non-polar material, and polyethylene terephthalate (PET), a polar material. They found that the values of the work of adhesion for PE/PE and PE/PET, which are dominated by the Lifshitz-van

der Waals interactions, are quite similar, i.e. 66 and 77 mJ/m^2, respectively. However, for the PET/PET system, where acid-base interactions are also present, the work of adhesion exhibits a considerably high value of 122 mJ/m^2.

The preceding discussions suggest that further examinations are warranted of the effects of acid-base interactions on practical adhesion. Compared to the untreated fibers, amine-silanated fibers displayed a stronger acid-base interaction with polystyrene, hence also a stronger practical adhesion. This observation agreed with the finding of Beshay and Hoa (1990), who reported that amine silanation of wood fibers improved the tensile property of fiber/polystyrene composites. This observation, on the other hand, contradicted the study of Felix *et al.* (1993), where cellulose fibers pre-treated with amino-silanes yielded a fiber/polystyrene composite of inferior tensile strength. Such a discrepancy originated from the extent of silanation which influenced the surface chemical properties of the treated fibers. In the present study, the amine-silanated fibers had both acidic and basic characteristics although the basicity was more prominent (K_A=0.33; K_B = 0.52; Table 5.5). Such a bipolar characteristic enhances interactions with polystyrene, which is also bipolar (K_A=0.28; K_B = 0.46; Table 5.5) so that the acidic sites from the fibers can interact with the basic cites from the polystyrene, or vise versa. In the study of Felix *et al.* (1993), however, the amine-silanation was performed, presumably with a more complete surface coverage, to yield a monobasic surface (K_A = 0.05; K_B = 0.35; see Table 5.5). The monobasic surface

bonded poorly with polystyrene, which is weak in acidity. In brief, the above discussion reinstates the worthiness of measuring acid-base characteristics for understanding material interactions and predicting the properties of the composites.

Figure 5.4 plots the relationship between τ_{max} and I_{a-b}. The data points for all silanated fibers form a positive, linear trend line, showing an increase of the level of practical adhesion with the increase of acid-base interactions between cellulose fibers and polystyrene. The trend line, however, overestimates the untreated cellulose fibers and styrene copolymer esterified (SMA) fibers. The outlying nature of these two data points may be attributed to the fewer number of available or accessible sites for acid-base interactions. Indeed, noting from Equation 5.9, the number of sites participating in the acid-base interactions (N) is as important as the energy of the interactions ($-\Delta H^{AB}$ or I_{a-b}) in affecting the work of adhesion. The silanated fibers have increased acid-base sites because of the silane polymerized networks that could possibly form by attaching to merely a bonding site on the cellulose fibers. The general trend line observed for all silanated fibers is an indication that the silanes polymerized to more or less similar extents thereby, allowing similar accessibility for acid-base sites, leaving only I_{a-b} as the influencing factor for determining the extent of fiber/polymer adhesion. On the other hand, the grafted styrene copolymer is expected to form on fibers as chains of loops and tails that intermingle with one another. This typical polymeric nature resulted in an interphase that impeded polystyrene penetration and reduced accessible interaction sites.

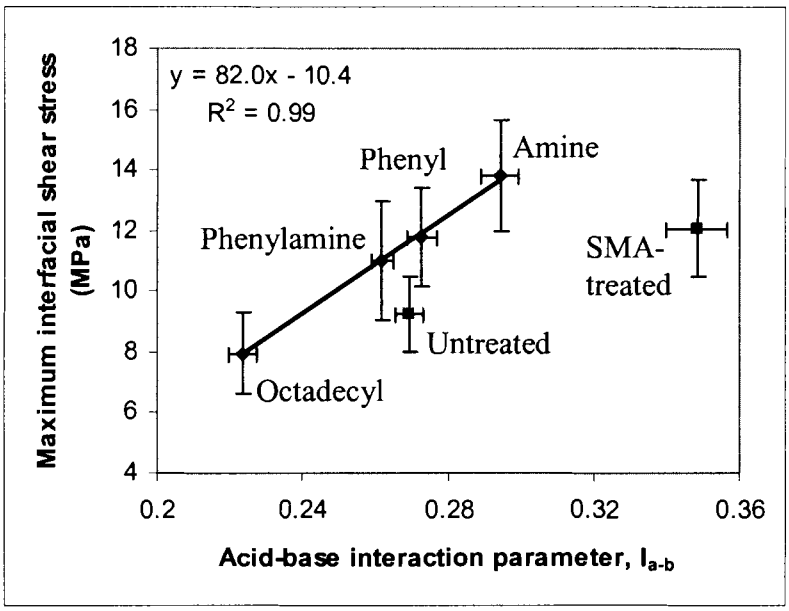

Figure 5.4 Effects of acid-base interaction on maximum interfacial shear stress. Note: Error bars correspond to the 95% confidence interval of the mean. The regression analysis did not include untreated and SMA-treated fibers.

In an attempt to account for the effects of penetration or interdiffusion at the fiber/polymer interphase, the chemical compatibility at the interphase was examined with respect to the level of practical adhesion. From the published literature, the silane/polymer interdiffusion, as determined by sputtered neutral mass spectrometry, was found to relate to the solubility parameters of the silane functional groups and the matrix polymer – the closer the solubility parameters of the two components, the higher the interdiffusion (Gentle *et al.* 1992). It was hypothesized that in adhesion, chemical compatibility has the role of ensuring a more intimate and a larger number of contacts between two interacting species to realize their potential interactions. Therefore, the subsequent attempt in this study was to examine how chemical compatibility influenced the effects of acid-base interactions on the fiber/polymer (practical) adhesion.

A model that relates (practical) adhesion to chemical compatibility and acid-base interactions is readily available from Equation 5.17. Based on Hansen's approach of incompatibility (Equation 5.15), Equation 5.17 can be rewritten as follows:

$$-\Delta G_{adh} = -V\phi_1\phi_2(\overline{\Delta\delta})^2 - \Delta H^{AB}. \tag{5.19}$$

A general expression was then made to relate the free energy of adhesion (ΔG_{adh}) and the maximum interfacial shear stress (τ_{max}), analogous to that established (Equation 5.6) by Wu (1982) for the relationship between fundamental and practical adhesion:

$$-\Delta G_{adh} = k_5 \tau_{\max} + k_6, \tag{5.20}$$

where k_5 and k_6 are empirical constants. By inserting Equations 5.12 and 5.20 into Equation 5.19, the following equation was derived:

$$k_5 \tau_{\max} + k_6 = -V\phi_1\phi_2(\overline{\Delta\delta})^2 + k_3 I_{a-b} - k_4, \text{ or}$$

$$\tau_{\max} = \left(\frac{-V\phi_1\phi_2}{k_5}\right)(\overline{\Delta\delta})^2 + \left(\frac{k_3}{k_5}\right) I_{a-b} + \left(\frac{-k_4 - k_6}{k_5}\right). \tag{5.21}$$

Multiple regression analyses can be performed based on Equation 5.21. All the k parameters in the equation are constant values. Therefore, if $V\phi_1\phi_2$ values are considerably constant for all the data points, a multiple regression analysis of $\tau_{\max}$ versus $(\overline{\Delta\delta})^2$ and I_{a-b} should result in a negative coefficient (slope) for $(\overline{\Delta\delta})^2$, a positive coefficient for I_{a-b}, and an intercept constant. Indeed, the regression results turned out as expected:

$$\tau_{\max} = -0.004\ (\overline{\Delta\delta})^2 + 30.4\ I_{a-b} + 3.0, \tag{5.22}$$

except that the correlation between $\tau_{\max}$ and both the $(\overline{\Delta\delta})^2$ and I_{a-b} is unsatisfactory, with a low R-square of 0.63. However, if the regression analysis was performed without the SMA-grafted fibers, the outcome of the regression analysis becomes:

$$\tau_{max} = -0.005\ (\overline{\Delta\delta})^2 + 75.0\ I_{a-b} - 8.4, \qquad (5.23)$$

with a high R-square of 0.99.

Table 5.7 shows values of the maximum interfacial shear stress predicted using Equation 5.23. The prediction was within a deviation of $\pm$ 0.5 MPa for the respective average τ_{max} for all silanated fibers. The prediction was also accurate for the untreated fibers, which earlier presented an outlying data point in Figure 5.4. This success is an indication that chemical compatibility between untreated fibers and polystyrene accounts for the number of accessible acid-base sites, which in turn, influences the effects of acid-base interactions on the fiber/polymer (practical) adhesion.

For SMA-grafted fibers, however, the prediction (Table 5.7) overestimates the practical adhesion level (by 6 MPa), hence suggesting that factors other than solubility parameters also come into play. To attain the experimental τ_{max} value, the measured I_{a-b} should be reduced by 20% of the measured value (from 0.34 to 0.27), or the multiplier for $(\overline{\Delta\delta})^2$ must be increased about 80 times (from -0.005 to -0.46). The first possibility implies that the I_{a-b} value, determined from the adsorption of small molecules in IGC studies, was overestimated for the polymer chain (in SMA-fibers) where accessibility is largely restrained because of steric effects. The second possibility implies that the $V\phi_1\phi_2$ value, hence the copolymer grafting density and interfacial volume, is excessively large thereby, based on Equations 5.13 and 5.14, resulted in

Table 5.7 Predicted maximum shear stress (τ_{max}) values for the cellulose-fiber/polystyrene interphase.

Cellulose (lyocell) fiber	Predicted maximum interfacial shear stress (MPa)	Accuracy of the prediction: predicted - experimental (MPa)
Untreated	9.4	0.1
Amino-silanated	13.3	-0.5
Phenylamino-silanated	11.1	0.1
Phenyl-silanated	11.8	0.0
Octadecyl-silanated	7.6	-0.4
SMA-grafted	17.8	5.7

Note: The prediction was based on: $\tau_{max} = -0.005\ (\overline{\Delta\delta})^2 + 75.0\ I_{a-b} - 8.4$ (Equation 5.23), using values of $\overline{\Delta\delta}$ from Table 5.3, and I_{a-b} from Table 5.6.

a decreased mixing. Lin *et al.* (1996), who bonded polystyrene to glass fibers that were pre-tethered with polystyrene chains, also reported that the densely attached polymeric chain reduced the penetration of the matrix chain, hence decreasing the interfacial toughness of the resulting composites. Both possibilities, nevertheless, support the earlier postulation that the adhesion between SMA-fibers and polystyrene is affected by the reduced accessibility of the matrix polystyrene to the acid-base interaction sites on the fibers.

Another possible reason for reduced accessibility which is not accounted for by the thermodynamic approach, i.e. $(\overline{\Delta\delta})^2$, $V\phi_1\phi_2$, or I_{a-b}, is the kinetic contribution. The interdiffusion of the styrene-copolymer and matrix polystyrene, though favored by the good chemical compatibility, may not be optimized considering the short time scale of the polymer droplet deposition and the fast solidification (solvent evaporation) process.

5.6. Conclusions

This study was conducted to examine the effects of interfacial chemistry on the maximum interfacial shear stress or practical adhesion level of the cellulose-fiber/polystyrene composites. The data show that the extent of practical adhesion can be increased by increasing the acid-base interaction parameter (I_{a-b}) and the chemical compatibility (reducing $\overline{\Delta\delta}$) between fibers and the matrix polymer. Therefore,

interfacial chemistry plays a central role in the practical adhesion between cellulose fibers and amorphous polymers. More importantly, the contributions of interfacial chemistry to practical adhesion can be predicted using a modified diffusion model where I_{a-b} is considered in addition to $\overline{\Delta\delta}$. The (practical) adhesion for SMA-grafted fibers was lower than estimated possibly because of the high grafting density which decreased matrix penetration, overestimation of the acid-base interaction parameter which did not account for steric effects, and kinetic contributions where the time scale of the polystyrene deposition and solidification process was too short for optimum interdiffusion. Overall, the predictability of the fiber/polymer practical adhesion has been enhanced. Such an achievement, coupled with the existing knowledge of the bulk properties of fibers and matrix polymer, ultimately leads to a better engineering of composite properties.

5.7. References

Berg, J. C. 1993. The importance of acid-base interactions in wetting, coating, adhesion, and related phenomena. Nordic Pulp and Paper Research Journal. 1:75-85.

Beshay, A. and S. V. Hoa. 1990. Reinforcement of polyvinyl chloride (PVC) and polystyrene (PS) with cellulosic fibers treated with silane. Journal of Thermoplastics Composite Materials. 3:264-274.

Brewis, D. M. and D. Briggs. 1985. An overview. Pages 1-14 in D.M. Brewis and D. Briggs, eds. Industrial adhesion problems. John Wiley and Sons, New York.

Chamis, C. C. 1974. Mechanics of load transfer at the interface. Pages 31-77 in E. P. Plueddemann, ed. Interfaces in polymer matrix composites. Academic Press, New York.

Coupas, A. –C., H. Gauthier, and R. Gauthier. 1998. Inverse gas chromatography as a tool to characterize ligno-cellulosic fibers modified for composite applications. Polymer Composites. 19(3):280-286.

Dutschk, V., E. Pisanova, S. Zhandarov, and B. Lauke. 1998. "Fundamental" and "practical" adhesion in polymer-fiber systems. Mechanics of Composites Materials. 34(4):309-320.

Fafard, M., M. El-Kindi, H. P. Schreiber, G. Dipaola-Baranyi, and A. M. Hor. 1994. Estimating surface energy variations of solid by inverse gas chromatography. Journal of Adhesion Science and Technology. 8(12):1383-1394.

Felix, J. M., P. Gatenholm, and H. P. Schreiber. 1993. Control interactions in cellulose-polymer composites: I. Effect on mechanical properties. Polymer Composites. 14(6):449-457.

Fowkes, F. M. 1962. Determination of interfacial tensions, contact angles and dispersion forces in surfaces by assuming additivity of intermolecular interaction in surfaces. Journal of Physical Chemistry. 66:382.

Fowkes, F. M. 1983. Acid-base interactions in polymer adhesion. Pages 583-603 in K. L. Mittal, ed. Physicochemical aspects of polymer surfaces. Vol. 2. Plenum Press, New York.

Fowkes, F. M. and M. A. Mostafa. 1978. Acid-base interactions in polymer adsorption. Industry Engineering and Chemistry: Products Research and Development. 17(1):3-7.

Gentle, T. E., R. G. Schmidt, B. M. Naasz, A. J. Gellman, and T. M. Gentle. 1992. Organofunctional silanes as adhesion promoters: direct characterization of the polymer/silane interphase. Journal of Adhesion Science and Technology. 6(2):307-316.

Hansen, C. M. 1969. The universatility of the solubility parameter. Industry Engineering and Chemistry: Products Research and Development. 8(1):2-11.

Hansen, C. M. and A. Björkman. 1998. The ultrastructure of wood from a solubility parameter point of view. Holzforschung. 52:335-344.

Harding, P. H. and J. C. Berg. 1997. The role of adhesion in the mechanical properties of filled polymer composites. Journal of Adhesion Science and Technology. 11(4):471-493.

Hildebrand, J. and R. L. Scott. 1950. The solubility of nonelectrolytes. 3rd edition. Reinhold, New York. 488 pp.

Hoecker, F. and J. Karger-Kocsis. 1996. Surface energetics of carbon fibers and its effects on the mechanical performance of CF/EP composites. Journal of Applied Polymer Science. 59:139-153.

Hoy, K. L. 1985. The Hoy tables of solubility parameters. Solvent and Coatings Materials Research and Development Department, Union Carbide Corporation, South Charleston, WV, USA. 144 pp.

Kim, J. and Y. Mai. 1998. Engineered interfaces in fiber reinforced composites. Elsevier, Oxford, U. K. 401 pp.

Kinloch, A. J. 1987. Adhesion and adhesive science and technology. Chapman and Hall, New York. 441 pp.

Kontominas, M. G., R. Gavara, and J. R. Giacin. 1994. The adsorption of hydrocarbons on polystyrene by inverse gas chromatography: infinite dilution concentration region. European Polymer Journal. 30(2):265-269.

Lin, R., R. P. Quirk, J. Kuang, and L. S. Penn. 1996. Toughening of impenetrable interfaces by monodisperse tethered polymer chains: effect of areal attachment density. Journal of Adhesion Science and Technology. 10(4):341-349.

Liu, P. F. 1994. Characterizing interfacial adhesion between wood fibers and a thermoplastic matrix. Ph.D. dissertation. West Virginia University. Morgantown, WV., USA. 170 pp.

Maldas, D., B. V. Kokta, R. G. Raj, and C. Daneault. 1988. Improvement of the mechanical properties of sawdust wood fiber-polystyrene composites by chemical treatment. Polymer. 29:1255-1265.

Mangipudi, V., M. Tirrell, and A. V. Pocius. 1994. Direct measurement of molecular level adhesion between poly(ethylene terephthalate) and polyethylene films: determination of surface and interfacial energies. Journal of Adhesion Science and Technology. 8(11):1251-1270.

Matuana, L. M., R. T. Woodhams, J. J. Balatinecz, and C. B. Park. 1998. Influence of interfacial interactions on the properties of PVC/cellulosic fiber composites. Polymer Composites. 19(4):446-455.

Matuana, L. M., J. J. Balatinecz, R. N. S. Sodhi, and C. B. Park. 2001. Surface characterization of esterified cellulosic fibers by XPS and FTIR spectroscopy. Wood Science and Technology. 35:191-201.

Miller, A. C., M. T. Knowlton, and J. C. Berg. 2000. The use of UNIFAC for the estimation of adhesion enhancement between polymers and mineral surfaces treated with silane coupling agents. Journal of Adhesion Science and Technology. 14(12):1471-1484.

Mittal, K. L. 1975. Surface chemical criteria for maximum adhesion and their verification against the experimentally measured adhesive strength values. Pages 129-171 in L. Lee, ed. Adhesion science and technology. Plenum Press, New York.

Mukhopadhyay, P. and H. P. Schreiber. 1994. Aspects of polymer surface characterization by inverse gas chromatography. Journal of Polymer Science: Part B: Polymer Physics. 32:1653-1656.

Papirer, E., E. Brendle, H. Balard, and C. Vergelati. 2000. Inverse gas chromatography investigation of the surface properties of cellulose. Journal of Adhesion Science and Technology. 14(3):321-337.

Park, S. J. and J. B. Donnet. 1998. Anodic surface treatment on carbon fibers: Determination of acid-base interaction parameter between two unidentical solid surfaces in a composite system. Journal of Colloid and Interface Science. 206:29-32.

Pisanova, E. and E. Mäder. 2000. Acid-base interactions and covalent bonding at a fiber-matrix interface: contribution to the work of adhesion and measured adhesion strength. Journal of Adhesion Science and Technology. 14(3):415-436.

Schultz, J. and M. Nardin. 1994. Some physico-chemical aspects of the fibre-matrix interphase in composite materials. Journal of Adhesion. 45:59-71.

Thomason, J. L. and G. E. Schoolenberg. 1994. An investigation of glass fibre/polypropylene interface strength and its effect on composite properties. Composites. 25(3):197-203.

Wu, S. 1982. Polymer interface and adhesion. Marcel Dekker, New York. 630 pp.

6. CONCLUSIONS AND RECOMMENDATIONS

6.1. Conclusions

The overall objective of this dissertation was to gain an understanding of the relationship between interfacial chemistry and the micromechanics of the cellulose-fiber/polymer composites. Regenerated cellulose (lyocell) fibers and polystyrene were chosen as the fiber/matrix combination. The fibers were treated with amine-, phenylamine-, phenyl-, and octadecyl-silanes, and also styrene-maleic anhydride (SMA) copolymer.

Inverse gas chromatography indicates that all the treatments examined in this study reduced the dispersive component of the surface free energy of the cellulose fibers from 49 mJ/m^2 to average values that ranged from 38-48 mJ/m^2. Fibers esterified with styrene-maleic anhydride (SMA) copolymer displayed an increase in the average K_A value from 0.36 (untreated) to 0.42. Fibers treated with silanes exhibited very similar Lewis acid characters (K_A = 0.32-0.34), and this could be contributed by the acidic silicon atom or the uncondensed silanols (Si-OH). Overall, the different types of chemical treatments performed in this study produced fibers whose mean K_B values spanned from 0.27 to 0.57. These fibers of different surface chemistry were expected to form interphases of different chemical natures with the polystyrene matrix.

The adsorption of ethylbenzene onto cellulose fibers with different surface-chemical properties reveals that the enthalpies of specific adsorption ($-\Delta H_A^{sp}$) are closely correlated to the interaction parameter (I_{a-b}) values which were calculated by matching the K_A and K_B values between fibers and the matrix polymer. This observation implies that the fiber/matrix acid-base interaction can be conveniently predicted from the respective acid-base characters (K_A and K_B) of the components prior to forming a composite.

The concept of solubility was also used to predict chemical compatibility at the fiber/polymer interphase. The solubility parameter for cellulose suggested by Hansen based on dextran is 38.6 $J^{1/2}/cm^{3/2}$ while the solubility parameter for polystyrene calculated from the Hoy approach was 19.3 $J^{1/2}/cm^{3/2}$, hence demonstrating an incompatibility between the two materials. The cellulose/polystyrene compatibility could be increased by introducing phenyl molecules onto cellulose, as evidenced from the low values of the incompatibility parameters ($\overline{\Delta\delta} < 4$ $J^{1/2}/cm^{3/2}$) calculated for phenyl-silane, phenylamino-silane, and the styrene copolymer. All other surface-modifying agents in this study have organofunctional groups that display $\overline{\Delta\delta}$ values (incompatibility with polystyrene) of up to 10 $J^{1/2}/cm^{3/2}$.

The Raman micro-spectroscopic studies demonstrate that the local tensile strain and stress are not uniform along the fiber/polymer interphase. The interfacial strain and stress are highest at the edge of the droplet, and these values tend to decline from the edge region to the middle region of the drop. The maximum of these local strains

corresponds to a strain-control fracture of the matrix polymer. The minimum of the local tensile stress corresponds to the extent of fiber-to-matrix load transfer whose efficiency should also be indicative of the matrix-to-fiber load transfer in practical applications of fiber-reinforced composites. The slope of the tensile stress profile along the interface region allows for an estimation of the maximum interfacial shear stress which is indicative of the level of fiber/polystyrene adhesion. As such, a novel micro-Raman tensile technique has been established for evaluating the practical adhesion of a potentially wide range of fiber/polymer systems, especially for combinations involving ductile fibers and brittle polymers such as the lyocell/polystyrene system in the present study.

The micro-Raman tensile techniques provided maximum interfacial shear stress values of 8.0 to 13.8 MPa, ranking functional groups of fibers according to their practical adhesion to polystyrene: alkyl< untreated < phenyl = phenylamine = styrene copolymer < amine. Overall, the fiber/polymer adhesion can be increased by increasing the acid-base interactions (I_{a-b}), or reducing the chemical incompatibility ($\overline{\Delta\delta}$) between the fibers and matrix. Therefore, interfacial chemistry plays a central role in the practical adhesion of cellulose-fibers and polystyrene. These conclusions should also be applicable to wood-plastic composites involving lignocellulosic fibers and amorphous polymers.

An important implication from this study is that the contributions of interfacial chemistry to (practical) adhesion can be predicted using a modified diffusion model. The model, though failed to predict the (practical) adhesion between polystyrene and fibers grafted with styrene-maleic anhydride molecules (SMA), still provided a framework for explaining the anomaly. The practical adhesion of SMA-grafted fibers was lower than estimated possibly because of the high grafting density which decreased matrix penetration, overestimation of the acid-base interaction parameter which did not account for steric effects, and kinetic contributions where the time scale of the polystyrene deposition and solidification process was too short for optimum interdiffusion. Overall, the predictability of the fiber/polymer practical adhesion has been enhanced.

6.2. Recommendations for Future Studies

This dissertation employed a molecular approach (chromatography and spectroscopy) in relating interfacial chemistry and micromechanics. The next step in the composite engineering design, which is recommended for future studies, is to produce composites under the conditions of the optimized practical adhesion so that the mechanical performance of the composite system can be evaluated and further optimized.

Another recommended investigation is to examine the grafting of copolymer with different maleic anhydride (MA) contents and molecular weights. High MA content coupling is expected to result in a better coverage of the fiber surfaces, while high molecular weight coupling is anticipated to cause a brush-like interphase that is more likely to engage in molecular entanglement with the matrix polymer (Snijder and Bos 1999). Studying these different types of interphases at different grafting intensities (weight percent gain) should shed light to the efforts of accounting interfacial volume fraction for predicting (practical) adhesion using the modified diffusion model.

Another important study is to subject the micro-composites to heat and water to investigate the hygrothermal attack on the fiber/polymer interphase. For example, the attack of water is expected to result in fiber (restraint) swelling at the interphase which should be manifested from the changes in interfacial stresses if Raman mapping is performed. Also, stress relaxation at the fiber/polymer interphase can be potentially studied by collecting Raman spectra at a fixed location at the interphase as a function of time while holding a strained fiber in position. The outputs of these investigations are expected to provide insights on how the fiber/polymer interphase responds to environmental attack.

The other worthwhile investigation is to study crystalline polymers such as polyethylene and polypropylene whose crystallinity can be nucleated by the fibers at the fiber/polymer interphase. Collecting Raman spectra of cellulose along the fiber/polymer interphase, as performed in the present study, will allow examination of

the stress distributions and adhesion at the interphase. On the other hand, collecting spectra of polymer across the fiber/polymer interphase will allow determination of the gradients of the crystallinity degrees at the interphase. Indeed, the peak intensities of the 808 cm^{-1}, 830 cm^{-1}, and 840 cm^{-1}bands of polypropylene have been employed to determine its degree of crystallinity and the results approximated 93% of the values determined using the differential scanning calorimetry (Nielsen *et al.* 2002).

6.3. References

Nielsen, A. S., D. N. Batchelder, and R. Pyrz. 2002. Estimation of crystallinity of isotactic polypropylene using Raman spectroscopy. Polymer 43:2671-2676

Snijder, M. H. B. and H. L. Bos. 1999. Reinforcement of commodity plastics by annual plant fibers: optimization of the coupling agent efficiency. Pages 123-129 in Proceedings of the Fifth International Conference on Woodfiber-Plastic Composites. Forest Products Society, Madison, WI, USA.

REFERENCES

Ahmad, H. and M. Yaseen. 1979. Application of a chemical group contribution technique for calculating solubility parameters of polymers. Polymer Engineering and Science. 19(12):858-863.

Atalla, R. and B. E. Dimick. 1975. Raman-spectral evidence for differences between the conformations of cellulose I and cellulose II. Carbohydrate Research. 39:C1-C3.

Balard, H., E. Brendle, and E. Papirer. 2000. Determination of the acid-base properties of solid surfaces using inverse gas chromatography: advantages and limitations. Pages 299-316 in K. L. Mital, ed. Acid-base interactions: Relevance to adhesion science and technology. Vol. 2. VSP, Zeist, The Netherlands.

Banwell, C. N. 1972. Fundamentals of molecular spectroscopy. 2nd edition. McGraw-Hill, London. 348 pp.

Berg, J. C. 1993. The importance of acid-base interactions in wetting, coating, adhesion, and related phenomena. Nordic Pulp and Paper Research Journal. 1:75-85.

Beshay, A. and S. V. Hoa. 1990. Reinforcement of polyvinyl chloride (PVC) and polystyrene (PS) with cellulosic fibers treated with silane. Journal of Thermoplastics Composite Materials. 3:264-274.

Beshay, A. and S. V. Hoa. 1992. Improved interface bonding between cellulosic fibers and thermoplastics. Science and Engineering of Composite Materials. 2(2):85-97.

Brewis, D. M. and D. Briggs. 1985. An overview. Pages 1-14 in D.M. Brewis and D. Briggs, eds. Industrial adhesion problems. John Wiley and Sons, New York.

Cave, N. G. and A. J. Kinloch. 1992. Self-assembling monolayer silane films as adhesion promoters. Polymer. 33(6):1162-1170.

Chamis, C. C. 1974. Mechanics of load transfer at the interface. Pages 31-77 in E. P. Plueddemann, ed. Interfaces in polymer matrix composites. Academic Press, New York.

Clemons, C. 2002. Wood-plastic composites in the United States: The interfacing of two industries. Forest Products Journal. 52(6):10-18.

Conder, J. R. and C. L. Young. 1979. Physicochemical measurements by gas chromatography. Wiley-Interscience, New York. 632 pp.

Coupas, A. –C., H. Gauthier, and R. Gauthier. 1998. Inverse gas chromatography as a tool to characterize ligno-cellulosic fibers modified for composite applications. Polymer Composites. 19(3):280-286.

Cox, H. L. 1952. The elasticity and strength of paper and other fibrous materials. British Journal of Applied Physics. 3:72-79.

Defosse, M. 1999. Processors focus on differentiation in window profiles. Modern Plastics. Sept.:74-79.

Desiraju, G. R. and T. Steiner. 1999. The weak hydrogen bond in structural chemistry and biology. Oxford University Press, Oxford. 508 pp.

Donnet, J. B., S. J. Park, and H. Balard. 1991. Evaluation of specific interactions of solid surfaces by inverse gas chromatography. Chromatographia. 31(9/10):434-440.

Dorris, G. M. and D. G. Gray. 1980. Adsorption of n-alkanes at zero surface coverage on cellulose paper and wood fibers. Journal of Colloids and Interface Science. 77(2):353-362.

Drzal, L. T. 1990. The role of the fiber-matrix interphase on composite properties. Vacuum. 41(7-9):1615-1618.

Dutschk, V., E. Pisanova, S. Zhandarov, and B. Lauke. 1998. "Fundamental" and "practical" adhesion in polymer-fiber systems. Mechanics of Composites Materials. 34(4):309-320.

Eckert, C. 2000. Opportunities for natural fibers in plastic composites. In: Proceedings, Progress in Woodfibre-Plastic Composites Conference 2000. University of Toronto, Toronto.

Egan, A. and S. M. Shaler. 2000. Fracture and mechanics of fracture for resin coated single wood fibers. Pages 95-103 in G. Hague, M. McLauchlin, and T. Skinner, eds. Proceedings of the Fourth Panel Products Symposium. The Biocomposites Centre, Bangor, U.K.

Eichhorn, S. J., M. Hughes, R. Snell, and L. Mott. 2000. Strain induced shifts in the Raman spectra of natural cellulose fibers. Journal of Materials Science Letters. 19:721-723.

Eichhorn, S. J. and R. J. Young. 2001. The Young's modulus of a crystalline cellulose. Cellulose. 8:197-207.

Eichhorn, S. J., J. Sirichaisit, and R. J. Young. 2001a. Deformation mechanisms in cellulose fibres, paper and wood. Journal of Materials Science. 36:3129-3135.

Eichhorn, S. J., R. J. Young, and W.–Y. Yeh. 2001b. Deformation processes in regenerated cellulose fibers. Textile Research Journal. 71(2):121-129.

Erickson, P. W. and E. P. Plueddemann. 1974. Historical background of the interfaces – Studies and theories. Pages 1-29 in E. P. Plueddemann, ed. Interfaces in polymer matrix composites. Academic Press, New York.

Fafard, M., M. El-Kindi, H. P. Schreiber, G. Dipaola-Baranyi, and A. M. Hor. 1994. Estimating surface energy variations of solid by inverse gas chromatography. Journal of Adhesion Science and Technology. 8(12):1383-1394.

Fan, C. F., D. A. Waldman, and S. L. Hsu. 1991. Interfacial effects on stress distribution in model composites. Journal of Polymer Science: Part B: Polymer Physics. 29:235-246.

Felix, J. M., P. Gatenholm, and H. P. Schreiber. 1993. Control interactions in cellulose-polymer composites: I. Effect on mechanical properties. Polymer Composites. 14(6):449-457.

Felix, J. M., P. Gatenholm, and H. P. Schreiber. 1994. Plasma modification of cellulose fibers: effects on some polymer composite properties. Journal of Applied Polymer Science. 51:285-295.

Flory, P. J. 1942. Thermodynamics of high polymer solutions. Journal of Chemical Physics. 10:51-61.

Fowkes, F. M. 1962. Determination of interfacial tensions, contact angles and dispersion forces in surfaces by assuming additivity of intermolecular interaction in surfaces. Journal of Physical Chemistry. 66:382.

Fowkes, F. M. 1983. Acid-base interactions in polymer adhesion. Pages 583-603 in K. L. Mittal, ed. Physicochemical aspects of polymer surfaces. Vol. 2. Plenum Press, New York.

Fowkes, F. M. and M. A. Mostafa. 1978. Acid-base interactions in polymer adsorption. Industry Engineering and Chemistry: Products Research and Development. 17(1):3-7.

Franko, A., K. C. Seavey, J. Gumaer, and W. G. Glasser. 2001. Continuous cellulose fiber-reinforced cellulose ester composites III. Commercial matrix and fiber option. Cellulose. 8:171-179.

Gaur, U. and B. Miller. 1989. Microbond method for determination of the shear strength of a fiber/resin interface: Evaluation of experimental parameters. Composites Science and Technology. 34:35-51.

Gauthier, R., C. Joly, A. C. Coupas, H. Gauthier, and M. Escoubes. 1998. Interfaces in polyolefin/cellulosic fiber composites: chemical coupling, morphology, correlation with adhesion and aging in moisture. Polymer Composites. 19(3):287-300.

Gentle, T. E., R. G. Schmidt, B. M. Naasz, A. J. Gellman, and T. M. Gentle. 1992. Organofunctional silanes as adhesion promoters: direct characterization of the polymer/silane interphase. Journal of Adhesion Science and Technology. 6(2):307-316.

Gu, X. and R. J. Young 1997. Deformation micromechanics in model carbon fiber reinforced composites. Part II. The microbond test. Textile Research Journal. 67(2):93-100.

Gutmann, V. and E. Wychera. 1966. Coordination reactions in non aqueous solutions – The role of the donor strength. Inorganic and Nuclear Chemistry Letters. 2:257-260.

Gutmann, V. 1968. Coordination chemistry in non-aqueous solutions. Springer-Verlag, New York. 174 pp.

Hansen, C. M. 1969. The universatility of the solubility parameter. Industry Engineering and Chemistry: Products Research and Development. 8(1):2-11.

Hansen, C. M. and A. Björkman. 1998. The ultrastructure of wood from a solubility parameter point of view. Holzforschung. 52:335-344.

Harding, P. H. and J. C. Berg. 1997. The role of adhesion in the mechanical properties of filled polymer composites. Journal of Adhesion Science and Technology. 11(4):471-493.

Herrera-Franco, P. J. and L. T. Drzal. 1992. Comparison of methods for the measurement of fiber/matrix adhesion in composites. Composites. 23:2-27.

Hiemenz, P. C. and R. Rajagopalan. 1997. Principles of colloid and surface chemistry. 3rd edition. Marcel Dekker, New York. 650 pp.

Hildebrand, J. and R. L. Scott. 1950. The solubility of nonelectrolytes. 3rd edition. Reinhold, New York. 488 pp.

Hoecker, F. and J. Karger-Kocsis. 1996. Surface energetics of carbon fibers and its effects on the mechanical performance of CF/EP composites. Journal of Applied Polymer Science. 59:139-153.

Hoy, K. L. 1985. The Hoy tables of solubility parameters. Solvent and Coatings Materials Research and Development Department, Union Carbide Corporation, South Charleston, WV, USA. 144 pp.

Huggins, M. L. 1942. Theory of solutions of high polymers. Journal of the American Chemical Society. 64:1712-1719.

Kamdem, D. P. and B. Riedl. 1991. IGC characterization of PMMA grafted onto CTMP fiber. Journal of Wood Chemistry and Technology. 11(1):57-91.

Katz, S. and D. G. Gray. 1981. The adsorption of hydrocarbons on cellophane. I. Zero coverage limit. Journal of Colloid and Interface Science. 82:318-325.

Kim, J. and Y. Mai. 1998. Engineered interfaces in fiber reinforced composites. Elsevier, Oxford, U. K. 401 pp.

Kinloch, A. J. 1987. Adhesion and adhesive science and technology. Chapman and Hall, New York. 441 pp.

Kontominas, M. G., R. Gavara, and J. R. Giacin. 1994. The adsorption of hydrocarbons on polystyrene by inverse gas chromatography: infinite dilution concentration region. European Polymer Journal. 30(2):265-269.

Liang, B., L. Mott, S. M. Shaler, and G. T. Caneba. 1994. Properties of transfer-molded wood-fiber/polystyrene composites. Wood and Fiber Science. 26(3):382-389.

Lin, R., R. P. Quirk, J. Kuang, and L. S. Penn. 1996. Toughening of impenetrable interfaces by monodisperse tethered polymer chains: effect of areal attachment density. Journal of Adhesion Science and Technology. 10(4):341-349.

Liu, P. F. 1994. Characterizing interfacial adhesion between wood fibers and a thermoplastic matrix. Ph.D. dissertation. West Virginia University. Morgantown, WV., USA. 170 pp.

Liu, P. F., T. G. Rials, M. P. Wolcott, and D. J. Gardner. 1996. Interactions between wood fibers and amorphous polymers. Pages 74-81 in Woodfiber-plastic composites: Virgin and recycled wood fiber and polymers for composites. Forest Products Society, Madison, WI., USA.

Luner, P. and M. Sandell. 1969. The wetting of cellulose and wood hemicellulose. Journal of Polymer Science: Part C. 28:115-142.

Maldas, D., B. V. Kokta, R. G. Raj, and C. Daneault. 1988. Improvement of the mechanical properties of sawdust wood fiber-polystyrene composites by chemical treatment. Polymer. 29:1255-1265.

Mangipudi, V., M. Tirrell, and A. V. Pocius. 1994. Direct measurement of molecular level adhesion between poly(ethylene terephthalate) and polyethylene films: determination of surface and interfacial energies. Journal of Adhesion Science and Technology. 8(11):1251-1270.

Mapleston, P. 2001. It's one hot market for profile extruders. Modern Plastics. June:49-52.

Matuana, L. M., R. T. Woodhams, J. J. Balatinecz, and C. B. Park. 1998. Influence of interfacial interactions on the properties of PVC/cellulosic fiber composites. Polymer Composites. 19(4):446-455.

Matuana, L. M., J. J. Balatinecz, C. B. Park, and R. N. S. Sodhi. 1999. X-ray photoelectron spectroscopy study of silane-treated newsprint-fibers. Wood Science and Technology. 33:259-270.

Matuana, L. M., J. J. Balatinecz, R. N. S. Sodhi, and C. B. Park. 2001. Surface characterization of esterified cellulosic fibers by XPS and FTIR spectroscopy. Wood Science and Technology. 35:191-201.

Mayer, U., V. Gutmann, and W. Gerger. 1975. The acceptor number – a qualitative empirical parameter for the electrophilic properties of solvents. Monatshefte für Chemie. 106:1235-1257.

Mayer, U. 1979. A semiempirical model for the description of solvent effects on chemical reactions. Pure and Applied Chemistry. 51:1697-1712.

Mead, R., R. N. Curnow, and A. M. Hasted. 1993. Statistical methods in agriculture and experimental biology. 2nd edition. Chapman and Hall, London. 415 pp.

Mercado, J. 1992. Using digital image analysis to determine the reinforcement of wood fiber polyurethane composites. M.S. thesis. Michigan Technological University, Houghton, MI, USA. 71 pp.

Miller, A. C., M. T. Knowlton, and J. C. Berg. 2000. The use of UNIFAC for the estimation of adhesion enhancement between polymers and mineral surfaces treated with silane coupling agents. Journal of Adhesion Science and Technology. 14(12):1471-1484.

Miller, T. M. 1997. Atomic and molecular polarizabilities. Pages 10-199-10-213 in D. R. Lide, ed. Handbook of chemistry and physics. 78th edition. CRC Press, New York.

Mittal, K. L. 1975. Surface chemical criteria for maximum adhesion and their verification against the experimentally measured adhesive strength values. Pages 129-171 in L. Lee, ed. Adhesion science and technology. Plenum Press, New York.

Mott, L., S. M. Shaler, and L. H. Groom. 1996. A technique to measure strain distributions in single wood pulp fibers. Wood and Fiber Science. 28(4):429-437.

Mukhopadhyay, P. and H. P. Schreiber. 1994. Aspects of polymer surface characterization by inverse gas chromatography. Journal of Polymer Science: Part B: Polymer Physics. 32:1653-1656.

Nielsen, A. S., D. N. Batchelder, and R. Pyrz. 2002. Estimation of crystallinity of isotactic polypropylene using Raman spectroscopy. Polymer. 43:2671-2676.

Papirer, E., E. Brendle, H. Balard, and C. Vergelati. 2000. Inverse gas chromatography investigation of the surface properties of cellulose. Journal of Adhesion Science and Technology. 14(3):321-337.

Park, S. J. and J. B. Donnet. 1998. Anodic surface treatment on carbon fibers: Determination of acid-base interaction parameter between two unidentical solid surfaces in a composite system. Journal of Colloid and Interface Science. 206:29-32.

Pisanova, E. and E. Mäder. 2000. Acid-base interactions and covalent bonding at a fiber-matrix interface: contribution to the work of adhesion and measured adhesion strength. Journal of Adhesion Science and Technology. 14(3):415-436.

Rials, T. G., M. P. Wolcott, and D. J. Gardner. 1998. Characterizing the wood fiber/polymer interface. Pages 31-39 in L. H. Groom and A. G. Zink, eds. Techniques in experimental mechanics applicable to forest products research. USDA Forest Service Southern Research Station, Asheville, NC.

Riddle, F. L. Jr. and F. M. Fowkes. 1990. Spectra shifts in acid-base chemistry. 1. van der Waals contributions to acceptor numbers. Journal of the American Chemical Society. 112(9):3259-3264.

Saint Flour, C. and E. Papirer. 1982. Gas-solid chromatography: a method of measuring surface free energy characteristics of short glass fibers. 2. Through retention volumes measured near zero surface coverage. Industrial & Engineering Chemistry: Product Research and Development. 21(4):666-669.

Saint Flour, C. and E. Papirer. 1983. Gas-solid chromatography: A quick method of estimating surface free energy variations induced by the treatment of short glass fibers. Journal of Colloid and Interface Science. 91:69-75.

Schultz, J., L. Lavielle, and C. Martin. 1987. The role of the interface in carbon-fiber epoxy composites. Journal of Adhesion. 23(1):45-60.

Schultz, J. and M. Nardin. 1994. Some physico-chemical aspects of the fibre-matrix interphase in composite materials. Journal of Adhesion. 45:59-71.

Scott, R. L. 1949. The thermodynamics of high-polymer solutions. IV. Phase equilibria in ternary system: polymer-liquid1-liquid 2. Journal of Chemical Physics. 17:268-279.

Sears, K. D., R. Jacobson, D. F. Caulfield, and J. Underwood. 2002. Reinforcement of engineering thermoplastics with high purity wood cellulose fibers. Pages 27-34 in Proceedings of the Sixth International Conference on Woodfiber-Plastic Composites. Forest Products Society, Madison WI., USA.

Shaler, S. M. 1993. Mechanics of the interface in discontinuous wood fiber composites. Pages 9-14 in M. P. Wolcott, ed. Wood-fiber/polymer composites: fundamental concepts, processes, and material options. Forest Products Society. Madison, WI., USA.

Smith, P. M. 2001. U.S. woodfiber-plastic composite decking market. Pages 13-17 in Proceedings of the Sixth International Conference on Woodfiber-Plastic Composites. Forest Products Society, Madison, WI, USA.

Snijder, M. H. B. and H. L. Bos. 1999. Reinforcement of commodity plastics by annual plant fibers: optimization of the coupling agent efficiency. Pages 123-129 in Proceedings of the Fifth International Conference on Woodfiber-Plastic Composites. Forest Products Society, Madison, WI, USA.

Suh, K. W. and D. H. Clarke. 1967. Cohesive energy densities of polymers from turbidimetric titrations. Journal of Polymer Science: Part A-1. 5:1671-1681.

Thomason, J. L. and G. E. Schoolenberg. 1994. An investigation of glass fibre/polypropylene interface strength and its effect on composite properties. Composites. 25(3):197-203.

Trejo-O'Reilly, J. A., J. Y. Cavaillé, M. Paillet, A. Gandini, P. Herrera-Franco, and J. Cauich. 2000. Interfacial properties of regenerated cellulose fiber/polystyrene composite materials. Effect of the coupling agent's structure on the micromechanical behavior. Polymer Composites. 21(1):65-71.

Tuinstra, T. and J. L. Koenig. 1970. Characterization of graphite fiber surfaces with Raman spectroscopy. Journal of Composite Materials. 4:492-499.

Van Krevelen, D. W. 1990. Properties of polymers – Their correlation with chemical structure; their numerical estimation and prediction from additive group contributions. Elsevier, Amsterdam. 875 pp.

Wu, S. 1982. Polymer interface and adhesion. Marcel Dekker, New York. 630 pp.

APPENDICES

Appendix A. Equations and Data Reduction Procedures for the Probe Polarizability Approach in the Inverse Gas Chromatographic Studies

In the probe polarizability approach of the inverse gas chromatographic (IGC) studies, the polarizability index is given by $[(h\nu_L)^{1/2}\alpha_{O,L}]$, where h is the Planck's constant (6.626 x 10^{-34} J s), ν is the characteristic electronic frequency (in s^{-1}) of the probe, α_O is the deformation polarizabilities (in C m^2 V^{-1}) of molecules, and the subscript L refers to the probe liquid. The energy term, $(h\nu)$, can be calculated from (Hiemenz and Rajagopalan 1997):

$$h\nu = \frac{1}{2\pi}\sqrt{\frac{e^2}{\alpha_O m_e}}, \tag{A1}$$

$$\text{or } h\nu = \frac{1}{2\pi}\sqrt{\frac{(1.602)^2}{\alpha_O 8.187}} x1.986x10^{-37} \tag{A2}$$

where e is the elementary charge (1.602 x 10^{-19} Coulomb), m_e is the mass of electron (9.109 x 10^{-31} kg or 8.187 x 10^{-14} J), α_O is in C m^2 V^{-1}, and the factor 1.986 is for converting the calculated $(h\nu)$ value to the unit of J. Equation A2 can be simplified to:

$$h\nu = \frac{5.56x10^{-38}}{\pi}\sqrt{\frac{1}{\alpha_O}} \tag{A3}$$

Based on Equation A3, the polarizability index (in $C^{3/2}$ m^2 $V^{-1/2}$) can be expressed as:

$$(h\nu)^{1/2}\alpha_O = \left[\frac{5.56x10^{-38}}{\pi}\sqrt{\frac{1}{\alpha_O}}\right]^{1/2}\alpha_O$$

$$\text{or } (h\nu)^{1/2}\alpha_O = 2.358x10^{-19}\frac{\alpha_O^{3/4}}{\sqrt{\pi}} \qquad \text{(A4)}$$

For ethylbenzene, the deformation polarizability (α_O) was given in the Chemistry Handbook (Miller 1997) as 14.2 x 10^{-24} cm^3 which can be converted to 1.580 x 10^{-39} C m^2 V^{-1} (1 cm^3 = 1.113 x 10^{-16} C m^2 V^{-1}). Using Equation A4, the polarizability index was calculated as 10.5 x 10^{-49} $C^{3/2}$ m^2 $V^{-1/2}$ (see Table 2.1). The values of $[(h\nu_L)^{1/2}\alpha_{O,L}]$ for other IGC probes in Table 2.1 had been calculated in the same way by Donnet *et al.* (1991).

Regardless of the molecular descriptors (vapor pressure, polarizability etc.), the total free energy of adsorption (ΔG_A; in kJ/mol) is generally expressed as (Dorris and Gray 1980):

$$\Delta G_A = -\frac{RT}{1000}\ln\left(\frac{V_N}{10^6}\frac{P_{s,g}}{S\pi_s}\right), \qquad \text{(A5)}$$

where R is the gas constant (8.3145 J K^{-1} mol^{-1}), T is the column temperature (in K), V_N is the net specific retention volume per gram of sample (in ml/g), S is the specific

surface area of the sample (in m^2/g), $P_{s,g}$ is the adsorbate vapor pressure in the gaseous standard state (1.013×10^5 Pa or N/m^2), and π_s is the surface or spreading pressure of the gas in the standard adsorption state (3.38×10^{-4} N/m according to De Boer's definition of the standard state, and 6.08×10^{-4} N/m according to Kemball and Rideal's definition; Mukhopadhyay and Schreiber 1994). The factor 1000 in the equation converts the energy unit from J to kJ, while the factor 10^6 converts the retention volume from ml to m^3. Using a constant, K_1, to represent the multiplication of V_N, S, $P_{s,g}$, π_s, and 10^{-6}, Equation A5 can be rewritten as:

$$\Delta G_A = -\frac{RT}{1000}\left(\ln V_N + \ln K_1\right), \text{ or}$$

$$-\Delta G_A = \frac{RT}{1000}\ln V_N + \frac{RT}{1000}\ln K_1, \text{ or}$$

$$-\Delta G_A = \frac{RT}{1000}\ln V_N + C, \qquad \text{(A6)}$$

where C represents $[10^{-3}\ RT \ln K_1]$, which is a constant value for the IGC column at a given temperature.

In the probe polarizability approach, the London dispersive interaction between an adsorbate (probe) and an adsorbent (solid sample) is equated to the potential energy of interaction between two non-identical molecules, expressed as (Donnet *et al.* 1991):

$$-\Delta G_A^d = \frac{1}{1000}\left[\frac{3}{4}\frac{N}{(4\pi\varepsilon_O)^2}\left(\frac{1}{r_{S.L}}\right)^6\right](h\nu_S)^{1/2}\alpha_{O,S}(h\nu_L)^{1/2}\alpha_{O,L}, \text{ or} \qquad \text{(A7)}$$

$$-\Delta G_A^d = \frac{K}{1000}(h\nu_S)^{1/2}\alpha_{O,S}(h\nu_L)^{1/2}\alpha_{O,L}, \qquad \text{(A8)}$$

where ΔG_A^d is the London dispersive component of the free energy (in kJ/mol) of adsorption, ε_O is the permittivity in vacuum (8.8542 x 10^{-12} C^2 J^{-1} m^{-1}), $r_{S,L}$ is the distance between adsorbent (solid; subscript S) and adsorbate (liquid; subscript L) molecules (assuming constant as 0.3 x 10^{-9} m), K in Equation A8 is the collective constant (in J^2 C^{-4} m^{-4} mol^{-1}) involving N, π, ε_O, and $r_{S,L}$ of Equation A7. The factor 1000 converts the energy unit from J to kJ.

For adsorption of non-polar probes, the London interaction (ΔG_A^d) is also the total free energy of adsorption of the probes (ΔG_A), and through substitution with Equations A6 and A8, the following equation is obtained:

$$-\Delta G_A = -\Delta G_A^d, \text{ or}$$

$$\frac{RT}{1000}\ln V_N + C = \left[\frac{K}{1000}(h\nu_S)^{1/2}\alpha_{O,S}\right](h\nu_L)^{1/2}\alpha_{O,L}. \qquad \text{(A9)}$$

Based on Equation A9, a linear regression can be performed on the plots of [$RT\ln V_N$] versus [$(h\nu_L)^{1/2}\alpha_{O,L}$] (the polarizability index tabulated in Table 2.1) for a series of n-alkanes (Figure 2.2). The intercept obtained will include the constant, C. The slope

obtained is the representation of $[K(h\nu_S)^{1/2}\alpha_{O,S}]$ which is related to the London dispersive component (γ_S^d) of the solid surface, and is characteristic of a given solid sample.

For adsorption of polar probes, the same regression constants established in the preceding paragraph can be used. The polarizability index $[(h\nu_L)^{1/2}\alpha_{O,L}]$ of the polar probe liquid (from Table 2.1) was inserted into the regression formulae to predict the value of $[RT\ln V_N]$, and hence Equation A9 can be more specifically expressed as:

$$\frac{RT}{1000}\ln V_N^{ref} + C = \left[\frac{K}{1000}(h\nu_S)^{1/2}\alpha_{O,S}\right](h\nu_{PL})^{1/2}\alpha_{O,PL}, \qquad \text{(A10)}$$

where the superscript ref means value predicted from the reference alkane line, and the subscript PL refers to polar probe liquid. Based on Equations A8, Equation A10 can be rewritten to express the $-\Delta G_A^d$ (in kJ/mol) of the polar-probe adsorption onto the solid samples:

$$\frac{RT}{1000}\ln V_N^{ref} + C = -\Delta G_A^d, \qquad \text{(A11)}$$

The specific, or Lewis acid-base, interaction of a polar probe [ΔG_A^{sp}; in kJ/mol] with the solid sample was calculated by subtracting the London dispersive component from the total free energy of adsorption:

$$\Delta G_A^{sp} = \Delta G_A - \Delta G_A^d, \text{ or}$$

$$-\Delta G_A^{sp} = (-\Delta G_A) - (-\Delta G_A^d) \qquad \text{(A12)}$$

By inserting Equations A6 and A11, Equation A12 becomes:

$$-\Delta G_A^{sp} = \left[\frac{RT}{1000}\ln V_N + C\right] - \left[\frac{RT}{1000}\ln V_N^{ref} + C\right]$$

$$= \left[\frac{RT}{1000}\ln V_N\right] - \left[\frac{RT}{1000}\ln V_N^{ref}\right]$$

$$= \frac{RT}{1000}\ln\frac{V_N}{V_N^{ref}} \qquad \text{(A13)}$$

The expression in Equation A13 (which is similar to Equation 2.7) is graphically depicted in Figure 2.2 [plots of $RT\ln V_N$ versus $(h\nu_L)^{1/2}\alpha_{O,L}$]. In the plots, the $-\Delta G_A^{sp}$ value is determined from the vertical difference between a point of [$RT\ln V_N$] and the corresponding alkane line.

Appendix B. A Modified Diffusion Model for Fundamental Adhesion

In the study of Liu (1994), the fundamental adhesion mechanism was considered to consist of two processes: (1) interfacial adsorption of the matrix polymer onto the fibers, and (2) interdiffusion (mixing) across the fiber/matrix interface. Therefore, the free energy of adhesion (ΔG_{adh}) is a summation of the free energies of adsorption (ΔG_A) and mixing (ΔG_m):

$$\Delta G_{adh} = \Delta G_A + \Delta G_m , \tag{B1}$$

The enthalpies of the two processes could then be summed up to obtain the enthalpy of adhesion (ΔH_{adh}):

$$\Delta H_{adh} = \Delta H_m + \Delta H_A , \text{ or}$$

$$\Delta H_{adh} = V\phi_1\phi_2(\delta_1 - \delta_2)^2 + \Delta H^{AB} \tag{B2}$$

where the first term of Equation B2 represents the enthalpy of diffusion or mixing (ΔH_m; given in Equation 5.14), and the second term of the equation refers to the enthalpy of adsorption (ΔH_A), which according to Fowkes and Mostafa (1978), is dominated by the acid-base interactions (ΔH^{AB}) in the case of non-polyolefin polymers and fillers.

The entropy of adhesion (ΔS_{adh}) could be summed up likewise, but the entropy of adsorption can be neglected because the conformation of the fiber and matrix surfaces is not expected to change much during the adsorption process (Liu 1994). The entropy of adhesion, therefore, is solely contributed by the entropy of mixing (ΔS_m; Flory 1942; Huggins 1942; Scott 1949):

$$\Delta S_{adh} = \Delta S_m, \text{ or}$$

$$\Delta S_{adh} = -\frac{RV}{V_r}\left(\frac{\phi_1 \ln \phi_1}{x_1} + \frac{\phi_2 \ln \phi_2}{x_2}\right), \tag{B3}$$

where R is the gas constant, V_r is the molar volume of monomer repeat unit, x is the degree of polymerization, while the subscripts 1 and 2 are for component 1 (wood/copolymer) and 2 (polystyrene). Other symbols bear the same meaning as Equation 5.14.

The free energy of adhesion (ΔG_{adh}) can also be expressed as:

$$\Delta G_{adh} = \Delta H_{adh} - T\Delta S_{adh}, \tag{B4}$$

but the contribution of ΔS_{adh} can be neglected because this quantity, based on Equation B3, decreases rapidly to zero as the degree of polymerization (x) becomes very large for

polymer of high molecular weight (Liu 1994). Under such a situation, the free energy of adhesion (ΔG_{adh}) is only affected by ΔH_{adh} (Equation B2), and can be expressed as:

$$\Delta G_{adh} = V\phi_1\phi_2(\delta_1 - \delta_2) + \Delta H^{AB}, \text{ or} \tag{B5}$$

$$-\Delta G_{adh} = -V\phi_1\phi_2(\delta_1 - \delta_2) - \Delta H^{AB}. \tag{B6}$$

Appendix C. An Example of Calculations for Solubility Parameter Components of an Amorphous Polymer Based on the Method of Hoy (1985)

Polystyrene, an amorphous polymer, was used to illustrate the calculations of solubility parameter components based on the method of Hoy (1985). The structural groups of polystyrene and the corresponding values of molar attraction functions are presented in Table C.1.

Table C.1 Structural groups of polystyrene and the calculated molar attraction function.

..Group, i	No. of functional groups, N_i	$\Sigma F_{t,i}$ $(J\ cm^3)^{1/2}/mol$	$\Sigma F_{p,i}$ $(J\ cm^3)^{1/2}/mol$	ΣV_i (cm^3/mol)	$\Sigma \Delta_{T,i}^{(P)}$
$-CH_2-$	1	269	0	15.55	0.020
$-\overset{\vert}{C}H-$	1	176	0	9.56	0.013
$CH_{aromatic}$	5	1205	312.5	67.10	0.090
$C_{aromatic}$	1	201	65.0	7.42	0.015
	Total:	1851	377.5	99.63	0.138

Note: Refer to Table 5.1 for the values of group contributions to the molar attraction function.

The calculations, using the values from table C.1, are as follows:

The molecular aggregation number,

$$\alpha^{(P)} = \frac{777\Delta_T^{(P)}}{V} = \frac{777(0.138)}{99.63} = 1.076$$

The number of repeating units per effective chain segment of the polymer,

$$\bar{n} = \frac{0.5}{\Delta_T^{(P)}} = \frac{0.5}{0.138} = 3.623$$

Solubility parameter (in $J^{1/2}/cm^{3/2}$),

$$\delta_t = \frac{F_t + \frac{B}{\bar{n}}}{V} = \frac{1851 + \frac{277}{3.623}}{99.63} = 19.35$$

Polar force contribution to the solubility parameter (in $J^{1/2}/cm^{3/2}$),

$$\delta_p = \delta_t \left(\frac{1}{\alpha^{(P)}} \frac{F_p}{F_t + \frac{B}{\bar{n}}} \right)^{1/2} = 19.35 \left[\left(\frac{1}{1.076} \right) \left(\frac{377.5}{1851 + \frac{277}{3.623}} \right) \right]^{1/2} = 8.25$$

Hydrogen-bonding contribution to the solubility parameter (in $J^{1/2}/cm^{3/2}$),

$$\delta_h = \delta_t \left(\frac{\alpha^{(P)} - 1}{\alpha^{(P)}} \right)^{1/2} = 19.35 \left(\frac{1.076 - 1}{1.076} \right)^{1/2} = 5.15$$

Dispersion force contribution to the solubility parameter (in $J^{1/2}/cm^{3/2}$),

$$\delta_d = \left(\delta_t^2 - \delta_p^2 - \delta_h^2\right)^{1/2} = \left(19.35^2 - 8.25^2 - 5.15^2\right)^{1/2} = 16.72$$

Note that the solubility parameter of polystyrene determined from experiments is 18.6 $J^{1/2}/cm^{3/2}$ (or 9.1 $cal^{1/2}/cm^{3/2}$; Suh and Clarke 1967; Ahmad and Yaseen 1979) which is close to our calculated value.

Appendix D. Permission to Use Published Material

August 18, 2003.

Forest Products Society
2801 Marshall Court
Madison, WI 53705-2295, USA

Dear Madam/Sir

Ref.: Permission to Use Published Materials

I am writing to request permission to use two figures from your publications for my Ph.D. dissertation under the title of "Effects of Fiber/Matrix Interactions on the Interfacial Deformation Micromechanics of Cellulose-Fiber/Polymer Composites", University of Maine, 2003. The two figures that I am seeking permission to use are:

(a) Figure 5 from the article: Mechanics of the interface in discontinuous wood fiber composites by S. M. Shaler; pages 9-14 in **Wood-fiber/polymer composites: fundamental concepts, processes, and material options** (published in 1993), and

(b) Figure 1 from the article: Interactions between wood fibers and amorphous polymers by P. F. Liu, T. G. Rials, M. P. Wolcott, and D. J. Gardner; pages 74-81 in **Woodfiber-plastic composites: Virgin and recycled wood fiber and polymers for composites** (published in 1996).

This request includes international distributions by ProQuest Information and Learning Company (PQIL), which will supply, on demand, copies of my dissertation. The request also includes all future editions and revisions, in all languages. Credit to the original source will be included.

Thank you.

Sincerely

William Tai-Yin Tze
5793 AEWC Building,
University of Maine,
Orono, ME 04469-5793, USA

Please sign below and return to me.
Permission is granted on the terms stated in this letter.

Signature: Erin Bosch
Date: 8/20/03
Print Name: Erin Bosch
Title: Editor
Company: Forest Product Society

BIOGRAPHY OF THE AUTHOR

William Tai-Yin Tze was born in Kota Kinabalu, State of Sabah, Malaysia, on May 27, 1966. From 1979 to 1986, he attended La Salle Secondary School for a six-year secondary education and a two-year pre-university education. He proceeded to the then Agricultural University of Malaysia (now Universiti Putra Malaysia) and obtained, in 1992, his Bachelor of Forestry Science degree with a concentration in wood industry. William worked as a Shift-in-charge in the pulp and paper plant of the Sabah Forest Industry, Malaysia from 1992-1993. He later joined the Sepilok Forest Research Center of Malaysia to work as a Wood Science and Utilisation Research Officer. William entered the graduate program of Michigan Technological University in 1996, and graduated with an M.S. degree in Forestry in 1998. In the fall of 1998, he began his graduate study in The University of Maine and obtained the 5^{th} year Certificate in Pulp and Paper Management in 1999. William is a candidate for the Doctor of Philosophy degree in Forest Resources from The University of Maine in August, 2003.